Lens-based fluorescence nanoscopy

Christian Eggeling[1,2], Katrin I. Willig[1], Steffen J. Sahl[1] and Stefan W. Hell[1]*

[1] Department of NanoBiophotonics, Max Planck Institute for Biophysical Chemistry, 37070 Göttingen, Germany
[2] MRC Human Immunology Unit, Weatherall Institute of Molecular Medicine, University of Oxford, Oxford OX3 9DS, UK

Abstract. The majority of studies of the living cell rely on capturing images using fluorescence microscopy. Unfortunately, for centuries, diffraction of light was limiting the spatial resolution in the optical microscope: structural and molecular details much finer than about half the wavelength of visible light (∼200 nm) could not be visualized, imposing significant limitations on this otherwise so promising method. The surpassing of this resolution limit in far-field microscopy is currently one of the most momentous developments for studying the living cell, as the move from microscopy to super-resolution microscopy or 'nanoscopy' offers opportunities to study problems in biophysical and biomedical research at a new level of detail. This review describes the principles and modalities of present fluorescence nanoscopes, as well as their potential for biophysical and cellular experiments. All the existing nanoscopy variants separate neighboring features by transiently preparing their fluorescent molecules in states of different emission characteristics in order to make the features discernible. Usually these are fluorescent 'on' and 'off' states causing the adjacent molecules to emit sequentially in time. Each of the variants can in principle reach molecular spatial resolution and has its own advantages and disadvantages. Some require specific transitions and states that can be found only in certain fluorophore subfamilies, such as photoswitchable fluorophores, while other variants can be realized with standard fluorescent labels. Similar to conventional far-field microscopy, nanoscopy can be utilized for dynamical, multi-color and three-dimensional imaging of fixed and live cells, tissues or organisms. Lens-based fluorescence nanoscopy is poised for a high impact on future developments in the life sciences, with the potential to help solve long-standing quests in different areas of scientific research.

* Author for Correspondence: Stefan W. Hell, Department of NanoBiophotonics, Max Planck Institute for Biophysical Chemistry, 37070 Göttingen, Germany.
Email: hell@nanoscopy.de

1. Introduction: from far-field light microscopy to nanoscopy

Biophysical studies strongly rely on microscopy, since it can directly deliver images of the distributions of specific molecules in the living cell. Among all the different microscopes, optical fluorescence microscopes have been established as key instruments in the life sciences. This stems from the fact that the use of light allows least-invasive access to the interior of living cells and organisms and, when combined with fluorescence readout, offers the specific and highly sensitive detection of cellular constituents. To keep these advantages, optical microscopy of the living cell is usually applied in the far-field: a lens-based system allows the excitation and detection of fluorescent molecules micrometers to millimeters away from any optical element, preserving the non-invasiveness and the ability to image deep inside living cells or tissue. However, the concomitant focusing of light introduces the most prominent limit of this technique: due to the diffraction of light, details far below the wavelength of light λ, i.e. in the range of below 200–300 nm, cannot be directly resolved in an image and remain hidden to the observer (Abbe, 1873). This diffraction barrier has major implications for biophysical studies of the cell, since a complete understanding of cellular structure and function requires observations at the molecular level, i.e. with molecular-scale resolution. Until not very long ago, obtaining a spatial resolution on the nanometer scale with a far-field fluorescence microscope was considered impossible (Alberts *et al.* 2002).

Several ideas had been put forward to improve the resolution, including special illumination patterns and mathematical approaches (Bertero *et al.* 1990; Toraldo di Francia, 1952). One of them is structured illumination microscopy (SIM) (Ash & Nicholls, 1972; Bailey *et al.* 1993; Frohn *et al.* 2000; Gustafsson, 2000; Gustafsson *et al.* 2008; Lukosz, 1966; Schermelleh *et al.* 2008). SIM allows (three-dimensional (3D) live-cell) imaging with a two-fold increase in spatial resolution over the conventional diffraction limit, i.e. ∼100 nm. Similarly, 4-Pi or I^{5}M microscopy significantly improve the axial resolution of far-field microscopy (Gustafsson *et al.* 1995, 1996, 1999; Hell, 1992; Hell *et al.* 1994; Hell & Stelzer, 1992). Unfortunately, these techniques are rather complex with respect to both instrumentation and image processing, and they do not break the diffraction barrier, because they are still limited by diffraction; they only push diffraction to its very limits.

It was not until the early 1990s that viable concepts emerged to truly break the physical barrier given by diffraction. It was realized that this could be achieved using basic molecular transitions (Hell, 1994; Hell & Kroug, 1995; Hell & Wichmann, 1994). By exploiting a transition between states of different emission properties of the fluorescent molecules, such as between a dark and a bright state, it would become possible to control the fluorescence emission in such a way that adjacent molecules emit sequentially in time (Hell, 2004; Hell *et al.* 2003). This has led to far-field imaging of fluorescently tagged objects with unprecedented spatial resolving power and heralded the move from microscopy to 'super-resolution' microscopy or 'nanoscopy'. For further reviews see, for example, (Bates *et al.* 2008; Chi, 2009; Clausen *et al.* 2013; Dedecker *et al.* 2008; Dempsey *et al.* 2011; Eggeling *et al.* 2013; Evanko, 2009; Fernandez-Suarez & Ting, 2008; Heilemann *et al.* 2009a; Heintzmann & Ficz, 2007; Heintzmann & Gustafsson, 2009; Hell, 2003, 2007, 2009a, b; Hell *et al.* 2004; Huang, 2010; Huang *et al.* 2009, 2010; Lippincott-Schwartz & Manley, 2009; Moerner, 2006; Muller *et al.* 2012; Patterson *et al.* 2010; Rice, 2007; Tinnefeld *et al.* 2015). Two major concepts have evolved so far: (1) the coordinate-targeted approach, as realized in a stimulated emission depletion (STED) (Hell & Wichmann, 1994), ground state depletion (GSD) (Hell & Kroug, 1995) or reversible saturable/switchable optical linear (fluorescence) transition (RESOLFT) (Hell, 2003, 2004; Hell *et al.* 2003) nanoscope, reversibly inhibits the occupation of a molecular state (such as the bright, emissive state) everywhere but at specific points in space such that a detected signal (such as the spontaneous fluorescence) is only allowed in coordinate regions of sub-diffraction size. Scanning of these points realizes a super-resolved image. (2) The coordinate-stochastic approach such as realized in fluorescence photoactivated localization microcopy ((F)PALM) (Betzig *et al.* 2006; Hess *et al.* 2006) or stochastic optical reconstruction microscopy (STORM) (Rust *et al.* 2006) inhibits the population of a molecular state (the bright, emissive state) everywhere but from single molecules per region of diffraction (i.e. the spatial extent in which the diffraction limit applies), whose spatial position can then be determined with sub-diffraction precision. Subsequent stochastic state transitions of all (individual) molecules and the determination of their positions allow the reconstruction of a super-resolved image.

In this review we will describe the fundamentals of far-field microscopy and its diffraction barrier, outline the details of breaking this barrier using different fluorophore transitions and detail the basics and different modalities of the current far-field nanoscopes. We will however not review every work in this field. By outlining the basic concepts of the various super-resolution microscopy or nanoscopy approaches, we rather aim at presenting the prospects and any current limitations of these nanoscopes for their use in biophysical and biomedical studies.
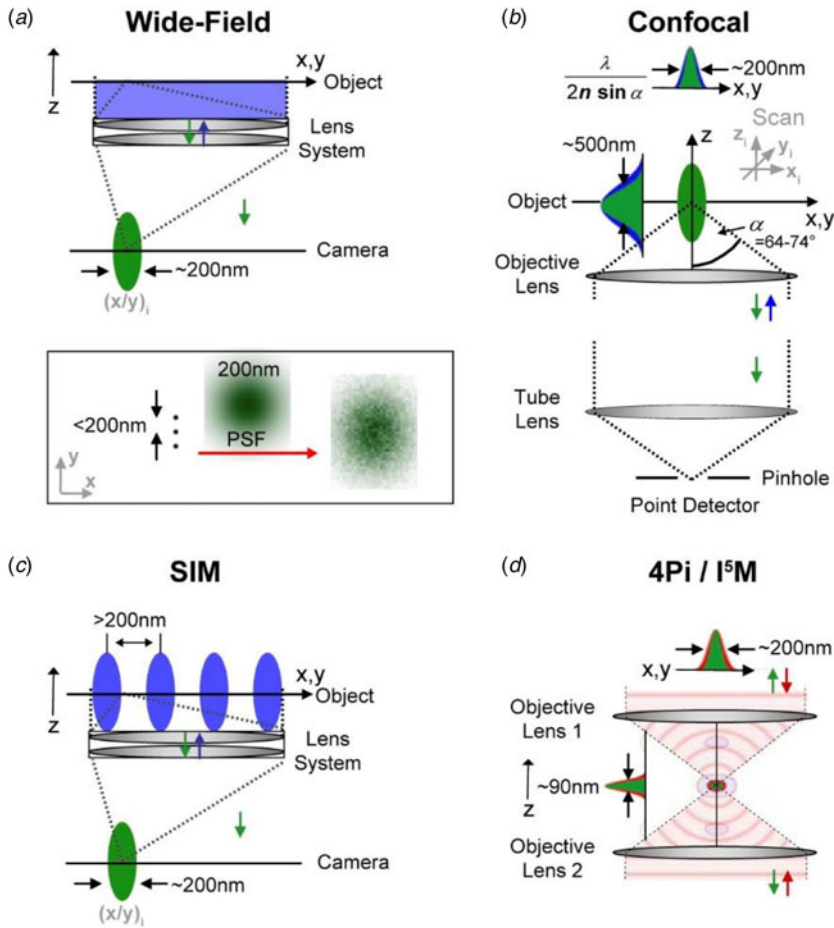
1.1 The diffraction limit

Far-field fluorescence microscopy (or far-field optical light microscopy in general) employs focused light. A lens system (the objective lens) is used to excite and collect fluorescence in the sample and to image it onto a photon detector. This is usually realized in a wide-field mode, where a large area is excited at once and imaged onto a camera, or in a point-scanning approach (e.g. the confocal microscope), where only a small spot (volume) is excited, its fluorescence detected by a point detector, and the final image formed by scanning the spot over the sample (Fig. 1*a, b*). The lens causes the focused propagating light to interfere constructively at a certain point in space, called the focal point. Diffraction, however, results in a light intensity pattern which features a central maximum and a width whose full-width-at-half-maximum (FWHM) is $d \approx \lambda/(2n \sin \alpha)$ along the lateral and $\Delta z \approx \lambda/(n \sin^2 \alpha)$ along the optic axis, governed by the wavelength λ of the light and the focusing strength of the lens (given by its semi-aperture angle α and the refractive index n of the object medium, $NA = n \sin \alpha$ is referred to as the numerical aperture of the objective lens) (Born & Wolf, 2002). This finite-width point-spread-function (PSF) of the lens rules both the fluorescence excitation and collection process, and for both the wide-field and single-point scanning variant precludes the discerning of simultaneously emitting molecules which lie within this PSF. For visible light ($\lambda \approx 500$ nm) structural details below approximately 200 nm thus appear blurred and indiscernible in the final image (Box in Fig. 1).

Several strategies have been thought of to push this resolution barrier. A straightforward way is to reduce the wavelength λ of the light. Ultraviolet (UV) light is however known to introduce photostress on the sample, stronger photobleaching of the fluorescent molecules under study, significant autofluorescence (especially in the cellular environment), and a demand for UV-specific optics, thus making it rather impractical for live-cell studies. An increase of the numerical aperture is ultimately limited by the technical feasibilities of manufacturing objective lenses, currently delivering maximum NA in the range of 1·4–1·5.

A logical consequence of the limits brought about by using focused light was to give up the use of the far-field objective lenses and confine the light by means of a sub-diffraction-sized aperture or tip (Ash & Nicholls, 1972; Synge, 1928). The light evolves out of the tip as an evanescent field, meaning that it fades out exponentially within a distance of $\sim\lambda/2$. Keeping the tip within a distance of $\cong << \lambda/2$ (i.e. a few nm) and scanning it across the sample allows the recording of images with a spatial resolution far better than the diffraction limit, given approximately by the size of the tip itself (Lewis *et al.* 1984; Pohl *et al.* 1984). Such near-field scanning optical microscopy (NSOM) has been applied in many areas (Novotny & Hecht, 2006), including biological imaging (Betzig *et al.* 1993; Kirsch *et al.* 1996). For example, with spatial resolutions of down to 80 nm, NSOM has given insights into the nanoscale organization of proteins on the plasma membrane of (living) cells (de Bakker *et al.* 2007; van Zanten *et al.* 2010). Unfortunately, the requirement of keeping the tip very close to the sample comes at a high cost: on one hand, an elaborate feedback mechanism has to be applied to keep the sample-tip distance constant (especially for dynamic living cells) (Koopman *et al.* 2004). On the other hand, one is bound to imaging surfaces, and this precludes the use of NSOM to explore the (3D) nanoscopic interior of the living cell. With this drawback, the applicability of NSOM will remain limited, which may be a reason why most biophyiscal observations keep on relying on far-field optics.

Total-internal-reflection fluorescence (TIRF) microscopy relies on evanescent fields as well. Here the evanescent field is created at the microscope's cover glass–sample interface by illuminating with (laser) light that is totally internally reflected at the glass–water interface (Axelrod,

Fig. 1. Diffraction-limited far-field fluorescence microscopy. An object is illuminated with excitation light (blue) and its fluorescence (green) imaged onto a detector using a lens system, whereby the object is placed >µm away from any optics. (*a*) In a wide-field microscope a large area of the object is illuminated at once and signal imaged onto a camera. (*b*) In a point-scanning confocal microscope a diffraction-limited volume is illuminated, signal detected on a point-detector through a pinhole, and the final image formed by scanning the spot over the object. The size of the focused and observed spot is governed by the focusing strength of the objective lens (given by the angle α), the wavelength λ of the applied light, and the refractive index n of the object medium. *Box:* Due to the focusing of light one cannot image point-like objects to dimensions smaller than approximately 200 nm in the lateral (x,y) and 600 nm in the axial (z) directions for visible light. This finite-sized, diffraction-limited point spread function (PSF) precludes the discerning of alike objects closer together than these 200 nm and results in blurred images at these spatial scales. Different versions of far-field microscopy have been implemented with the goal to push the diffraction barrier to its limits. (*c*) A two-fold increase in spatial resolution has been realized by SIM using, for example, a standing wave pattern in a wide-field mode with the pattern maxima separated by more than the 200 nm. (*d*) Using two opposing objective lenses for illumination and/or detection, the axial resolution of a wide-field or point-scanning/confocal microscope can be enhanced multi-fold, denoted I^{5}M or 4Pi, respectively. (Here, red: excitation, and green: fluorescence)

1981). With a finite penetration depth of the evanescent excitation field of typically <100 nm, TIRF microscopy only detects the fluorescence emitted from near the cover glass–sample interface. Consequently, TIRF microscopy is not a far-field optical technique, but virtually a two-dimensional (2D) microscopy technique that is not really applicable to explore the interior of a

cell. Nevertheless, TIRF efficiently suppresses the background from out-of-focus structures, and it is therefore well suited to explore the cellular boundaries, such as the plasma membrane and ligand–receptor interactions (see, e.g. Lieto *et al.* 2003).

Starting in 2000, the idea was put forward to use negative refractive index metamaterials (Pendry, 2000) for imaging with sub-diffraction resolution in the far-field. Introduced as a hyperlens (Liu *et al.* 2007; Smolyaninov *et al.* 2007), evanescent waves were converted into propagating waves forming a magnified image of the sample on a distant screen. Considered as a far-field image projection, the use of negative refractive index metamaterials (the hyperlens) also relies on collecting an evanescent wave, i.e. it requires the placing of the sample into very close proximity to the hyperlens – more specifically into its near-field. Hence, although it introduces a very interesting approach of employing evanescent waves, the hyperlens in its current state cannot be regarded as a far-field imaging device capable of observing inner-cellular structures (Podolskiy & Narimanov, 2005).

1.2 Pushing the limits of the diffraction barrier

It is due to the above limits of other techniques why most biophysical and biomedical applications still relied on the use of far-field optics, and several ideas have been put forth to address the resolution problem. These ideas included the use of special illumination patterns, like first suggested in 1952 by Toraldo di Francia (1952) or later on followed by Cremer and Cremer (1978). The use of these concepts was rendered impractical by either strong side lobes of the focused light (Toraldo di Francia, 1952), or the fact that it is impossible to achieve light convergence to a sub-diffraction focal spot (in the absence of relayed near-field components) (Cremer & Cremer, 1978). Purely mathematical processing of the imaging data has also been suggested several times to overcome the diffraction barrier (Bertero & Boccacci, 1998; Bertero *et al.* 1990; Conchello & McNally, 1996). Such computational methods usually required *a priori* knowledge of parameters of the imaging system (e.g. the PSF) and/or of the imaged object. Due to a potential lack of accurate *a priori* information, these approaches were however prone to artifacts and rarely exceeded a two-fold increase in spatial resolution. These limitations might be partially mitigated through additional *a priori* constraints such as the objects featuring different absorption or emission spectra (Burns *et al.* 1985), but marking all features in the sample with different labels – and hence achieving a general imaging strategy for the sub-diffraction interrogation of arbitrary structures – becomes itself difficult, if not impossible.

In a spot-scanning confocal microscope the sample is illuminated with a diffraction-limited focused spot and the fluorescence emission confocally detected with a symmetrically arranged point detector, which is usually realized by inserting a detection pinhole (Fig. 1*b*). The confocal detection does, however, not really provide a higher resolution. Theoretically, the width of the effective focal spot or PSF is reduced by a factor of $\sqrt{2}$ (Minsky, 1961; Pawley, 2006; Wilson & Sheppard, 1984). This improved spatial information is however usually heavily damped and thus lost in noise. The biggest benefit of detecting through a pinhole is a superb background rejection, which significantly improves 3D-imaging and which is the reason why the confocal laser scanning microscope can be considered as the workhorse of fluorescence 3D-microscopy (Pawley, 2006; Wilson & Sheppard, 1984).

Another approach that has often been connected with resolution improvement is the use of two-photon excitation. Here, the simultaneous absorption of two photons results in excitation of the fluorophore. The wavelength of the excitation light is thereby usually chosen to be double

the wavelength λ that would be used for conventional one-photon excitation (Bloembergen, 1965; Denk *et al.* 1990; Sheppard & Kompfner, 1978). The resulting non-linear squared dependence of the fluorescence emission on the excitation intensity establishes a clear reduction of the width of the effective focal spot or PSF by a factor of $\sqrt{2}$. Unfortunately, doubling the wavelength (2λ) comes with a doubling of the size of the diffraction spot (Denk *et al.* 1990), i.e. in total the spatial resolution of a two-photon microscope is usually slightly poorer than its one-photon counterpart (Schönle *et al.* 1999). The same arguments are valid for *m*-photon absorption processes, because they usually require an even longer wavelength $m\lambda$. The advantage of a multi-photon microscope lies in other factors such as a deep penetration depth, low scattering and the restriction of photobleaching to the focal spot.

Several approaches have suggested the use of structured illumination for increasing the spatial resolution of a far-field fluorescence microscope (e.g. Ash & Nicholls, 1972; Bailey *et al.* 1993; Lukosz, 1966). Structured Illumination Microscopy (SIM) by a standing wave pattern (Fig. 1*c*) is nowadays a well-established microscopy technique allowing the far-field imaging of living cells with a two-fold improvement in the lateral and axial resolution (Frohn *et al.* 2000; Gustafsson, 2000; Gustafsson *et al.* 2008; Schermelleh *et al.* 2008). Similarly, SIM has also been realized based on a software-based confocal CCD detection approach using scanning single- (Muller & Enderlein, 2010) or multi-spot (York *et al.* 2012) illumination, or it has been combined with TIRF (Fiolka *et al.* 2008). The use of two opposing objectives in either a spot-scanning 4Pi (Hell, 1992; Hell & Stelzer, 1992; Hell *et al.* 1994) or a widefield I^{5}M (Gustafsson *et al.* 1995, 1996, 1999) microscope realized an improvement of the axial resolution of a far-field microscope from 400–800 nm down to 70–150 nm (Fig. 1*d*). The latter approaches are often of special interest to microscope users since the axial resolution of any standard far-field light microscope is at least 3-times poorer than the lateral resolution in the focal plane. This particularly limits the 3D imaging of transparent objects such as cells. Both SIM and 4Pi microscopes are nowadays commercially available systems, and the enhanced resolution of both techniques has allowed the observation of live cellular structures with larger detail, giving a significantly improved insight into cellular functions (Bewersdorf *et al.* 2006; Egner & Hell, 2005; Egner *et al.* 2002, 2004; Gugel *et al.* 2004; Gustafsson *et al.* 2008; Schermelleh *et al.* 2008; Weil *et al.* 2012). However, the spatial resolution of these microscopes is still limited, i.e. they do not break the diffraction barrier, but they rather push diffraction to its limits.

1.3 Breaking the diffraction barrier

While the rationales of all previously mentioned methods such as SIM or 4Pi/I^{5}M, or NSOM, are based on modifying the propagation of light in one way or another, a real breakthrough for the surpassing of the diffraction barrier was the insight that the properties of the fluorophore itself can be used to attain in principle unlimited (actually molecular-size) spatial resolution in the far-field (Hell, 1994; Hell & Kroug, 1995; Hell & Wichmann, 1994). It was realized that one can take advantage of the transitions between different states (ground, excited and dark states) of the fluorescent label, i.e. its spectroscopic properties, to modify the fluorescence emission in such a way as to neutralize the limiting role of diffraction (Hell, 1994). Until then, fluorophores were primarily regarded as indicators of molecular species or environmental conditions (such as pH, ion concentrations). That they should also hold the key to nanoscale resolution in a far-field microscope was thus a major change in the perception of the fluorophores' role and capability in microscopy. The implementation of this idea started with STED (Hell &
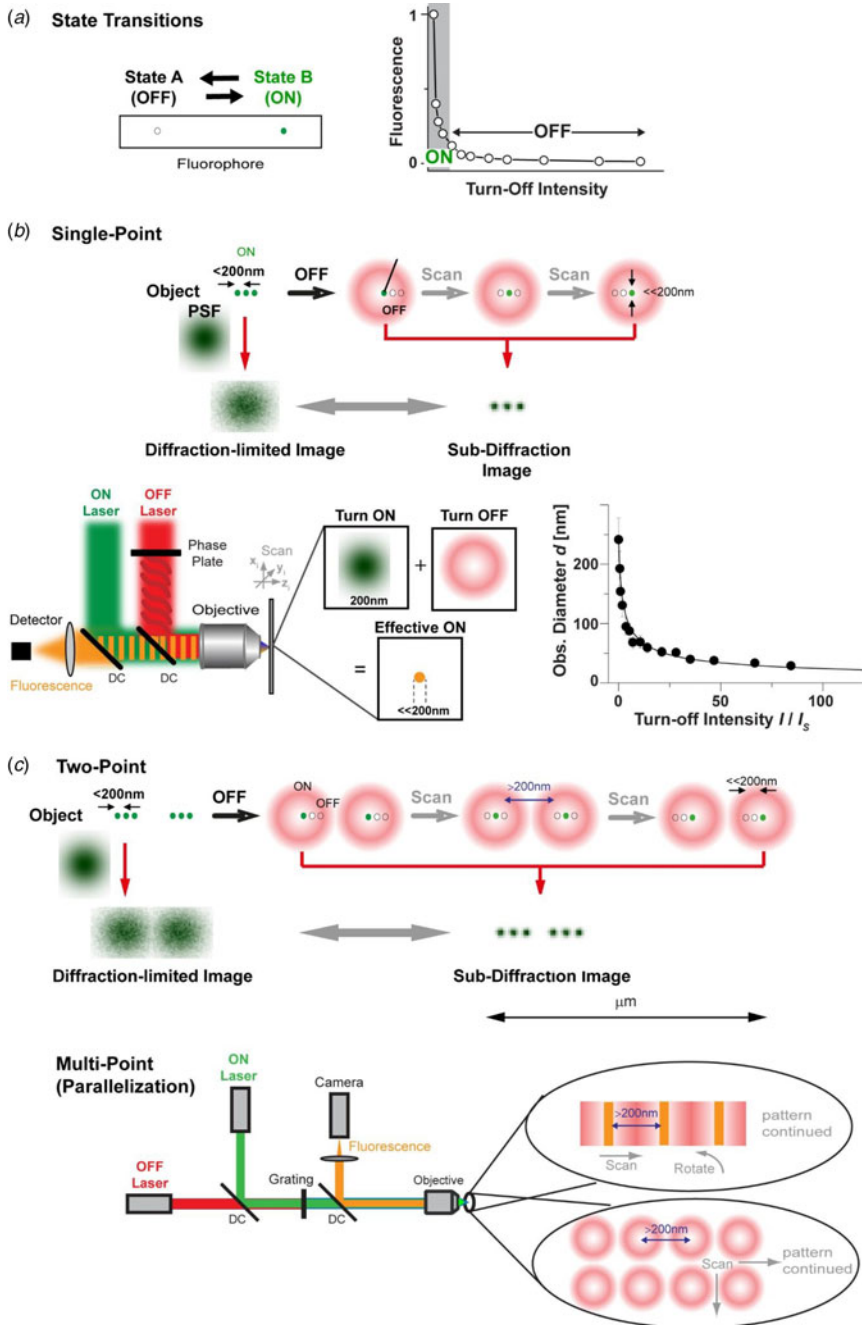
Fig. 2. Sub-diffraction imaging by the coordinate-targeted (deterministic) approach (STED/RESOLFT): driving molecular transitions in space. (*a*) Sub-diffraction imaging is based on reversibly inducing transitions between molecular states of different fluorescence emission properties (such as a bright ON- and a dark OFF-state), where at least one of the transitions such as the ON-to-OFF transition is driven by light (left). Increasing the intensity of the turn-off light above a certain threshold turns off the fluorescence emission (right). (*b*) In its single-spot scanning version the diffraction-limited spot of the fluorescence excitation or turn-on laser (green) is overlaid with an additional turn-off laser which features a central intensity zero (red). Increasing the intensity I of the turn-off laser far above a threshold value

Wichmann, 1994; Klar & Hell, 1999; Klar *et al.* 2000), GSD (Bretschneider *et al.* 2007; Hell & Kroug, 1995) and RESOLFT (Hell, 2004; Hell *et al.* 2003; Hofmann *et al.* 2005) microscopy, which thus emerged as the first concrete and viable physical concepts to overcome the limiting role of diffraction in a lens-based optical microscope. While these approaches reversibly inhibit the occupation of a molecular state (usually the emissive state) at defined spatial coordinates using deterministic scanning, subsequent developments such as (F)PALM (Betzig *et al.* 2006; Hess *et al.* 2006) or STORM (Rust *et al.* 2006) transfer the fluorophores to their emissive state stochastically in space and utilize the spatial localization of single isolated molecules based on the emitted fluorescence pattern of the individual molecules, to assemble the final image. Still, the basic requirement remains the same: the preparation of at least two transient states of the fluorescent labels with discernible emission properties. The most prominent example is a pair of a bright (fluorescent) ON- and a dark (non-fluorescent) OFF-state, where at least one transition such as the ON-to-OFF transition is driven by light. The molecular states involved do not necessarily have to be dark and bright states. They can also differ in other fluorescence properties such as absorption cross-section, emission wavelength, fluorescence lifetime or another property, i.e. their detected signal has to be discernible. For simplicity, we keep to the notation of ON- and OFF-states and denote the light driving the OFF–ON and ON–OFF transition by 'turn-on' and 'turn-off' light.

The prospects of these super-resolution microscopes or nanoscopes to image the living cell with conceptually unlimited (presently ∼10–50 nm) spatial resolution is revolutionizing modern microscopy and has a major impact on biophysical and biomedical research.

2. The coordinate-targeted approach

The initially developed coordinate-targeted approaches STED, GSD or RESOLFT utilize an illumination pattern. Specifically, an intensity distribution of either the turn-on or turn-off laser is created that features at least one intensity zero to transiently confine the occupation of usually the ON-state, i.e. the fluorescence emission, to sub-diffraction sized areas or volumes (Fig. 2). Increasing the intensity of this modified laser above a certain threshold basically then turns off the detected fluorescence emission (Fig. 2*a*). The restriction of the occupation of ON-states and thus (detected) fluorescence emission to sub-diffraction dimensions is ensured by (1) an overlay of the turn-off laser with the fluorescence excitation (or turn-on) laser, and (2) an intensity of the turn-off laser above the mentioned threshold.

A unique feature of this principle is that the size of the effective observation area/volume and thus the spatial resolution of the microscope is tuned by the intensity of the turn-off laser. More specifically, it has been shown that, for example, the lateral resolution as given by the diameter (or

(I_S) confines the volume in which fluorescence emission is allowed to sub-diffraction dimensions, i.e. it creates an observation spot with diameter $d \ll 200$ nm (orange). Insets: respective focal intensity distributions. Lower right: Diameter of the observation spot *versus* intensity of the turn-off laser (example data for STED). With the spatial coordinates known, scanning of this spot realizes imaging with sub-diffraction resolution, and thus the discerning of alike objects closer together than 200 nm (upper panel). (*c*) In a multi-spot realization, the added turn-off light features several intensity zeros, such as realized for a wide-field microscope by a standing-wave pattern or many doughnuts with the pattern maxima or doughnut minima separated by more than the 200 nm. Increasing $I \gg I_S$ restricts fluorescence emission to multiple spots or lines of sub-diffraction dimension, and scanning of these spots or lines over the sample realizes images with sub-diffraction resolution.

FWHM) of the observation area $d \approx \lambda/(NA\sqrt{(1 + I/I_S)})$ approximately scales with the inverse square-root of the intensity I of the turn-off laser (Harke *et al.* 2008a; Hell, 2004; Hell *et al.* 2003). Here, I_S is the above-mentioned threshold intensity (often denoted saturation intensity), which is a characteristic of the fluorophore (involving the light absorption cross-section of the ON–OFF transition and the lifetime of the involved states) and of the steepness of the edges of the intensity zeros. Driving the intensity I further and further up thus creates continuously smaller observation areas down to the size of a single molecule.

In usual practice, the wavefront of the turn-off laser is modified by the insertion of a phase plate or grating in such a way that the focusing creates one or multiple intensity zeros. In the case of the single-point scanning microscope usually a doughnut-like intensity distribution with a central intensity zero is preferred (Fig. 2*b*) (Keller, 2006; Willig *et al.* 2006a). Scanning of the reduced-size observation spot then renders a direct image of the distribution of fluorescently marked molecules with nanoscale spatial resolution. However, as will be discussed later on, other intensity distributions have been realized as well, for example confining the fluorescence along the axial z-direction (Klar *et al.* 2000) or even along all spatial directions, creating an almost isotropic spot (Harke, 2008; Harke *et al.* 2008a, b; Schmidt *et al.* 2008). In the case of the wide-field microscope, usually a standing-wave-like pattern with multiple zero-intensity lines such as in SIM is created. The camera images recorded for multiple scanning positions of the zeros are then post-processed to reconstruct the final image (Gustafsson, 2005; Heintzmann *et al.* 2002; Rego *et al.* 2012; Schwentker *et al.* 2007). As shown recently, a preferred mode is to scan multiple points or doughnuts instead of rotating entire lines (Chmyrov *et al.* 2013). In any case, for $I \gg I_S$ alike features closer together than the diffraction-limited 200 nm are now distinguishable, since they are switched on and thus detected separately in time. For the wide-field approach, this requires neighboring intensity zeros to be separated by more than the diffraction-limited 200 nm.

It is obvious that the increased image resolution comes along with a reduction of the scanning step size; the molecules that were 'off' initially have to be turned 'on' later, etc. Therefore, an accurate acquisition of nanoscale details requires an increased number of scanning steps and consequently longer acquisition times. Nevertheless, this coordinate-targeted approach offers all features of a conventional microscope from multicolor and 3D image acquisition over single-molecule detection to deep-tissue or *in-vivo* imaging. In the following, we will present these capabilities of coordinate-targeted scanning nanoscopy, starting with the so far most developed technique, STED nanoscopy.

2.1 STED nanoscopy

In STED nanoscopy, the pair of molecular states are the fluorophore's ground (dark OFF) state S_0 and the excited (fluorescent ON) state S_1, respectively. Being initially in the S_0 OFF-state, excitation to the S_1 ON-state and thus fluorescence emission is driven by the excitation laser, while switching back to S_0 is realized by stimulated emission using a second laser, the STED laser. The wavelength of the STED laser is usually chosen in the far red part of the fluorophore's emission spectrum to ensure for the STED light (1) a sufficiently large cross-section for stimulated S_1 to S_0 de-excitation, (2) a close-to-zero probability for S_0 to S_1 excitation and (3) a straightforward way to block the stimulated emission and STED light from the detection of the spontaneous fluorescence emission. Above a certain threshold intensity the STED light causes a more efficient stimulated than spontaneous S_1 to S_0 de-excitation, i.e. an inhibition of the detected (spontaneous)

emission. The threshold or saturation intensity $I_S = (\tau\,\sigma_{STED})^{-1}$ of the STED light is defined by the photon cross-section σ_{STED} of stimulated emission at the wavelength λ_{STED} of the STED laser and the lifetime τ of the excited S_1 state. With lifetimes in the range of 1–4 ns and stimulated emission cross-sections in the range of 10^{-17} cm^2 (i.e. photon cross-sections $\sigma_{STED} \approx 25$–30 cm^2/J) STED intensities of usually $I_S \gg 1$–10 MW/cm^2 have to be applied to realize a sufficiently large fluorescence inhibition. Therefore, a preferred implementation of the STED concept is the use of pulsed excitation and STED lasers, where the concomitant high pulse peak intensities and the optimized timing (with the STED laser swiftly following the excitation pulse) result in very efficient stimulated emission (Donnert *et al.* 2009; Klar *et al.* 2000) (compare chapter 2.1.6).

One of the first biologically relevant experiments in STED imaging related to the observation of synaptic vesicles (Willig *et al.* 2006c). Synaptic transmission is mediated by neurotransmitters that are stored in synaptic vesicles and released by exocytosis upon activation. The vesicular membrane is retrieved by endocytosis, and synaptic vesicles are regenerated and re-filled with neurotransmitter. While many aspects of vesicle recycling are well understood, the fate of vesicle membranes after fusion was still unclear. Do their components diffuse on the plasma membrane, or do they remain together? This question had been difficult to answer because, with a size of approximately 40 nm in diameter, synaptic vesicles are too small to be resolved by conventional diffraction-limited fluorescence microscopes. With STED microscopy, individual synaptic vesicles were visualized in the synapse at a resolution of 65 nm (Fig. 3*a*). It was shown that synaptotagmin I, a protein resident in the membrane, remains clustered in isolated patches on the presynaptic plasma membrane.

Similarly, with its improved spatial resolution STED nanoscopy could uncover new details of various cellular structures, protein clusters or DNA (e.g. Blom *et al.* 2011; Dyba *et al.* 2003; Kellner *et al.* 2007; Kittel *et al.* 2006; Lau *et al.* 2012; Muller *et al.* 2012; Opazo *et al.* 2012; Persson *et al.* 2011; Schmidt *et al.* 2008, 2009; Sieber *et al.* 2007; Wagner *et al.* 2012), making a STED microscope a uniquely helpful tool nowadays in cell-biological laboratories (Clausen *et al.* 2013). Furthermore, STED has important applications outside biology, ranging from nanoscale imaging of assemblies of colloidal particles and polymeric structures (Friedemann *et al.* 2011; Harke *et al.* 2008b; Ullal *et al.* 2009, 2011) to solid-state physics (Wildanger *et al.* 2011). With its capabilities and simplifications steadily growing, as outlined further on, and commercial instrumentation improving (Clausen *et al.* 2013), STED nanoscopy may become a workhorse of imaging facilities, greatly extending the resolving power of confocal microscopes.

2.1.1 Multicolor STED nanoscopy

In most cellular applications it is desirable not only to resolve a single structure at a time, but to highlight the relative sites and proximities of different molecules. In fluorescence microscopy this is usually realized by tagging the different molecules with different fluorescent labels, whose emission is then distinguished by its specific color, lifetime or potentially other fluorescence parameters. In a preferred implementation, the wavelength of the emitted light is chosen as a delimiter, and the fluorescence emission of the different labels is excited with lasers of different wavelength and detected on separate detectors monitoring different wavelength ranges. This principle is transferable to STED microscopy, however with the requirement of supplying a multitude of additional STED lasers, strictly speaking one for each label used. While this approach has rendered two-color STED imaging (Donnert *et al.* 2007b) possible, and revealed the co-localization of different proteins and structures on the nanometer-scale (Meyer *et al.* 2008), it entails a rather
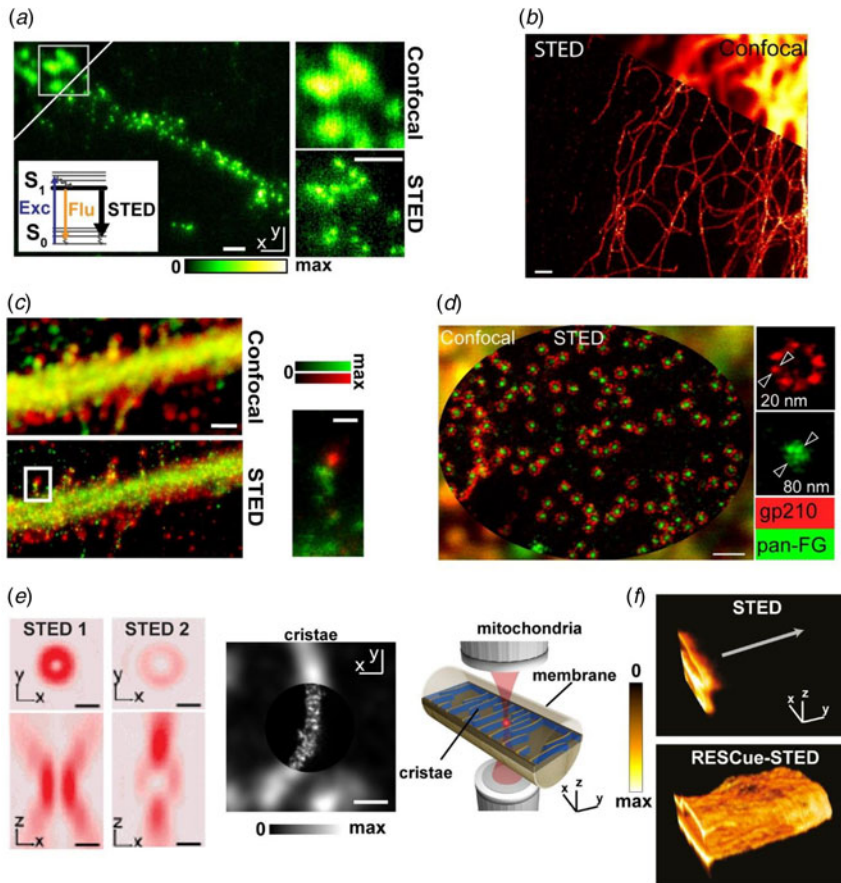
Fig. 3. STED nanoscopy. (*a*) A reversible molecular transition is realized by stimulated emission (inset): the turn-on light excites (Exc) the fluorophores from their (dark) ground S_0 to their (bright) excited S_1 state, where de-excitation by spontaneous fluorescence emission (Flu) is overruled by the addition of the STED laser inducing stimulated emission. Example scanning STED nanoscopy image of fluorescently labeled synaptotagmin I in fixed cultured hippocampal neurons, exemplifying the superior spatial resolution over conventional confocal microscopy and revealing that this protein is clustered in isolated patches on the presynaptic plasma membrane after synaptic vesicle exocytosis (adapted from (Willig *et al.* 2006c)). Scale bar: 1 µm. (*b*) Confocal (upper right) and STED images of immunolabeled microtubules in fixed mammalian cells (adapted from Wurm *et al.* 2012). Scale bar: 500 nm. (*c*) Multi-color STED nanoscopy determining the co-localization of different molecules with sub-diffraction resolution, as exemplified for the D1 dopamine receptor and Na1,K1-ATPase in cultured striatal neurons (lower image: confocal recording, adapted from (Blom *et al.* 2012)). Scale bars: 1 µm (in enlarged image: 200 nm). (*d*) Multi-color STED and confocal (peripheral parts) recordings of immunolabeled subunits in amphibian nuclear pore complexes (NPCs) of cultured *Xenopus* cells with close-ups (right) of the spatial organization of the peripheral gp210 and central pore pan-FG proteins in a single NPC (adapted from Göttfert *et al.* 2013). Scale bar: 500 nm. (*e*) 3D STED nanoscopy realized by overlapping two STED beams featuring confinement along the lateral x/y and axial z direction, respectively (left: x–y (upper) and x–z (lower) projections of the intensity distributions of the two STED lasers, scale bars: 200 nm), and by the use of two opposing microscope objectives (O1 and O2, right). The resulting isotropic observation spot of diameter below 40 nm allows the recording of super-resolved 3D images, as exemplified by resolving mitochondrial christae (middle, scale bar: 1 µm, adapted from (Schmidt *et al.* 2009)). (*f*) RESCue STED: Reduction of photobleaching in 3D STED imaging by applying an intelligent light exposure scheme that minimizes the number of excitation/de-excitation events a fluorophore has to undergo during recording of a scanning image: conventional (upper) and RESCue (lower) 3D STED

complex setup with the correct alignment of four lasers, two excitation and two STED beams. Furthermore, the simultaneous recording of the two colors proves itself somewhat difficult, since the more blue-shifted STED laser usually leads to a strong excitation and thus massive photo-bleaching of the more red-emitting dye. Therefore, initial two-color STED images were recorded sequentially. This limitation has been solved by straightforward optimizations of the choices of labels and wavelengths: (1) the combination of two labels with overlapping emission spectra and with a long (Stokes) shift between the excitation and emission spectrum of one of the labels allows the recording of two-color STED images with two excitation lasers but only one STED laser (serving both labels) (Clausen *et al.* 2013; Dean *et al.* 2012; Friedemann *et al.* 2011; Pellett *et al.* 2011; Schmidt *et al.* 2008). (Quasi-) simultaneous recording of both colors is possible in either a line-by-line or a pulse-interleaved excitation scheme, in both cases rapidly switching between the two excitation lasers. (2) Nanoscopic co-localization studies of various different proteins have been enabled by a carefully optimized choice of two conventional Stokes-shifted fluorophores, whose spectra differ by only about 60 nm, the use of two pairs of excitation/STED lasers timed in a pulsed interleaved excitation scheme, and with an elimination of the detection cross-talk by applying linear unmixing algorithms (Fig. 3*c, d*) (Blom *et al.* 2012; Dean *et al.* 2012; Neumann *et al.* 2010; Opazo *et al.* 2010; Reisinger *et al.* 2011; Osseforth *et al.* 2013). In this scheme, the number of distinguishable labels could be increased to four by separating the emission based on emission wavelength and lifetime (Bückers *et al.* 2011). (3) Recent two-color STED imaging has been realized using two excitation and a single STED laser only, e.g. 594 and 640nm excitation in combination with a 775nm STED laser (Göttfert *et al.* 2013). (4) Instituting rigorous linear unmixing with a single excitation and a single STED laser were sufficient to record two-color STED images of labels such as the yellow fluorescent protein (YFP) and green fluorescent protein (GFP), whose spectra are separated by about 20 nm (Tonnesen *et al.* 2011). Similarly, combining two reversibly photoswitchable fluorescent proteins (RSFPs) with opposite activation properties, two-color STED images were recorded with just one pair of excitation and STED lasers, without the necessity of applying linear unmixing, but with the addition of blue-light photoswitching (Willig *et al.* 2011). With the ongoing development of fluorescent labels and lasers, the number of fluorophores and matching excitation/STED laser pairs useful for multi-color STED imaging schemes will increase further.

2.1.2 3D STED nanoscopy

So far we have presented images recorded with STED nanoscopes which confine fluorescence emission and thus improve spatial resolution along the lateral direction only (using, e.g. the previously mentioned doughnut-like intensity distribution). The combination of this modality with an evanescent wave illumination (TIRF) scheme for excitation (Gould *et al.* 2011; Leutenegger *et al.* 2012) is sufficient for selectively imaging membranes of flat cells with penetration depths of <100 nm, and the combination with two-photon excitation realized imaging in ~800 nm thick sections with deep penetration depths (Bethge *et al.* 2013; Bianchini & Diaspro, 2012; Ding *et al.* 2009; Li *et al.* 2009b; Moneron & Hell, 2009; Takasaki *et al.* 2013). However, the imaging of intra-cellular structures such as the Golgi apparatus or mitochondria often requires both a

---

recordings of fluorescent immunostained nuclear lamina in fixed neuroblastoma cells (arrow: third dimension scanning direction (*y*), adapted from (Staudt *et al.* 2011)). Length of coordinate bars: *x*/*z* 1 μm, *y* 0·5 μm.

deeper penetration depth and an improvement of the spatial resolution along the axial z-direction as well. Four approaches have been applied so far: (1) The use of a phase plate that, upon interference, inhibits fluorescence along z and preferentially its combination with the doughnut-shaping plate creates the desired fluorescence restriction along all spatial directions (Fig. 3e) (Harke *et al.* 2008a, b; Klar *et al.* 2000; Wildanger *et al.* 2009b; Osseforth *et al.* 2013). (2) The use of the doughnut-shaped STED focus in conjunction with illumination by two opposing objectives (as for 4Pi) has realized spatial resolution along the axial direction of down to 33 nm (Dyba & Hell, 2002; Dyba *et al.* 2003), or was used to create an effective isotropic observation volume with a spatial resolution of down to 30 nm along all spatial directions (Hell *et al.* 2009; Schmidt *et al.* 2008). Such an isoSTED microscope has given new insights into mitochrondrial structure, for example for the first time resolving the mitochondrial cristae with an optical microscope (Fig. 3f) (Schmidt *et al.* 2009). (3) Recently, a combination of STED with single plane illumination microscopy (SPIM) realized an almost two-fold improvement in axial resolution along with an 1·3-fold improvement along the lateral directions compared to conventional SPIM. Applying this illumination scheme, STED-SPIM should allow penetration depths of >100 µm and thus realize imaging inside zebra fish (Friedrich *et al.* 2011). (4) Adaptive optics allows the correction of aberrations occurring predominantly when imaging in 3D deep inside tissue (Gould *et al.* 2012, 2013).

2.1.3 Photo-physical and -chemical considerations in STED nanoscopy

The signal strength and observation time of fluorescence experiments is limited by the population of metastable dark states and the photobleaching of the fluorophore label (e.g. Eggeling *et al.* 1998, 1999; Tsien *et al.* 2006). Fluorescence emission follows the excitation of the fluorophore from its ground to its excited electronic state by, for example, laser light. The frequency and number of emitted photons depend on how fast and how many times one can cycle the fluorophore between the ground and excited state, respectively. In the excited state, the fluorophore becomes more fragile as reaction pathways to non-fluorescent species (such as ionization and/or breaking of double bonds) are opened up which can result in photobleaching, an irreversible loss of the ability to fluoresce. Furthermore, in the excited state the fluorophore may cross to metastable dark states of microsecond- to second-long lifetimes (such as the triplet state or radical states for usual organic dyes or fluorescent proteins), where the fluorophore is disengaged from the fluorescence cycling process, thus reducing the number of emitted photons. These long-lived dark states are much more prone to photobleaching than the first excited singlet state. For example, the triplet state efficiently interacts with molecular oxygen, generating highly reactive singlet oxygen (for a review see e.g. Eggeling *et al.* 1999). On the other hand, high laser irradiances as for example used in scanning confocal microscopy open up new efficient photobleaching pathways by further exciting the already excited fluorophore to higher electronic states (e.g. Eggeling *et al.* 1998, 2005; Widengren & Rigler, 1996). In aqueous environments, these excited species couple quite efficiently with ionic states and are thus highly reactive (e.g. Anbar & Hart, 1964; Reuther *et al.* 1996), usually characterized by more than ten-fold higher photobleaching probabilities than found from the first excited electronic states (e.g. Eggeling *et al.* 1998, 2005). Such non-linear photobleaching mechanisms are exceedingly efficient from the dark states due to their relatively long lifetime.

The accommodation of a large number of continuous excitation/de-excitation cycles and thus the maximization of the fluorescence signal has been approached by choosing experimental conditions which minimize the reactivity of the excited states as well as the populations of dark and

higher excited states. This can either be done by choosing an appropriate dye with low photo-bleaching probabilities, low absorption cross-sections of the excited states and low dark state populations (e.g. Dittrich & Schwille, 2001; Eggeling *et al.* 1999, 2006; Tsien *et al.* 2006), or by the addition of chemicals (such as radical quencher or mercapto-compounds) that result in a reduction of photobleaching probabilities (especially of the higher excited electronic states) or in a quenching of the dark states (e.g. Dave *et al.* 2009; Dittrich & Schwille, 2001; Eggeling *et al.* 1999, 2006; Rasnik *et al.* 2006; Vogelsang *et al.* 2008; Widengren *et al.* 2007). Unfortunately, an appropriate fluorophore may not always exist, or the addition of (sometimes toxic) chemicals is often invasive and not live-cell compatible. The minimization of dark state populations and non-linear photobleaching processes therefrom was approached with a method termed dark- or triplet-state relaxation (D- or T-Rex) microscopy (Donnert *et al.* 2006, 2007a). The D- or T-Rex principle makes use of low-repetition pulsed laser light (Donnert *et al.* 2006, 2007a) or of ultra-fast scanners (Donnert *et al.* 2009) to allow for an efficient depopulation of any dark state population in-between excitation events, thereby minimizing dark-state build-up and non-linear photobleaching from these states. The use of fast beam-scanning microscopes, where D-/T-Rex is effectively implemented, is especially suitable for live-cell fluorescence imaging experiments (Borlinghaus, 2006; Conchello & Lichtman, 2005; Tsien *et al.* 2006; Vukojevic *et al.* 2008; Webb *et al.* 1990).

In STED, the fluorophores are forced to undergo numerous transitions between their ground and excited state from which photobleaching or a dark-state transition may occur (Fig. 4*a*) (Donnert *et al.* 2006; Dyba & Hell, 2003). In addition, increasing the irradiance of the STED laser to increase the gain in spatial resolution requires an adaptation of the scanning imaging process, with smaller pixel sizes and thus a larger number of scanning steps, unfortunately increasing the number of cycles that a molecule has to undergo during the recording of an image. Therefore, a key to sub-diffraction STED (or, similarly, GSD and RESOLFT) imaging is to ensure that the marker is able to switch repeatedly between its ON and OFF states in the presence of both the switch-on and switch-off light.

Stimulated emission reduces the lifetime of the excited state and therefore in principle increases the photostability of the fluorophore in comparison to action of the excitation laser only (Fig. 4*b*). However, unwanted excitation to the higher excited states usually antagonizes this process (Fig. 4*a*). As a consequence, it was the realization of D- or T-Rex (see above) STED imaging that demonstrated for the first time down to 20 nm macro-molecular spatial resolution in cells (Donnert *et al.* 2006), and it is the implementation of fast beam-scanning that nowadays allows routine live-cell STED nanoscopy (compare Section 2.1.5) (Fig. 4*c*) (Moneron *et al.* 2010). Additionally, STED nanoscopy becomes much more feasible by choosing fluorophores with a low absorption cross-section of the first excited state at the wavelength of the STED laser (Hotta *et al.* 2010), or by appropriately adapting the latter to minimize non-linear photobleaching (Fig. 4*d*) (Rankin *et al.* 2011). This has recently allowed STED imaging in an intact living organism, namely *Caenorhabditis elegans* expressing eGFP (Rankin *et al.* 2011). STED at nitrogen temperatures attempted to minimize photobleaching and to maximize the efficiency of stimulated emission (Fig. 4*e*) (Giske, 2007), unfortunately making live-cell studies less feasible. The choice of other promising emitters such as the very photostable nitrogen vacancy (NV) centers in diamond has recently allowed STED imaging with a spatial resolution of down to 5 nm (see Section 2.3) (Han *et al.* 2012; Rittweger *et al.* 2009a). Similarly, special quantum dots (QDs) could be used in a STED-like fashion (Irvine *et al.* 2008). Unfortunately, the use of most conventional QDs for STED is so far impeded by their low Stokes shift and narrow band of emission. Nevertheless, a large range of appropriate fluorophores for STED nanoscopy is now known. Still, the
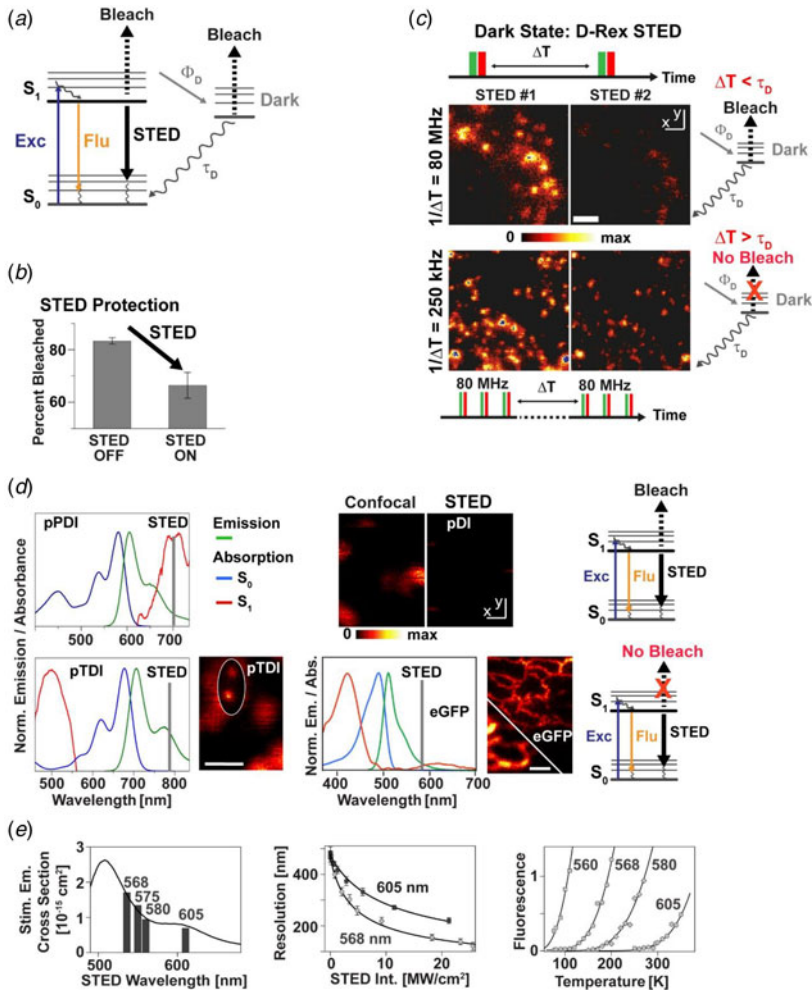
Fig. 4. STED nanoscopy: photophysics and bleaching. (*a*) Photobleaching pathways: excitation (Exc) elevates a fluorophore from its ground S_0 to its first excited electronic state S_1, from where it either returns to S_0 by spontaneous fluorescence emission (Flu) or by STED, or it traverses with probability Φ_D to a dark state whose lifetime τ_D (time before return to S_0) is much longer than that of S_1. Photobleaching may occur from S_1 and the dark state, and is most pronounced from higher excited electronic states after further absorption of excitation or STED light (higher-order photobleaching, dashed lines). Horizontal lines: electronic states (thick) and vibrational sub-states (thin). Curved lines: vibrational transitions. (*b*) Suppression of photobleaching rate by STED: stimulated emission shortens the lifetime of S_1 and thus the probability of photobleaching as exemplified by the percentage of signal bleached after scanning a layer of the organic dye KK114 with and without the addition of STED light (excitation at 488 nm with 9 kW/cm^2 and STED at 760 nm with 0·8 GW/cm^2, repetition rate 76 MHz, scanning dwell time 10 ms). (*c*) Higher-order photobleaching from long-lived dark states, as exemplified by subsequent scanning STED images of 40-nm sized fluorescent beads, showing a significant loss of signal due to irreversible photobleaching (upper images). D-Rex illumination, i.e. increasing the time ΔT between subsequent pairs of excitation and STED pulses (i.e. decreasing the repetition rate $1/\Delta T$) above the dark states lifetime τ_D allows the dark states to relax before incidence of the next pulses, avoiding higher-order photobleaching (lower images). D-Rex illumination by fast beam scanning (lower panel): for a fluorophore the incidence of only a few excitation-STED pulse pairs of high repetition rate (e.g. 80 MHz) is followed by a long resting period ΔT until the scanned beam pair hits the same spot again. (*d*) Higher-order photobleaching from the first excited electronic state S_1, as exemplified for the organic dyes pDI and pTDI and for eGFP. Absorption spectra of S_0 (blue) and S_1 (red) and fluorescence

development of new bright and photostable dyes, often specialized for STED applications, has and continuously will enhance the applicability and flexibility of experiments using this super-resolution technique (Boyarskiy *et al.* 2008; Kolmakov *et al.* 2010a, 2010b, 2012; Mitronova *et al.* 2010; Wurm *et al.* 2012).

The number of cycles that a molecule has to undergo is severely increased when recording 3D images, where one plane after the other is scanned at different optical (z) axis positions. Here, an intelligent light exposure scheme was put into practice. Related to controlled light exposure microscopy – introduced for decreasing photobleaching and increasing the number of detected fluorescence photons in scanning microscopy (Hoebe *et al.* 2007) – the reduction of state transition cycles (RESCue)-STED scheme uses an online feedback algorithm that rapidly switches off the excitation and STED light during a scanning step when no or only low signal is detected (Staudt *et al.* 2011). Thereby, the cycling of nearby fluorophores is minimized and the total number of on–off cycles significantly reduced. For 3D scanning imaging, this reduces the probability of dark state transitions and photobleaching in the adjacent axial planes, consequently increasing the number of planes that can be successively recorded (Fig. 3*f*).

2.1.4 Cluster analysis in STED nanoscopy

Clustering of molecules is key in a lot of cellular processes. Unfortunately, these clusters can often not be characterized accurately, especially in the living cell, mainly because their sizes are usually below the diffraction barrier and thus cannot be determined with conventional light microscopy. The use of a STED nanoscope is an obvious way to overcome this limitation. STED was applied to image various molecular assemblies in different cells, tissue or membranes. To name a few, STED imaging was used to study the clustering to ∼70-nm large spots of a synaptic vesicle protein after exocytosis (Fig. 3*a*) (Willig *et al.* 2006c), the anatomy of supra-molecular membrane protein clusters of approximately 50–60 nm in diameter (Sieber *et al.* 2007), the dynamics of approximately 80-nm large synaptic vesicle movements (Westphal *et al.* 2008), or the formation of domains in phase separated membrane bilayers of down to below 40 nm in diameter (Honigmann *et al.* 2013b, 2012). These examples have in common that previously blurred structures are now revealed as a multitude of single isolated clusters. Besides the cluster size, STED

---

emission spectra (green) show that excitation to higher excited states from S_1 by the STED light may be significant for pDI and for eGFP at >595 nm, but not for pTDI, and for eGFP at <595 nm, resulting in far less photobleaching for pTDI, exemplified in CW-STED images of single pDI and pTDI molecules (confocal images were taken prior to STED recordings, pTDI: STED (white circle) and confocal recording (outer region), scale bar 500 nm, adapted from (Hotta *et al.* 2010), and for eGFP the STED wavelength between 556 and 592 nm, exemplified in STED recordings of live Vero cells expressing eGFP in the endoplasmic reticulum (middle panel, lower left corner: confocal image, scale bar: 1 μm, adapted from (Rankin *et al.* 2011)). (*e*) STED at nitrogen temperatures. (Left) The cross-section of stimulated emission is highest at wavelengths close to the fluorescence emission maximum as exemplified for the organic dye Atto532 (columns: cross-sections of stimulated emission at selected wavelengths, black line: fluorescence emission spectrum scaled to the cross-section value at 568 nm). (Middle) As a consequence, less intensity of STED light is required for 568 nm compared to 605 nm to increase the spatial resolution in STED images of 80 nm-large Atto532-labeled beads, as determined for different intensities of the STED laser. (Right) STED imaging at 568 nm is however only possible at nitrogen temperatures, since the relative fluorescence emission evoked by the STED light increases for wavelengths closer to the emission maximum, but this anti-Stokes fluorescence excitation is efficiently suppressed at nitrogen temperatures <100 K, as exemplified for the dye Atto532 in polyvinyl-alcohol (PVA) (adapted from Giske 2007).

imaging also gives access to further parameters such as cluster brightness (and thus an estimate of the number of molecules per cluster) and the cluster density. An advantage of the STED approach is that it gives a direct image, i.e. cluster parameters such as cluster size can directly be inferred from the recorded image without having to introduce considerable image processing. In the following we will give an example of such a cluster analysis using STED nanoscopy.

We had previously shown that syntaxin 1A, a protein of the soluable N-ethylmaleimide-sensitive factor attachment protein receptors (SNARE) family of receptors which are involved in exocytosis, forms clusters of about 50–60 nm in diameter in the plasma membrane of PC12 cells (Sieber *et al.* 2006, 2007). An important question remains how these clusters change with increasing expression levels of syntaxin. For this, we created membrane sheets of PC12 cells, after fixation added labelled antibodies against syntaxin (HPC-1 monoclonal antibody and a secondary antibody decorated with the green-emitting dye Atto 532) and imaged their distribution using a custom-built STED nanoscope, as described previously (Sieber *et al.* 2006). To test the performance of our STED cluster analysis, we artificially created syntaxin clusters with a broad range of sizes and densities, as follows: (1) direct fixed: the cells were fixed directly after the membrane sheet preparation (i.e. after removing the upper part of the cell). (2) Patched 1: the sheets were incubated for 1 h at 37 °C prior to fixation (in 200 μl/CS sonication buffer with 1% BSA). (3) Patched 2: preparation as for patched 1 but with a polyclonal antibody during the 1 h incubation. For cases (2) and (3) we expect an enhanced (artificial) clustering of syntaxin, which should result in larger and brighter but less dense protein assemblies. Figure 5*a* shows representative STED images together with conventional confocal counterparts (circles) of these three different preparations. Clearly, the clusters can be much more accurately resolved with STED, and their density behaves as expected.

We applied three different statistical approaches to gain accurate values of cluster size, brightness and density. (1) Single cluster analysis (SCA): using an image analysis algorithm for identifying single isolated spots, clusters were separated and their brightness, diameter and the number of clusters per area determined (Willig *et al.* 2006c). (2) Image correlation analysis (ICS) (Petersen *et al.* 1986): the calculation and analysis of the autocorrelation function of the number of counts in the image pixels over space allows the determination of cluster size and density. (3) Fluorescence intensity distribution analysis (FIDA) or photon-counting-histogram (PCH) image analysis (Chen *et al.* 1999; Kask *et al.* 1999): The assembly and analysis of the histogram of the number of counts in the image pixels establishes relative values of cluster brightness and density (compare Digman *et al.* 2008; Sergeev *et al.* 2006). Applied to the STED images of the three different syntaxin preparations (direct fixed, patched 1 and patched 2), the three different analysis approaches (SCA, ICS and FIDA) congruently confirmed larger cluster brightness and sizes and lower densities for the patched compared to the direct fixed preparations, as expected (Fig. 5*a*). The advantage of ICS and FIDA over SCA is that these two analysis methods may still be applied to images with higher cluster densities, where SCA starts to fail at clearly separating single isolated spots, similar to advantages of fluorescence correlation spectroscopy (FCS) and FIDA over single fluorescence burst analysis in the study of diffusing molecules (e.g. Eggeling *et al.* 2001b).

With the cluster analysis of the STED images tested, we now studied the formation of syntaxin clusters under different levels of syntaxin expression. Figure 5*b* depicts a representative STED image and its confocal counterpart of the syntaxin clusters of the membrane sheets of three PC12 cells, each expressing different levels of syntaxin. The preparation and labelling of these sheets was performed as for the direct fixed case. Again, clusters can be much better resolved with STED, and their sizes, brightness and densities accurately determined from subsets of the STED images with ICS and FIDA, even for the highly expressing cell. We used the average
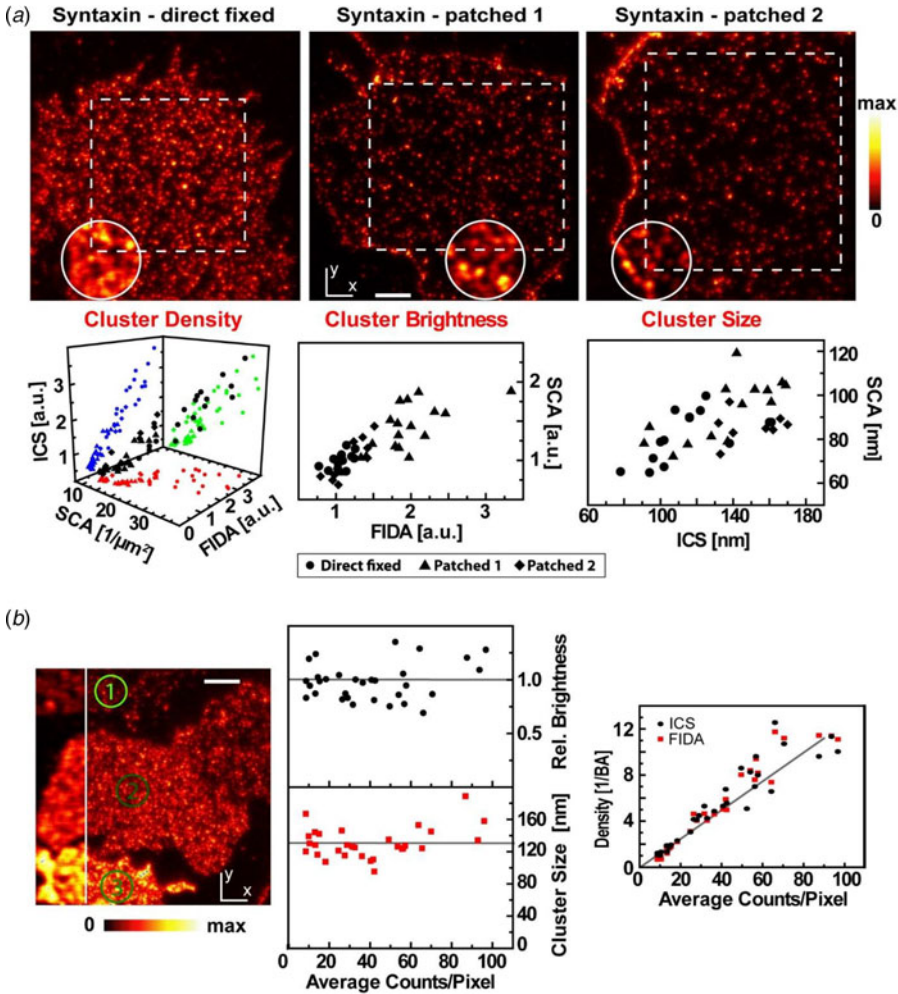
Fig. 5. STED nanoscopy: Cluster analysis. (*a*) ICS, FIDA and SCA analysis of syntaxin clusters recorded by STED. Upper panels: STED and confocal (circled areas) images of membrane sheets of PC12 cells immunolabeled for syntaxin for three different preparations (directly fixed (left) and patched 1 (middle) and 2 (right)). For the latter two, clustering is reinforced and cluster density decreased, dashed rectangles: analysed area, scale bar: 500 nm. Lower panels: values of cluster density (left), brightness (middle) and size (right) determined for different cells of the different preparations (dots: direct fixed, triangles: patched 1, diamonds: patched 2); left panel: 3D data (black) and projections to different value pairs (blue, green, red) of cluster density by ICS, FIDA and SCA, showing agreeing results by the different analysis techniques. (*b*) Syntaxin cluster morphology is independent of its expression level. Left panel: STED and confocal (left part) image of three representative membrane sheets generated from PC12 cells expressing different levels of immunolabeled myc syntaxin 1A (cell 1 with a low (probably endogenous) level of syntaxin, and cells 2 and 3 with different overexpression levels, adapted from (Sieber *et al.* 2006)). Plot of cluster brightness (upper middle), size (lower middle) and density (right) against the expression level (~average pixel brightness) determined by ICS (black) and FIDA (red) from the STED images of different cells, revealing no variation of brightness and size with expression level, and a linear increase of density with expression level.
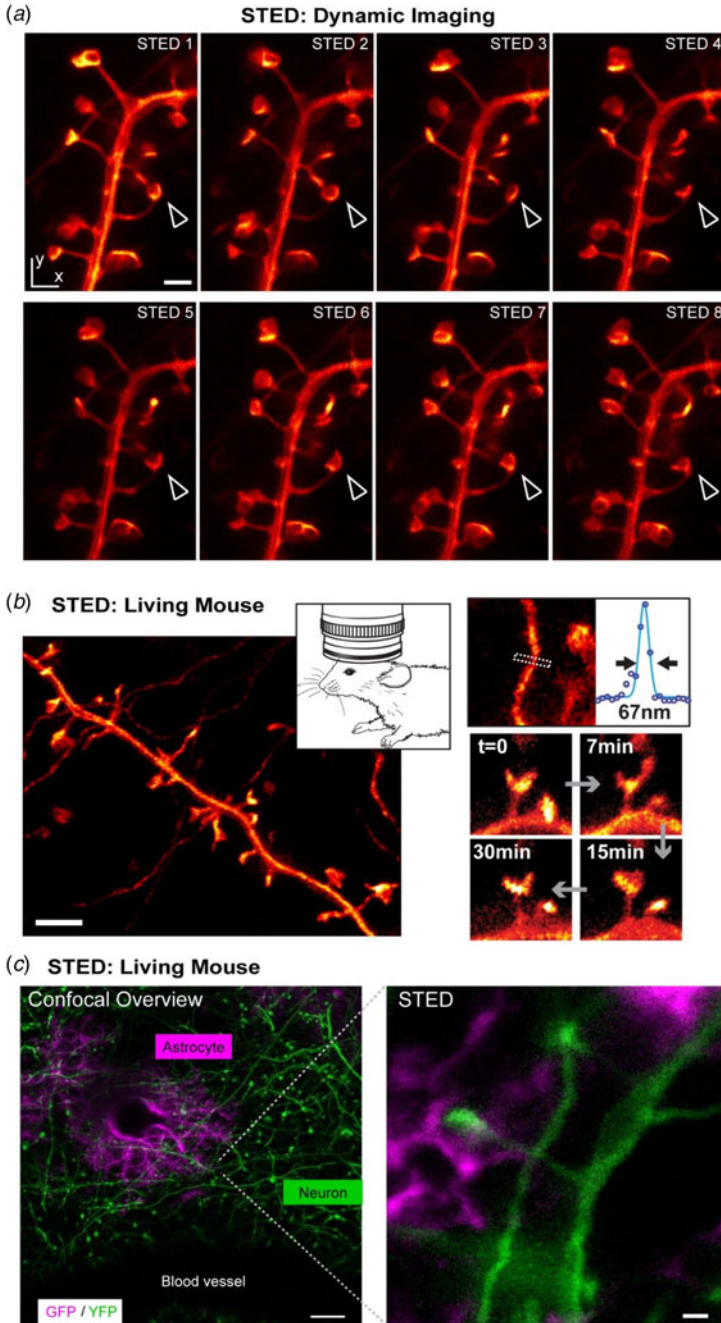
Fig. 6. Live-cell STED nanoscopy. (*a*) Time-lapse STED imaging of dendritic processes in a living hippocampal slice culture labeled with the fluorescent protein YFP (1 frame every 40 s, adapted from (Nägerl *et al.* 2008)). Arrows indicate a change in shape over time of a cup-like spine head. Scale bar: 1 μm. (*b*) *In-vivo* STED nanoscopy of a YFP-labeled neuron in the molecular layer of the somatosensory cortex of a mouse (left, inset depicts imaging setup). A maximum intensity projection of dendritic and axonal structures proves a spatial resolution of <70 nm (upper right). Temporal dynamics of spine morphology (lower right). Scale bar: 1 μm. Adapted from (Berning *et al.* 2012). (*c*) Two-color *in-vivo* STED imaging of astrocytes and neurons offers the possibility to study the influence of the astrocyte on

number of counts per pixel as a relative measure of the expression level in each image subset. As a result we could recognize that the expression level only determined the density but not the size and brightness (i.e. number of molecules) of the clusters. This is an important insight into the characteristics of the protein clusters (Sieber *et al.* 2006, 2007): increasing the concentration of the protein more than ten-fold seems to increase only the number of clusters formed, but not their composition.

2.1.5 Live-cell and *in-vivo* STED nanoscopy

Due to the aforementioned potential phototoxic effects of the image recording schemes, STED imaging was for long believed to be non-compatible with the study of living cells. However, first images of YFP-labeled endoplasmatic reticulum (ER) and microtubular networks in PtK2 cells proved the opposite (Hein *et al.* 2008). Especially the use of fast scanning units nowadays allows a straightforward use of STED nanoscopy for the study of the living cell using genetically encoded markers such as fluorescent proteins (Bethge *et al.* 2013; Eggeling *et al.* 2009; Hein *et al.* 2008; Li *et al.* 2009b; Moneron & Hell, 2009; Morozova *et al.* 2010; Nägerl *et al.* 2008; Rankin *et al.* 2011; Tonnesen *et al.* 2011; Urban *et al.* 2011; Willig *et al.* 2006b), or tagging proteins such as SNAP-, HALO- or CLIP-tags for proteins (Eggeling *et al.* 2009; Hein *et al.* 2010; Lukinavicius *et al.* 2013; Pellett *et al.* 2011; Schröder *et al.* 2008) or specifically for actin or microtubule-networks (Lukinavicius *et al.* 2014), or fluorogen-activating tags (Fitzpatrick *et al.* 2009) that covalently bind functionalized and membrane-permeable organic dyes. Ranging from the study of the nanoscale dynamics of different cellular molecules, molecular assemblies and structures such as the cytoskeleton, ER, mitochondria, peroxisomes, caveolae, membrane lipids and proteins or vesicles (e.g. Eggeling *et al.* 2009; Hein *et al.* 2008, 2010; Moneron & Hell, 2009; Morozova *et al.* 2010; Muller *et al.* 2012; Pellett *et al.* 2011; Rankin *et al.* 2011; Tonnesen *et al.* 2011; Westphal *et al.* 2008; Willig *et al.* 2011), live-cell STED nanoscopy experiments have also been realized with multi-color detection (Bethge *et al.* 2013; Pellett *et al.* 2011; Tonnesen *et al.* 2011; Willig *et al.* 2011), and video-rate STED imaging has been pushed to a time resolution of up to 80–200 frames per second. The STED method is therefore the fastest reported super-resolution imaging mode to date (Lauterbach *et al.* 2010a, b; Westphal *et al.* 2007, 2008).

In an application to neurobiology it was shown that it is possible to image dendritic spines of YFP-positive or organic-dye-filled hippocampal neurons in organotypic slices (Fig. 6*a*) (Ding *et al.* 2009; Nägerl *et al.* 2008; Urban *et al.* 2011). Spines are the dendritic processes that form the postsynaptic part of most excitatory synapses in the mammalian brain. In neurobiology, confocal and two-photon microscopy are widely used to study activity-dependent changes in synaptic morphology by recording time lapse images. However, the diffraction-limited resolution of light microscopy is often inadequate, forcing researchers to complement the live-cell imaging strategy by electron microscopy. Time-lapse STED nanoscopy outperforms confocal microscopy in revealing important structural details and can be used for quantification of morphological parameters, such as the neck width and curvature of the heads of spines, which play critical roles for the function and plasticity of synaptic connections (Urban *et al.* 2011), and can be correlated to

synaptic transmission *in vivo*. Confocal overview (left, $100 \times 100\ \mu m$, scale bar: $10\ \mu m$) and STED close-up image (right, scale bar: 500 nm) of the somatosensory cortex in a double transgenic mouse expressing cytosolic EYFP in neurons (TgN(Thy1-EYFP)) and cytosolic GFP in astrocytes (TgN(GFAP-EGFP) GFEC).

synaptic signaling (Tonnesen *et al.* 2014). Here, the use of aberration-reducing optics has realized STED imaging deep inside scattering biological tissue with penetration depth of up to 120 μm (Urban *et al.* 2011).

With STED nanoscopy available to study the living cell it will be exciting to see where it can unravel fundamental details. The imaging of spines is a good example because synaptic function is related to its shape. Super-resolution is necessary because the size of the spine neck is below the diffraction barrier. However, the main function of neurons is information processing by forming connections with their neighbours. This can only be studied where they are embedded in their natural environment and, if possible, in the living animal. Therefore, STED imaging was adapted to resolve neurons and their subtle dynamics in the cerebral cortex of a living mouse with so far unachieved spatial resolution. An upright STED nanoscope was constructed and adapted to the spectroscopic properties of YFP. The somatosensory cortex of the anaesthetised mouse was exposed through a glass-sealed hole in the skull (Berning *et al.* 2012). Figure 6*b* shows an image of the setup as well as of dendritic processes within the molecular layer of a TgN (Thy1-YFP) mouse taken by STED. The line profile shows that the smallest structures are <70 nm in diameter, indicating that the resolution is at least of that order. Recording images over 30 min in the living organism revealed that the dendritic spine can undergo morphologic changes and movements on the time scale of minutes. Furthermore, multi-colour STED recordings of the somatosensory cortex in double transgenic mice have the potential to study the influence of astrocytes on synaptic transmission *in vivo* (Fig. 6*c*). This shows that STED nanoscopy can be a tool to study brain function or the origin of brain diseases which are related to a structural change.

2.1.6 Lasers for STED

The development of the STED method has significantly benefited from improvements in laser technologies. STED nanoscopy was first realized with pulsed and high-repetition (∼80 MHz) Ti: Sa laser systems for stimulated emission and laser diodes for excitation (Klar *et al.* 2000). This configuration requires the exact timing of both lasers. This is usually accomplished by triggering the laser diodes using custom-built delay electronics, and stretching of the Ti:Sa pulses to 50–300 ps by, for example, glass rods and fibers. The triggering and pulse stretching optimize the timing and efficiency of the stimulated emission relative to the excitation laser pulses, and minimize bias due to polarization effects, jitters in the timing of the excitation and the STED pulses, multi-photon excitation processes, non-linear photobleaching via higher excited electronic states and direct excitation by the STED light (e.g. Dyba & Hell, 2003). While the Ti:Sa laser with wavelengths typically around 700–800 nm may directly be used for STED imaging of dyes emitting in the red spectrum (>600 nm), fluorescent labels such as GFP, YFP, Alexa 488, TMR and similar emit at around 500–590 nm and require STED wavelengths in the range of 590–650 nm. Pulsed laser light in this wavelength range and with average powers of 100–150 mW is delivered by an optical parametric oscillator (OPO) pumped by a Ti:Sa laser (Willig *et al.* 2006b, c). Such Ti: Sa arrangements are usually rather complex and costly. Nevertheless, the use of Ti:Sa lasers is still one of the preferred options for STED nanoscopy (e.g. Auksorius *et al.* 2008; Berning *et al.* 2012; Eggeling *et al.* 2009; Gould *et al.* 2011; Lau *et al.* 2012; Leutenegger *et al.* 2012; Nägerl *et al.* 2008; Pellett *et al.* 2011; Sieber *et al.* 2006, 2007; Westphal *et al.* 2008; Willig *et al.* 2006b, 2006c). Ti: Sa-based laser systems were employed in the first demonstration of two-color STED imaging (Donnert *et al.* 2007b; Meyer *et al.* 2008), have been integrated in a commercial system (Clausen *et al.* 2013; Fitzpatrick *et al.* 2009; Morozova *et al.* 2010; Schröder *et al.* 2008) and

have facilitated the D- or T-Rex modality (using a regenerative amplified (Rega) mode-locked Ti: sapphire oscillator) (Donnert *et al.* 2006).

Several options have been presented to reduce complexity and cost of the laser setup. Giving up the wavelength tunability, the use of single-wavelength pico- or nanosecond laser modules allows reducing costs (Westphal *et al.* 2003), and their high pulse peak powers have facilitated imaging with spatial resolutions of <10–20 nm (Göttfert *et al.* 2013; Rittweger *et al.* 2009a). The lowest-cost STED nanoscope to date has been realized by pulsing a 660 nm DVD-diode, i.e. a compact off-the-shelf laser diode (Schrof *et al.* 2011). Strong and compact single-wavelength lasers are therefore increasingly applied for STED, especially in new commercial STED nanoscopes. Multiple laser lines for STED and excitation can simultaneously be chosen from a pulsed white light or super-continuum laser, which offers highest flexibility for wavelength optimization, and disburdens from the necessity of synchronizing several lasers (Auksorius *et al.* 2008; Blom *et al.* 2011; Wildanger *et al.* 2008, 2009b). The advent of white light lasers alleviated the setup of multi-color STED instruments (Blom *et al.* 2012; Bückers *et al.* 2011; Neumann *et al.* 2010). In another development, a ~530 nm pico- or nanosecond microchip or fiber-amplified, frequency doubled laser was coupled into a standard single-mode fiber to produce a tunable spectrum of discrete peaks between 530 and 620 nm via stimulated Raman scattering (SRS) (Rankin & Hell, 2009; Rankin *et al.* 2008). This again allowed a flexible choice of STED laser wavelengths, demonstrating STED imaging with spatial resolution down to 20–30 nm (Rankin & Hell, 2009; Rankin *et al.* 2008, 2011).

Further simplification of the setup was achieved by realizing STED nanoscopy with continuous-wave (CW) lasers, since no laser-pulse preparation is required (Willig *et al.* 2007). CW-STED imaging was first realized with strong Argon–Krypton lasers (Willig *et al.* 2007) or Ti:Sa lasers running in CW mode (Ding *et al.* 2009; Harke, 2008), but since then it has been shown that it is possible to utilize compact fibre lasers (Bianchini & Diaspro, 2012; Moneron & Hell, 2009; Moneron *et al.* 2010), diode-pumped solid-state (DPSS) lasers (Honigmann *et al.* 2012; Mueller *et al.* 2012) or amplified diode lasers (Honigmann *et al.* 2013a) at wavelengths between 560 and 765 nm, also on commercial systems (Clausen *et al.* 2013; Friedemann *et al.* 2011). However, CW-STED comes with two drawbacks compared to the pulsed STED modality. Firstly, much higher average laser powers have to be applied (Harke, 2008; Willig *et al.* 2007). This follows from the fact that tightly synchronized trains of excitation and STED pulses, as realized in the pulsed modality, yield an optimized efficiency of stimulated emission: the pulses of the STED beam reach the focal plane virtually simultaneously with or a few picoseconds after the excitation pulses so as to instantly inhibit fluorescence emission from excited molecules. In contrast, in the CW-STED beam implementation the STED intensity and thereby the probability of stimulated de-excitation is lower. As a consequence, to achieve the same fluorescence inhibition efficiency by stimulated emission, $(\ln(2)\,f\tau)^{-1}$-fold larger time-averaged powers of the CW than of a pulsed STED laser have to be supplied (with fluorescence lifetime τ of the label and repetition rate f of the pulsed STED modality) (Harke, 2008; Willig *et al.* 2007). For usual parameters $f = 80$ MHz and $\tau = 3.5$ ns this amounts to about five-fold larger time-averaged CW powers, for example 800 mW in the CW compared to 160 mW in the pulsed case. Secondly, a further consequence of the CW STED modality is that a non-negligible fraction of the molecules emit fluorescence before having been exposed to much of the STED light, and thus residual fluorescence outside the zero-intensity point of the STED light leads to a pedestal in the effective observation spot, resulting in somewhat lower-contrast images (Leutenegger *et al.* 2010).

Besides the aforementioned simplifications of the laser arrangements (Kastrup *et al.* 2010), compact and more robust STED setups have been created by using optimized phase plates

for realizing the focal intensity distribution of the STED laser (Reuss *et al.* 2010; Wildanger *et al.* 2009a). Based on diffractive optical elements, a single-beam-path STED nanoscope has been constructed, which includes a phase plate that selectively modulates the STED beam but leaves the excitation beam unchanged. In this configuration the beams are aligned by design and the alignment is hence insensitive to mechanical drift (easySTED) (Wildanger *et al.* 2009a). Similarly, a birefringent device has been instituted which produces the doughnut-shaped focal spot with suitable polarization for the STED laser while leaving the excitation spot virtually intact, and which in addition can be adapted to reveal, through the resulting fluorescence image, the orientation of fluorophores in the sample, thus directly providing sub-diffraction resolution images of molecular orientation (Reuss *et al.* 2010). Using Wollaston prisms, a common beam-shaping device realized a parallelized STED nanoscope featuring four pairs of scanning excitation and STED beams. This arrangement provides four-fold increased imaging speed of a given sample area, while maintaining the advantages of a single-beam easy STED instrument (Bingen *et al.* 2011). Further increases in image acquisition speed are achieved by the use of even more parallelized scanning excitation and STED beams, as recently introduced by camera-based detection and wide-field excitation together with well-designed optical patterns for STED (Yang *et al.* 2014; Bergermann *et al.* 2015). Spatial light modulators have been applied to auto-align a STED nanoscope (Gould *et al.* 2013).

Overall, it is to be expected that further developments in laser and optical technology will create more and more compact and less costly systems, and thus will further facilitate the use of STED imaging in day-to-day biophysical and medical research.

2.1.7 Gated CW-STED nanoscopy

The problem of the pedestal inherent to the CW-STED modality can be solved by implementing a pulsed-laser excitation in combination with the CW-STED laser and a time-gated detection scheme (Moffitt *et al.* 2011; Vicidomini *et al.* 2011). Time-gated detection is often used in fluorescence microscopy for suppressing background (e.g. Eggeling *et al.* 2001a; Shera *et al.* 1990), and, in a pulsed STED scheme, it is well known that photons should be detected after the STED pulse has left (Schrader *et al.* 1995; Westphal & Hell, 2005), as shown in a recent experiment using time-correlated single photon counting (Auksorius *et al.* 2008). This is due to the fact that scattered laser light or residual fluorescence signal only occurs during the laser pulses. Time-gated detection also improves the contrast of CW-STED images by selectively suppressing image contents (or spatial frequencies) of low spatial resolution, i.e. the aforementioned pedestal or blurring (Fig. 7) (Moffitt *et al.* 2011; Vicidomini *et al.* 2011, 2013). This follows from the fact that fluorescence inhibition is lowest during the duration of the excitation pulse (usually <150 ps), while right afterwards only the CW-STED beam is acting and inhibiting fluorescence emission: the longer it lasts, the more likely it becomes that a fluorophore is switched off, i.e. the spatial resolution not only depends on the intensity of the STED light but also on the time span of the STED beam action (Hell *et al.* 2003; Vicidomini *et al.* 2013). This can also be rationalized in the sense that STED reduces the fluorescence lifetime τ of the excited fluorescent state. Ensuring that photons are collected only for delays significantly after the excitation pulse largely suppresses signal from strongly inhibited molecules: fluorescence light is recorded mainly from fluorophores from the zero-intensity doughnut center, where the STED beam is inherently weak (and thus the fluorescence lifetime rather long). Along with the improved image contrast, the selection of high spatial frequencies by the gated detection scheme also allows to apply lower
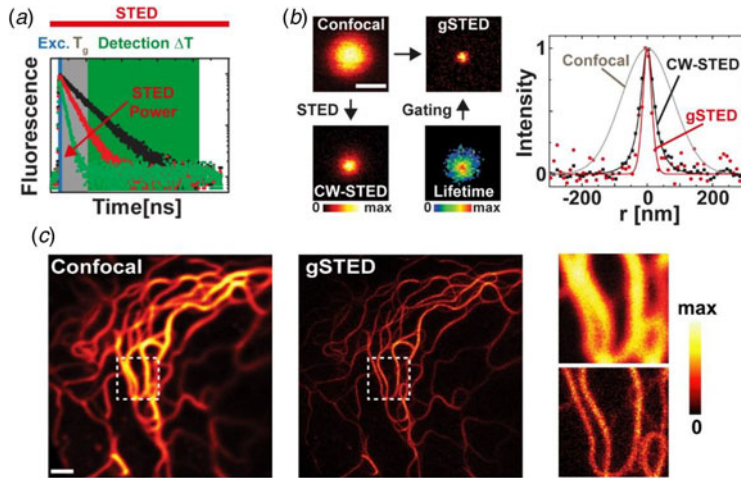
Fig. 7. gSTED nanoscopy. (*a*) Principle: the fluorescence lifetime of a fluorophore decreases with increasing STED power as depicted for representative fluorescence lifetime decays for different STED powers (left): using pulsed excitation (blue, Exc) and CW-STED (red) in conjunction with gated detection (detection within the time period ΔT (green) with a time lag T_g (grey) relative to the exciting pulse) favors signal from points of low STED power, i.e. from areas at or close to the intensity zero. (*b*) Scanning fluorescence intensity (left and upper right) and lifetime (lower right) images of a single fluorophore for confocal diffraction-limited (upper left), CW-STED (intensity: lower left, lifetime: lower right) and gSTED (upper right) recordings (scale bar: 200 nm), and (right panel) intensity line profiles through the middle images, indicating the removal of the pedestal of the CW-STED recordings (black) by the gated detection (gSTED, red). (*c*) Confocal and gSTED images (right: magnification of central area marked by the dashed white box) of keratin fused to the fluorescent protein citrine in a living PtK2 cell with low CW STED laser power. Scale bar: 1 μm. Adapted from (Vicidomini *et al.* 2011).

CW-STED powers compared to the non-gated CW-STED scheme to be able to similarly discern alike features (Vicidomini *et al.* 2011). This, and the fact that CW in comparison to pulsed beams may be less prone to induce phototoxic multiphoton processes, reduces light-induced stress on the sample. It is worth noting that these improvements always come with a reduction in signal, since the gating suppresses valuable signal as well (Vicidomini *et al.* 2013). Gated-STED (gSTED) nanoscopy has been realized for different fluorophores and in living cells, and has now been incorporated into a commercial system, allowing the recording of live-cell images with sub-diffraction spatial resolution at moderate CW STED powers <80 mW (Clausen *et al.* 2013; Vicidomini *et al.* 2011). Data acquisition for gSTED has been demonstrated by offline processing of time-correlated single-photon counting data, or in real-time using a fast electronic gate. As for CW-STED, gSTED nanoscopy can be realized with compact CW lasers, which are nowadays available at various wavelengths (Honigmann *et al.* 2012, 2013a; Mueller, 2012) and show improved performance with reduced noise levels (Hernandez *et al.* 2014a). Of all current STED modalities, gSTED provides the sharpest STED images at the lowest peak laser powers.

Besides the aforementioned improvement in image contrast, gated detection also allows to specifically suppress background signal. On one hand, discarding signal during the excitation pulse (as done for gSTED) reduces scattering signal from the excitation laser (e.g. Eggeling *et al.* 2001a; Shera *et al.* 1990). On the other hand, the rejection of signal for time delays after the excitation pulse much longer than the fluorescence lifetime τ of the fluorophore specifically suppresses continuous background signal such as fluorescence light excited by the CW-STED laser or detector

noise. This allows using wavelengths of the STED laser closer to the fluorescence emission maximum, which reduces the required laser powers (Vicidomini *et al.* 2012; Hernandez *et al.* 2014b). Consequently, gated detection introduces high flexibility, especially if the acquired data is post-processed by software. This will not only allow an optimization of the image contrast, but also the investigation of the very same data for different image contrasts, i.e. for different gating positions (Vicidomini *et al.* 2011).

### 2.1.8 STED-FCS: nanoscale single-molecule dynamics

The ongoing quest to study molecular dynamics not in the ensemble but at the molecular level calls for measurements both of molecular numbers and, crucially, with access to molecular spatial scales. Compared to ensemble measurements, studies at the single-molecule level reach a much increased sensitivity as they may reveal heterogeneities hidden in the ensemble and disclose deviations from the ergodic theorem (i.e. a time-averaged ensemble measurement may not be the same as the ensemble average of a large number of single-molecule measurements). Fluorescence microscopy has reached single-molecule detection sensitivity (Moerner & Kador, 1989; Orrit & Bernard, 1990; Shera *et al.* 1990; Weiss, 1999; Zander *et al.* 2002), and studies of single-molecule dynamics have given many new, detailed insights into physical, chemical and biological problems (e.g. Lord *et al.* 2010; Moerner, 2007). In this context, statistical analysis tools such as Fluorescence Correlation Spectroscopy (FCS) (Ehrenberg & Rigler, 1974; Haustein & Schwille, 2003; Magde *et al.* 1972) or photon-counting histogram analysis (PCH) (Chen *et al.* 1999) and Fluorescence Intensity Distribution Analysis (FIDA) (Kask *et al.* 1999) have been extremely helpful. However, further insights into a lot of (single-molecule) dynamical processes have been again impeded by the limited spatial resolution of common diffraction-limited fluorescence microscopy. 1) The concentration of fluorescently labeled molecules has to be very low (<nM) to reach the single-molecule level with conventional confocal observation volumes – a concentration which is often far below that of endogenous (biological) conditions. In contrast to performing measurements in zero-mode waveguides (Leutenegger *et al.* 2006; Levene *et al.* 2003; Wenger *et al.* 2007), or to photobleach (Moertelmaier *et al.* 2005) or switch off (Eggeling *et al.* 2007) large parts of the ensemble, the most obvious way to handle larger, endogenous concentrations would be to lower the observation spot's length scale (its size) (Blom *et al.* 2006; Kastrup *et al.* 2005; Weiss, 2000). 2) The conventional confocal observation spot usually averages over details of nanoscale molecular dynamics. For example, strongly localized trapping cannot directly be distinguished from slow but regular molecular diffusion (Eggeling *et al.* 2009). In the case of confocal FCS observations of molecular membrane dynamics, such discrimination has indirectly been realized, for example, by searching for anomalies in diffusion (Schwille *et al.* 1999), by extrapolating to the nanoscopic case (Wawrezinieck *et al.* 2005), or by probing in the near-field on nanostructures or -holes (Leutenegger *et al.* 2006; Manzo *et al.* 2011; Wenger *et al.* 2007). However, very direct measurements at the length scale of interest (i.e. observing diffusion dynamics through sub-diffraction-sized far-field observation spots) deliver much more reliable and model-independent results about nanoscopic details of molecular diffusion and interactions and, at the same time, allow indirect methods to access even smaller length scales.

In an attempt to access smaller length scales, non-invasive far-field microscopy was thus combined with single-particle tracking (SPT), utilizing the high spatial localization precision of down to the 1-nanometer level for bright marker particles (Geerts *et al.* 1987; Kusumi *et al.* 2005; Schutz *et al.* 1997; Sheetz *et al.* 1989; Yildiz *et al.* 2003). Yet this introduces other restrictions: to reach the

desired spatial localization precision, SPT often applies bright but rather large signal markers, which potentially influence the system under study (Clausen & Lagerholm, 2011). When using conventional fluorophore labeling the temporal resolution is lower. And while important insights can be gained in carefully optimized SPT experiments, for example if the full spatiotemporal resolution afforded by the fluorophore photon budget is harnessed in fast molecular tracking schemes (Sahl *et al.* 2010, 2014), the amount of data to be gathered for an accurate statement on an average molecular behavior is higher for SPT compared to FCS. In addition to the concentration issue, the stochastic sampling concomitant with SPT yields low statistics and random coverage from a single measurement only.

A remedy for these limitations is the combination of FCS with the STED principle (Eggeling *et al.* 2009; Kastrup *et al.* 2005; Ringemann *et al.* 2009). STED-FCS delivers high temporal and spatial resolution together with a high degree of statistical averaging. The most straightforward parameters measured with FCS are the average transit time τ_D of the fluorescent molecules through the observation area/volume and the average number N of fluorescing molecules in the observation volume. One expects both τ_D and N to decrease with the confinement of the observation spot, i.e. with the STED power. Figure 8*a* shows exemplarily FCS data for fluorophores in solution exhibiting 3D free diffusion. While the expected decrease of τ_D is observed, N does not decrease as strongly, and even increases for high STED powers due to a reduced signal-to-background ratio (SBR) (Ringemann *et al.* 2009). The low SBR is caused by non-inhibited, low-brightness fluorescence signals from out-of-plane volume shells. Contributions of the latter to the overall signal grow relative to the declining fluorescence signal from the more and more confined observation spot (Fig. 8*a*) (Ringemann *et al.* 2009). This degradation in SBR has on the one hand been observed for confinement along x/y only, but also for confinement along z or along all three spatial directions (Kastrup *et al.* 2005; Ringemann *et al.* 2009), even when using two-photon excitation (Moneron & Hell, 2009) or two opposing objectives in an iso-STED arrangement (Schmidt *et al.* 2008). The biased values of N can straightforwardly be corrected for by, for example, a combined or global FCS-FIDA analysis (Fig. 8*a*, right) (Ringemann *et al.* 2009). Therefore, while such reduction effects on the SBR might limit the sensitivity of STED-FCS experiments for 3D diffusion, it does not necessarily preclude such measurements, such as assessments of nanoscale molecular diffusion dynamics inside living cells.

The above out-of-plane background vanishes for 2D diffusion measurements such as within membranes, where no out-of-plane signal is present (Fig. 8*b*). Here, both τ_D and N decrease with increasing STED power, i.e. with the confinement of the observation area, as expected (Fig. 8*c*) (Ringemann *et al.* 2009). Recently, STED-FCS has also been combined with evanescent (TIRF) illumination to reject out-of-plane background (Leutenegger *et al.* 2012). However, the maximum achievable resolution of the TIRF-STED-FCS setup was only 50–60 nm due to side lobes inherent to the confocal TIRF illumination scheme. An important observation is that the STED mode reduces the transit times but hardly the detected fluorescence brightness (if the intensity zero of the STED focus is properly aligned, i.e. it really is close to zero). In Fig. 8*d*, the detected photon count-rate of a typical molecular trace of fluorescent lipids in multi-lamellar membrane layers peaks at 300–400 kHz which enables the analysis of single-molecule STED data at a good signal-to-noise ratio. Most importantly, signatures of single-molecule transits are only observable for small, sub-diffraction sized spots as created by STED, while the concentration is too high for conventional confocal recordings (Fig. 8d). Therefore, STED allows accurate single-molecule measurements on the cellular plasma membrane of living cells, and thus is a powerful tool for shedding new light on long-standing biological questions.
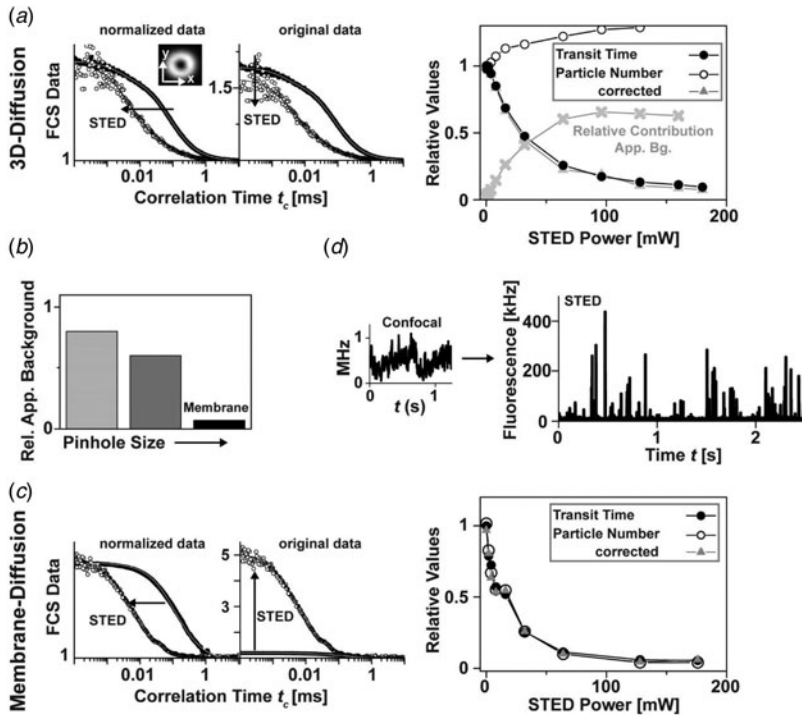
Fig. 8. STED-FCS. (*a*) STED-FCS analysis of free 3D-diffusion of the organic dye Atto647N in aqueous solution. Representative correlation data (left panels, left: normalized amplitudes, right: original data) for confocal (black) and STED recordings (open dots) and (right panel) relative values of transit time τ_D (black), particle number N (original open dots, background-corrected grey triangles), and signal fraction of apparent background (grey crosses) determined from FCS and FIDA data recorded for increasing power of the doughnut-shaped (inset left) STED laser. The size reduction of the observation spot by increasing the STED power shortens the dye's transit time, but also introduces an increasing contribution of apparent un-depleted low-brightness background, which introduces noise and dampens the FCS data's amplitude and thus results in an apparent increase of N, which can be corrected for by a global FCS-FIDA analysis. (*b*) Relative apparent background for the STED-FCS recordings for two different pinhole sizes (decrease from left to right), and for a fluorescent lipid analog diffusing in a multi-lamellar membrane. Reduction of the pinhole size reduces un-depleted out-of-plane low-brightness fluorescence signal (apparent background), which diminishes further when measuring two-dimensional diffusion in membranes, where out-of-plane signal is absent. (*c*) STED-FCS analysis of free 2D-diffusion of a fluorescent lipid analog in a multi-lamellar membrane. Representative correlation data (left panels, left: normalized amplitudes, right: original data) for confocal (black) and STED recordings (open dots) and (right panel) relative values of transit time τ_D (black) and particle number N (original open dots, background-corrected grey triangles) determined from FCS and FIDA data recorded for increasing power of the doughnut-shaped STED laser. The confinement of the observation spot by increasing the STED power reduces both τ_D and N, without an influence by out-of-plane signal contributions. (*d*) STED allows single-molecule observations at high concentrations. Fluorescence signal over time for the same concentration of a fluorescent lipid analog diffusing in a multi-lamellar membrane indicates diffusion of single molecules only for the STED (right) but not for the confocal (left) recordings. Adapted from (Ringemann *et al.* 2009).

2.1.9 STED-FCS: live-cell membrane dynamics

Many membrane-associated processes such as signaling events are considered to be closely re-lated to cholesterol-mediated interactions of some lipids such as sphingolipids (Brown &

London, 2000; Fielding, 2006; Hanzal-Bayer & Hancock, 2007; Jacobson *et al.* 2007; Simons & Ikonen, 1997). In contrast to phosphoglycerolipids, these lipids are assumed to form molecular complexes or integrate, assisted by cholesterol, into <200 nm sized lipid nanodomains, usually denoted 'rafts' (Simons & Ikonen, 1997). These interactions may disturb the diffusion of lipids and proteins in the plasma membrane, and on the other hand may compartmentalize cellular signaling (Pike, 2006). Although several experiments indicate their existence, such complexes and/or lipid 'rafts' remained controversial due to the lack of suitable techniques for detecting these small-sized objects in living cells (Hancock, 2006; Jacobson *et al.* 2007; Lommerse *et al.* 2004; Munro, 2003; Shaw, 2006). A common problem is once again that the <200 nm sized domains cannot be resolved by conventional confocal microscopes, and thus common fluorescence recovery after photobleaching (Feder *et al.* 1996; Yechiel & Edidin, 1987) or confocal FCS measurements (Fahey *et al.* 1977; Schwille *et al.* 1999; Wawrezinieck *et al.* 2005) average over nanoscale details of molecular diffusion. STED nanoscopy opens up a new avenue to elucidate lipid diffusion.

Figure 9 shows FCS analysis of lipid diffusion in the plasma membrane of living mammalian cells recorded with a STED nanoscope. The unique feature of the STED method to continuously downscale the size of the observation area with laser intensity and/or gated detection allows the determination of the average transit time τ_D for different diameters d of the observation, revealing different modes of diffusion (Fig. 9*d*) (Eggeling *et al.* 2009; He & Marguet, 2011; Ruprecht *et al.* 2011; Wawrezinieck *et al.* 2005). Unlike the confocal recordings, the STED-FCS data reveal distinct differences between fluorescent phosphoglycerolipid (PE) and sphingolipid (SM) analogs. Most importantly, it is revealed that while the PE lipids diffuse freely, the SM lipids diffuse heterogeneously on small spatial scales, being transiently (~10–20 ms) trapped in cholesterol-mediated molecular complexes with relatively slow-moving or immobilized binding partners. Such previously inaccessible molecular details depict how the non-invasive optical recording of molecular time traces and fluctuation data in tunable nanoscale domains is a powerful new approach to study the dynamics of biomolecules in living cells. Recent work could not detect any correlation between the nanoscale trapping as observed by STED-FCS in living cells and partitioning characteristics of the labeled lipids into liquid ordered domains of phase separated model membranes (which is often assumed as a physical model of lipid 'rafts') (Fig. 9*f*) (Eggeling, 2012; Mueller *et al.* 2011, 2013; Sezgin *et al.* 2012; Honigmann *et al.* 2014). Rather, the trapping characteristics and the dependence on cholesterol are highly dependent on the molecular structure of the lipid (however not on the dye label or the labeling position), identifying the ceramide or sphingosine group close to the water–lipid interface as well as the lipid's headgroup as the driving forces for molecular interactions (Fig. 9*g*) (Mueller *et al.* 2011). Therefore, we may recall our previous statement (Eggeling, 2012; Mueller *et al.* 2011, 2013), 'that the observed transient trapping with its rather strong binding to other membrane constituents follows a different molecular mechanism than that of the weak interactions responsible for the formation of ordered phases in model membranes. [...] If one pictures the STED-FCS observations in the context of lipid 'rafts', one may support a current view that (sphingo)lipid rafts may establish fluctuating nanoscale assemblies of sphingolipid, cholesterol and proteins that can be stabilized to coalesce, forming platforms that function in membrane signaling and trafficking (Lingwood & Simons, 2010). Here, the STED-FCS experiments may highlight the fluctuating nanoscale assemblies, which then seem to be highly diverse and strongly depending on the lipid structure. It remains to be shown whether these fluctuating nanoscale assemblies may be stabilized to coalesce to maybe more tightly packed domains (Joly, 2004; Lingwood & Simons, 2010). A fluorescent lipid analog that partitions
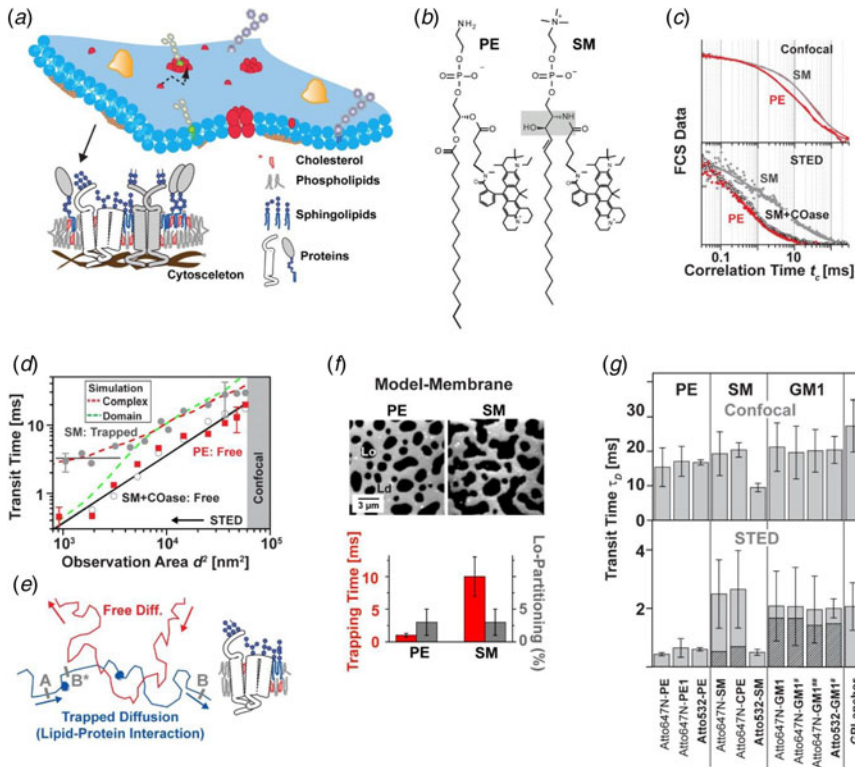
Fig. 9. STED-FCS analysis of lipid plasma membrane diffusion. (*a*) Lipids and proteins are heterogeneously distributed in the cellular plasma membrane, stemming from often cholesterol-assisted lipid–protein interactions (which may be the basis for the coalescence of transient signaling platforms, denoted membrane domains or lipid 'rafts', i.e. spatially confined molecular assemblies of different lipids and proteins which are essential for a cellular signaling event), an asymmetric molecular distribution to the inner and outer leaflet of the bilayer, the underlying cytoskeleton (which is membrane-anchored via proteins), and from membrane curvature and pits. Adapted from (Lingwood & Simons, 2010). (*b*) Structures of the fluorescent lipid analogs phosphoethanolamine (PE) and sphingomyelin (SM), both tagged with the organic dye Atto647N. Grey shaded area: ceramide or sphingosine group of the SM lipid. (*c*) Representative confocal and STED (observation diameter $d = 40$ nm) FCS data of PE (red), SM (black) and SM after cholesterol depletion by Cholesterol Oxidase (grey, SM+COase). The SM STED-FCS data can only be described by anomalous diffusion, revealing cholesterol-assisted hindered diffusion of the SM lipid analog. (*d*) The dependence of the transit time τ_D for different sub-diffraction sized observation areas $\sim d^2$ (as tuned by the STED laser power) shows an almost free diffusion (linear dependence, dark grey line diffusion coefficient 0.5 $\mu m^2/s$) for PE (red squares) and SM after cholesterol depletion (open circles), and a hindered diffusion (non-linear dependence) for SM (grey circles). The minimal change of τ_D for very small observation areas (grey horizontal line) and Monte-Carlo simulations indicate that the hindrance in diffusion is caused by transient complexes with either relatively slow-moving or immobilized membrane molecules (red dotted line) and not by incorporation into $\geqslant 20$ nm large domains, where diffusion is slowed down (green dotted line). The direct observation of these transient interactions is impossible with the large diffraction-limited confocal observation area (grey shaded area). (*e*) Schematic drawing of normal free (red) and hindered SM diffusion (blue, dots: points of interactions or complexes). (*f*) Comparison of live-cell and model membrane data. Phase separation into liquid-disordered (Ld) and liquid-ordered (Lo) domains of a model membrane bilayer composed of a ternary mixture: both the fluorescent PE and SM lipid analogs hardly enter the Lo phase (upper panel: confocal scanning fluorescence image, black: low signal, white: high signal, adapted from (Mueller *et al*. 2011)). Partitioning in model membranes and trapping characteristics observed by STED-FCS on live-cell plasma membranes are not correlated (lower panel): Trapping time (red, left axis, live-cell) and

into the liquid ordered phase of model membranes (like its natural counterpart) may be able to report on this coalescence.' Recently, such a lipid analog has successfully been tested in STED experiments (Honigmann *et al.* 2013b), and initial experiments in live-cell membranes indicated no difference to the liquid-disordered partitioning of fluorescent lipid analogs (Sezgin *et al.* 2012; Honigmann *et al.* 2014). Caution has to be taken when designating any lipid-based interaction or heterogeneous organization as a 'raft', since the basis of these may be highly diverse (Eggeling, 2012; Mueller *et al.* 2011, 2013; Sezgin *et al.* 2012).

2.2 Generalization: STED, GSD, SSIM/SPEM and RESOLFT

Stimulated emission is only one way to reversibly transfer molecules between states of different fluorescence properties. Similarly, other state transitions may be applied for sub-diffraction optical microscopy (nanoscopy). The key is to identify a pair of ON- and OFF-states between which at least one transition can be driven by light (Hell, 2004, 2009b; Hell *et al.* 2003). The different mechanisms used so far are summarized in Fig. 10*a*; they most significantly differ in the molecular states involved, the required laser intensities and the choice of label.

2.2.1 STED: stimulated emission

STED requires rather large laser intensities in order to induce de-excitation from S_1 more efficiently than the spontaneous decay (usually around 2–4 ns). Therefore, the threshold or saturation intensities required to inhibit half of the fluorescence are in the range of $I_S = 1$–10 MW/cm^2 (Fig. 10*a*). As mentioned in Section 2.1.6, a preferred implementation of STED is the use of pulsed lasers supplying high peak intensities. This STED modality provides an exponential, i.e. a very steep, dependence of the fluorescence inhibition on the STED laser, realizing a very sharp confinement of fluorescence emission (Harke *et al.* 2008a; Hell, 2009b). Inhibition of fluorescence by stimulated emission can be realized with basically any fluorophore. The spatial resolution of the STED concept is in principle limited only by the size of the quantum system to be imaged, i.e. by the molecule. (Section 2.3).

2.2.2 GSD: transient dark state shelving

GSD imaging was the second far-field nanoscopy concept concretely laid out (Hell & Kroug, 1995). In GSD, inhibition of fluorescence emission is realized by transiently shelving the fluorophore in a metastable dark state such as the triplet (Kasha, 1950) or other dark (redox) states populated therefrom (e.g. Vogelsang *et al.* 2008; Zondervan *et al.* 2003). Since the lifetime of the involved dark states is usually much longer (μs to s) than that of the S_1 (ns), GSD allows using

---

fraction of signal in Lo phase (grey, right axis, model membranes) of PE and SM (adapted from Sezgin *et al.* 2012). (*g*) STED-FCS analysis of the plasma membrane diffusion of different fluorescent lipid analogs, revealing lipid-specific interactions and independence on dye and label position. Average transit time τ_D for confocal ($d \approx 250$ nm, upper panel) and STED ($d \approx 40$ nm, lower panel) recordings of the Atto647N- or Atto532-labeled phosphoethanolamine (PE: head group and PE1: acyl-chain labeled), sphingomyelin (SM: acyl-chain and CPE: head-group labeled), ganglioside GM1 (GM1: acyl-chain, GM1[#]: head-group and GM1[##]: chain addition), and of an Atto647N-tagged transfected GPI-anchor. The meshed bars in the lower panel indicate the values of τ_D determined after cholesterol depletion by COase treatment. Error bars result from averaging over more than thirty measurements. No dependence of the STED-FCS data on the dye-label position has been observed, apart from using the dye Atto532 on the lipid's acyl chain, which accelerates diffusion and lowers trapping probability. Adapted from (Eggeling *et al.* 2009).
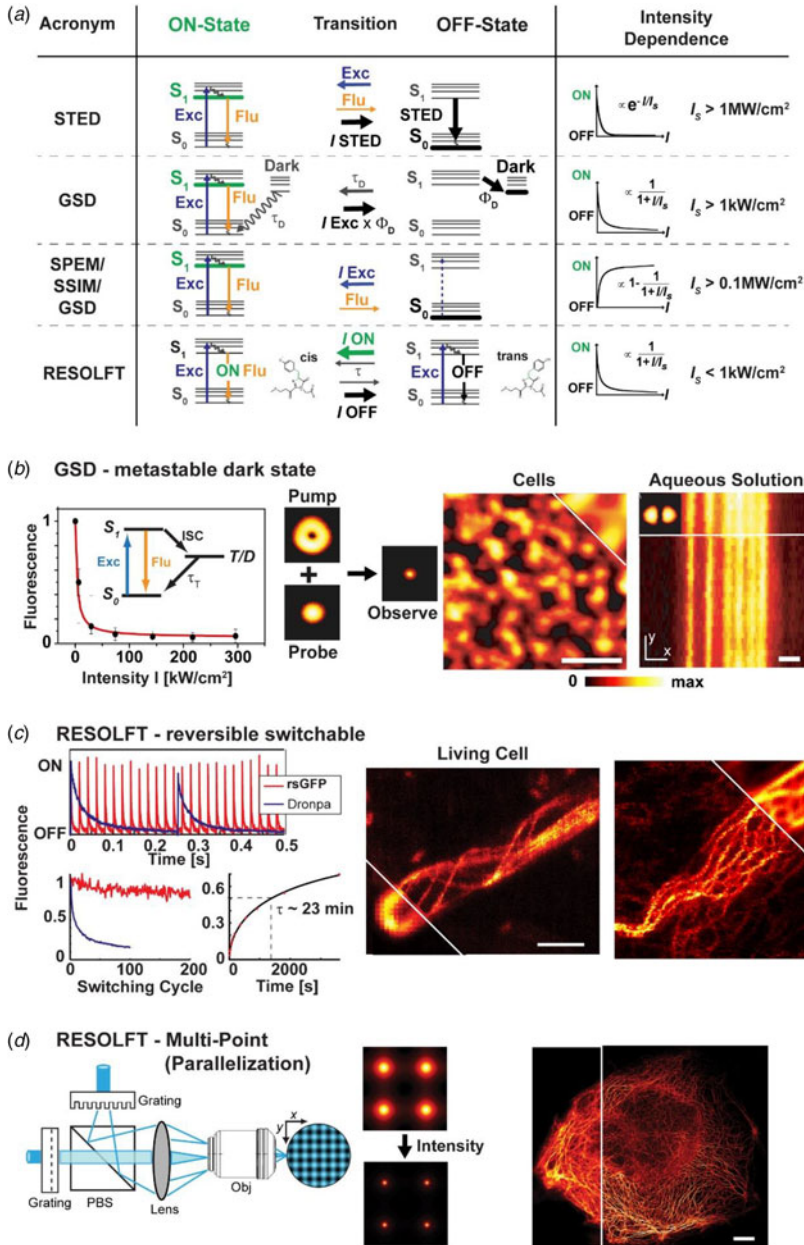
Fig. 10. Generalization of coordinate-targeted (deterministic) nanoscopy: the RESOLFT concept. (*a*) Different molecular states and transitions can be applied to reversibly inhibit fluorescence for coordinate-targeted nanoscopy ranging from STED (stimulated emission), over GSD (metastable dark states), SPEM/SSIM/GSD (ground state depletion by saturated excitation) to RESOLFT (e.g. photoswitchable fluorophores, different conformational states): acronyms (left), molecular states (middle) with energy level diagram of a fluorophore (ground S_0, excited S_1 and dark states) and transitions for ON (left middle) and OFF (right middle) direction (middle: ON-OFF transitions with excitation (Exc), fluorescence (Flu), stimulated emission (STED), metastable dark states (with crossing probability Φ_D and lifetime τ_D), bright (ON) and dark (OFF) conformational states (with on- and off-switching light and potential spontaneous transition lifetime τ) and intensity I of the corresponding lasers), intensity I dependence of switching with threshold intensities I_S (right), and approximate values of I_S. Adapted

much lower intensities than STED, in the range of 100–300 kW/cm^2 (Fig. 10*b*) (Bretschneider *et al.* 2007; Hell & Kroug, 1995). Since both dark state shelving and fluorescence excitation occur via S_1, i.e. most efficiently by the same laser line, a pump-probe scheme has been introduced in the experimental realization of GSD nanoscopy (Bretschneider *et al.* 2007). Here, the pump beam is arranged with one or several zero intensity points (such as the doughnut-shaped intensity distribution) and essentially prepares the observation area by restricting molecules that are left in the bright S_0–S_1 system to sub-diffraction sized volumes. A subsequent conventional, diffraction-limited fluorescence excitation beam probes these residual bright molecules. Super-resolution images are again realized by scanning the resulting nanoscopic observation spot over the sample, as depicted for immunolabeled SNAP-25 protein clusters on a cell membrane in Fig. 10*b*. The silenced fluorophores have to return to the S_0–S_1 system before each scanning step, which puts a lower limit on the image acquisition time (e.g. pixel dwell times of 60 ms in Fig. 10*b*). The implementation of the GSD concept is further challenged by the increased involvement of the dark states in photobleaching. Therefore, the experimental realization of GSD had to discover conditions for which (1) the dark state lifetime is within a reasonable range (1–100 ms) to minimize laser intensity for optical pumping but also to reduce pixel dwell and thus image acquisition times, and (2) photobleaching is low enough to allow a reasonable number of pump-probe cycles per fluorophore (Bretschneider *et al.* 2007). This has, for example, been realized using special mounting media (Bretschneider *et al.* 2007) or nitrogen temperatures (Schwentker, 2007) increasing both the dark state lifetime as well as the photostability. On the other hand, it was shown that the addition of UV or IR light after probing may shorten the return time to the S_0–S_1 system by reverse dark state/intersystem crossing (Giske, 2007; Ringemann *et al.* 2008), introducing an additional degree of freedom for the optimization of GSD data acquisition (Schwentker, 2007). A large list of fluorophores was introduced as potential labels for GSD nanoscopy (Bretschneider *et al.* 2007). Recently, GSD was realized with NV centers in diamond, featuring down to 12 nm spatial resolution (compare Fig. 11*b*) (Han *et al.* 2010). GSD nanoscopy will benefit from the

---

from (Hell, 2007). (*b*) GSD nanoscopy: (left) dependence of the inhibition of fluorescence on the excitation laser intensity, which is based on transient shelving into a metastable dark state (inset). (Middle) Pump-probe principle with pump light inducing dark state transitions and probe light exciting fluorescence of those molecules that are left in the bright state, resulting in a sub-diffraction observation spot. (Right) GSD and confocal (upper marked areas) images of immunolabeled SNAP-25 protein clusters on a fixed cell membrane (left) and an organic dye with a high triplet intersystem crossing rate, filling up a grooved nanostructure (right). Scale bars: 500 nm. Adapted from (Bretschneider *et al.* 2007). (*c*) RESOLFT nanoscopy using the reversibly photoswitchable protein rsGFP. (Left) rsGFP fulfills all requirements for coordinate-targeted nanoscopy: fast photoswitching (upper panel: fluorescence signal following repetitive on–off switching (red) with comparison to the RSFP Dronpa (blue)) with low switching fatigue (lower left panel: 'on' fluorescence *versus* number of on–off switching cycle (red) and comparison to Dronpa (blue)), and a long lifetime of the 'off' state (lower right panel: spontaneous temporal recovery of fluorescence after off-switching with half of the fluorescence recovered after 23 min). (Right) RESOLFT and confocal (lower or upper left corner) of an *Escherichia coli* bacterium expressing rsGFP–MreB (left) and a live mammalian cell expressing keratin-19–rsGFP (right). Scale bar: 1 µm. Adapted from (Grotjohann *et al.* 2011). (*d*) RESOLFT nanoscopy with more than hundred-thousand doughnuts. (Left) By overlapping the diffraction pattern generated by two perpendicularly arranged gratings, an illumination pattern of the switch-off light is generated, which features a large number of intensity zeros (PBS: polarization beam-splitter, Obj: objective lens) and which results in multiple simultaneous scanning points, whose dimension decreases with increasing intensity of the switch-off light (middle). (Right) Conventional (left part) and RESOLFT (right part) wide-field images of keratin 19–rsEGFP(N205S) in live mammalian cells (scale bar: 1 µm, adapted from (Chmyrov *et al.* 2013)).
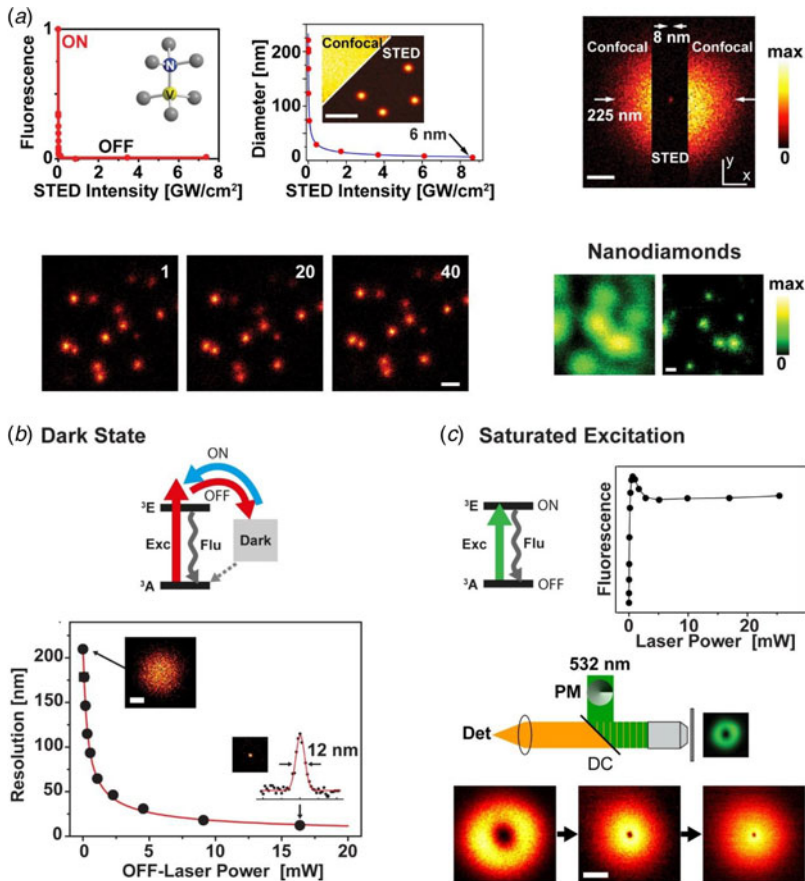
Fig. 11. The resolution of coordinate-targeted nanoscopy is in principle limited only by the size of the quantum system (molecule or emitter) to be distinguished: imaging nitrogen-vacancy (NV) centers in diamond. (*a*) STED imaging of NV centers. (Upper left) NV centers (inset: molecular structure) are a nearly perfect switch: fluorescence inhibition *versus* STED laser intensity. (Upper middle) STED images of single isolated NV centers in bulk diamond (inset: scanning image, with confocal counterpart in the upper left corner) reveal down to 6 nm spatial resolution (or diameters of the observation area) with increasing STED laser intensity. Scale bar: 100 nm. (Upper right) Scanning image of a single isolated NV center (fast axis along *y*) with STED laser switched on only in the marked area, exemplifying the vast increase in spatial resolution from confocal 225 nm down to 8 nm. Scale bar: 100 nm. (Lower left) Repetitive STED images of single isolated NV centers in diamond (frame number in the upper right corner), showing the ultimate stability of these emitters. Scale bar: 200 nm. (Lower right) Confocal (left) and STED (right) images of 35 nm large NV-containing nanodiamonds. Scale bar: 100 nm. Adapted from (Han *et al.* 2009; Rittweger *et al.* 2009a). (*b, c*) GSD nanoscopy of NV centers. (*b*) GSD by reversible laser-driven transitions into a long-lived dark state. (Upper panel) Energy level diagram of an NV center with ground ^3A, excited ^3E and dark states, transitions driven by red (excitation Exc and OFF-switching) and blue light (ON-switching), spontaneous fluorescence emission (Flu) and dark state return (dashed line, >100 s lifetime). (Lower panel) Spatial resolution *versus* power of the red laser driving the OFF transition, as determined by scanning images of isolated NV centers and respective intensity line profiles (insets, scale bar is 100 nm). Adapted from (Han *et al.* 2010). (*c*) GSD by saturated excitation. (Upper left panel) Energy level diagram of an NV center with ^3A (OFF) and ^3E (ON) states, and excitation by green light (Exc) and spontaneous fluorescence emission (Flu). (Upper right panel) Saturation of fluorescence signal: dependence of fluorescence signal of a single NV center on the power of the excitation laser. (Middle panel) Experimental setup with green 532 nm excitation laser, phase plate (PM) generating the doughnut-shaped intensity distribution (inset), dichroic mirror (DC), fluorescence signal (orange), and detector (Det). (Lower panels) Scanning images of a single NV center for increasing intensity of the excitation laser (left to right), depicting the confinement of the area in which no fluorescence is elicited. Adapted from (Rittweger *et al.* 2009b). Scale bar: 50 nm.

exploration of fluorophores and mounting or buffer conditions which realize large and controllable dark-state populations (Kolmakov *et al.* 2010a; Vogelsang *et al.* 2008). For example, special redox buffers have allowed the controlled and efficient photoswitching of conventional organic dyes by promoting the population of their dark states as well as their photostability (Vogelsang *et al.* 2008). Figure 10*b* on the other hand depicts GSD imaging in aqueous environment, where fluorophores usually exhibit dark state lifetimes in the range of μs. The image has been recorded with an organic dye which is characterized by a high intersystem crossing rate, i.e. a high triplet state yield (Chmyrov *et al.* 2008) and using somewhat larger laser intensities (Bretschneider *et al.* 2007). The use of dark states that are normally involved in bleaching pathways has however so far hampered the practicability of GSD for (live-) cell nanoscopy.

2.2.3 SPEM/SSIM: GSD via saturated excitation

Saturated Patterned Excitation Microscopy (SPEM) (Heintzmann *et al.* 2002) or Saturated Structured Illumination Microscopy (SSIM) (Gustafsson, 2005) also depletes the ground state, as in GSD. It differs from GSD (or STED) in that it confines the dark state S_0 rather than the emitting state S_1, thus creating sub-diffraction sized dark regions that are surrounded by bright areas. Scanning of such spots consequently produces 'negative data' and the final 'positive' images have to be reconstructed computationally (Gustafsson, 2005). The intensities necessary to create dark regions of sub-diffraction sized extent, i.e. to efficiently deplete S_0 and saturate the population of S_1 are of similar magnitude as in the STED concept, because both rely on the same states. Introduced theoretically a decade ago and also promising in principle molecular resolution (Heintzmann *et al.* 2002), SPEM/SSIM has so far experimentally been realized once with fluorescent beads, displaying a lateral resolution of 50 nm (Gustafsson, 2005). The limitations of this technique result from the use of very large excitation intensities, which cause enhanced photobleaching from higher excited (dark) states, as well as an optically induced depopulation of dark states, which prevents saturation of the S_1 (Giske, 2007; Ringemann *et al.* 2008; Schwentker, 2007). The aforementioned SPEM/SSIM experiment therefore implemented a D-/T-Rex-like illumination scheme, avoiding significant populations of long-lived dark states using a 5 kHz laser for excitation (Gustafsson, 2005). In other work, saturated excitation of ultra-stable NV centers in diamond yielded single-spot scanning GSD images with a spatial resolution of <10 nm (compare Fig. 11*c*) (Han *et al.* 2012; Rittweger *et al.* 2009b).

2.2.4 RESOLFT: reversible photoswitchable labels

All of the above approaches may be summarized under a general name, RESOLFT nanoscopy (Hell, 2004; Hell *et al.* 2003, 2004). The realization of STED or GSD led to the consideration of molecular switches between states of very long lifetimes (even longer than the metastable dark states introduced in the GSD concept). The advantage is obvious: the utilization of states with very long lifetimes τ (or even the elimination of spontaneous transitions) would allow applying very low laser intensities for driving a fluorophore to a certain state (Hell *et al.* 2003). Reversible photoswitching between states with very long τ can be realized through changes in molecular conformations. A prominent example is photoinduced cis–trans isomerization involving fluorescent and dark (or non-detectable) isomeric counterparts, which can be switched back and forth by light of different wavelengths. Cis–trans isomerization is for example known for cyanine dyes. The lifetime of these states for cyanines is however $\tau < \mu s$ in aqueous solution (Widengren & Schwille, 2000), impeding the move to very low intensities. Isomeric states may

be stabilized (and τ prolonged) for other molecules such as reversible switchable fluorescent proteins (RSFPs) or spiro-compounds, and/or by fixation in rigid environments (Ando *et al.* 2004; Bossi *et al.* 2006; Dickson *et al.* 1997; Feringa, 2001; Irie *et al.* 2002; Lukyanov *et al.* 2000; Sakata *et al.* 2005). In RSFPs the differently isomerized states are usually stabilized by the protein barrel surrounding the chromophore (and often involve differently protonated states) (Andresen *et al.* 2005, 2007; Habuchi *et al.* 2006; Wilmann *et al.* 2005). It was therefore an RSFP, asFP595 (Lukyanov *et al.* 2000), that was first used to experimentally prove the viability of the general RESOLFT concept in 2005 (Hofmann *et al.* 2005). asFP595 can be reversibly switched between a dark trans and a bright cis state with light of 405–460 and 560 nm, respectively, and the thermal lifetimes of $\tau > $ ms in aqueous solution enabled for the first time the use of ultra-low intensities ($<$kW/cm^2) for super-resolution microscopy. Similar sub-diffraction images were realized when using other RSFPs such as Dronpa (Ando *et al.* 2004; Bock, 2008; Dedecker *et al.* 2007; Hofmann, 2007), or when switching between an open and a closed form of a photochromic organic compound of the furyl-fulgides family in a polymeric matrix (Bossi *et al.* 2006). In the latter, the difference in fluorescence signal between the two forms had been realized by the photochromic compound serving as a reversible switchable energy acceptor for a fluorescent compound. Unfortunately, the uses of both asFP595 and the photochromic organic compound for cellular RESOLFT nanoscopy were limited. First of all, specific labeling with either was not feasible, since asFP595 was only present in a tetrameric form, and the organic compound could not successfully be functionalized. Furthermore, under the final imaging conditions the signal could not be switched off completely due to cross-talk between laser lines (e.g. $>$30% of the ON-state fluorescence in the case of asFP595), requiring computational post-processing of the recorded image (through, e.g. deconvolution) in order to fully extract the sub-diffraction image contents – a procedure which can be prone to noise and biases. In addition, the switching speed was rather slow, entailing scanning dwell times of $>$100 ms. Finally, and most importantly, both labels exhibited considerable switching fatigue. Therefore, deliberate screening for fast and high-contrast switching monomeric RSFPs which should hardly show spontaneous decay of the involved states and, most importantly, survive $>$1000 and more photoswitching cycles was performed (Stiel *et al.* 2007). This screen ended in a RSFP variant of GFP (rsGFP: reversible switchable GFP), and its use in RESOLFT nanoscopy realized down to 40 nm spatial resolution in live-cell imaging (Grotjohann *et al.* 2011). Similarly, the RSFP Dreiklang was created and applied to RESOLFT imaging, where suitable wavelengths for on and off switching and fluorescence excitation were completely disentangled, minimizing any action cross-talk (Brakemann *et al.* 2011). Applying laser intensities of only 1 kW/cm^2, the RESOLFT concept applying RSFPs is highly suited for live-cell applications. RESOLFT nanoscopy has in the meantime enabled the recording of live-cell dynamics even in 3D (Testa *et al.* 2012). Further improvements have come with the development of RSFPs with faster photoswitching times and decreased switching fatigue (Grotjohann *et al.* 2012), as well as with additional emission wavelength ranges (Stiel *et al.* 2008) for multi-color observations. Phototoxic effects of the (often UV) photoswitching light may be avoided by the use of IR light in a two-photon mode (Denk, 1996).

2.2.5 Parallelization

The image acquisition in coordinate-targeted nanoscopy can be accelerated significantly by employing multiple observation spots simultaneously. As already outlined in Section 2.1.6, this has been realized in STED nanoscopy with four parallel scanning spots using Wollaston prisms

(Bingen *et al.* 2011), or 100 or even 2000 parallel spots using optical standing wave patterns (Yang *et al.* 2014; Bergermann *et al.* 2015). Unfortunately, the laser intensities required for STED are still too high to allow further parallelization with currently available laser powers. The required average laser intensities in GSD – 10^5-fold lower compared to STED – allowed the use of larger numbers of intensity zeros in parallel (Schwentker, 2007). SSIM has so far been experimentally shown with structured illumination, i.e. with a multitude of zero-intensity lines (Gustafsson, 2005). The high laser intensities were delivered by a laser with large transient pulse peak powers but very low repetition rate, which again slows down the image acquisition process and makes live-cell imaging less feasible. This restriction has been lifted by employing RSFPs: the ultra-low intensities required for the RESOLFT concept allowed scanning with several intensity zeros and thus several sub-diffraction sized observation areas in parallel for live-cell nanoscopy (Rego *et al.* 2012; Schwentker *et al.* 2007). The combination of RESOLFT and structured illumination therefore promises <50–60 nm with sub-second image acquisition times of $>50 \times 50 \ \mu m^2$ fields of view (Rego *et al.* 2012). A more advanced illumination pattern than using parallel lines of high intensities as in conventional SIM is the scanning with thousands of parallelized points as in spinning-disc microscopy (McCabe *et al.* 1996) or in multifocal SIM (York *et al.* 2012). Similarly, more than 100 000 doughnuts were generated simultaneously for ultra-fast live-cell RESOLFT imaging of large fields of view with down to 70 nm spatial resolution (Chmyrov *et al.* 2013) (Fig. 10*d*). With the development of further optimized photoswitchers, RESOLFT is therefore a very promising tool for revolutionizing live-cell optical nanoscopy.

2.2.6 Nanoscale writing

Concurrently to the imaging of various nanostructures, the RESOLFT concept was extended to the writing of structures with sub-diffraction size and spacing using visible light. Proposed in the early times (Hell, 2004), writing of nanostructures based on the STED and RESOLFT concept has been experimentally realized using photochromic materials (Andrew *et al.* 2009; Fischer *et al.* 2010; Harke *et al.* 2012; Li *et al.* 2009a; Scott *et al.* 2009; Wiesbauer *et al.* 2013; Wollhofen *et al.* 2013) or RSFPs (Grotjohann *et al.* 2011). Analogously to imaging sub-diffraction features, an intensity distribution of a photoswitching laser exhibiting one or several intensity zeros is used to maintain molecules in a reactive ON-state (i.e. in a writable state that, in contrast to the OFF-state, can be transferred to a permanent state) only at the sub-diffraction spots defined by the zeros. Scanning then realizes writing of nanostructures. RESOLFT has thus evolved to a versatile concept to reach the nanoscale in far-field optical applications.

2.3 Ultimate limit

The spatial resolution of all of the above approaches scales inversely with the square root of the intensity of the laser light featuring the intensity zero(s) (Harke *et al.* 2008a; Hell, 2004; Hell *et al.* 2003). Therefore, driving up the intensity should entail observation spots going down to the size of a single emitter. Several test samples containing different fluorophores have been chosen to prove this. For example, STED on the organic dye JA26 in a polyvinyl-alcohol (PVA) matrix could for the first time experimentally prove the square-root law down to a spatial resolution of 16 nm along one lateral dimension (Westphal & Hell, 2005). T-Rex STED nanoscopy of protein assemblies in cells provided spatial resolution down to 20 nm along all lateral directions (Donnert *et al.* 2006). The square-root dependence and spatial resolutions of <20–30 nm were also demonstrated for STED measurements on fluorescent beads or single fluorescent molecules

under special photostabilizing buffer conditions (reducing and oxidizing system (ROXS) buffer) (Harke *et al.* 2008a; Kasper *et al.* 2010). Going beyond this, RESOLFT imaging was applied to NV centers in diamond (Han *et al.* 2009, 2010; Rittweger *et al.* 2009a, 2009b). These fluorescent color centers are extremely photostable, and were imaged by STED nanoscopy as well using very high laser intensities, exemplifying a nearly perfect switch in fluorescence emission. These experiments once again proved the square-root intensity dependence with spatial resolutions down to 6 nm (Fig. 11*a*), only limited by the insufficient stability of the microscope stage. The use of a solid-immersion lens has recently enabled imaging of single NV centers with a spatial resolution of below 3 nm (Wildanger *et al.* 2012). The NV centers could be imaged multiple times without any sign of photobleaching (Fig. 11*a*). With fluorescence lifetimes >10 ns, these fluorescent centers perform almost equally well in the pulsed or CW STED mode (Han *et al.* 2009), with further improvements realized through gated detection (Vicidomini *et al.* 2011). 20–35 nm large 'nano-diamonds' containing one or more NV centers could be imaged equally well (Fig. 11*a*) (Han *et al.* 2009; Vicidomini *et al.* 2011), and progress in their size reduction down to 5 nm (Smith *et al.* 2009) and functionalization (Fu *et al.* 2007; Krueger, 2008) aims at their applicability in cellular nanoscopy (Tzeng *et al.* 2011). Apart from cellular imaging, STED nanoscopy has allowed the optical detection of electron spin resonances from single NV centers in diamond located at sub-diffraction proximities (Wildanger *et al.* 2011), which is an important development for diverse areas of research such as quantum computation or magnetic resonance imaging (Balasubramanian *et al.* 2008; Jelezko & Wrachtrup, 2006; Maze *et al.* 2008).

The NV centers also exhibit dark states, transitions to which can specifically be addressed by light of different wavelengths: while red light (>600 nm) 'dumps' the NV centers into a >100 s long dark state, blue light efficiently depopulates this state (Han *et al.* 2010, 2012). Therefore, NV centers are also perfect candidates for GSD nanoscopy. Using this switching mechanism, the square-root law could be ascertained for the GSD approach with down to 12 nm spatial resolution (Fig. 11*b*), again limited by the stability of the microscope table and signal-to-noise (Han *et al.* 2010). The NV centers' ground state could be equally well inhibited, and emission of the fluorescence saturated, by simply raising the excitation intensity (Fig. 11*c*). Shaping the focal intensity distribution of the excitation laser in a way to present a local intensity zero (such as for the doughnut-shaped intensity distribution) and driving up its intensity consequently creates sub-diffraction sized dark holes, as presented above for the GSD-based SPEM/SSIM approaches (Section 2.2.3). Scanning of these dark spots over the sample and subsequent computations created images of single isolated NV centers in diamond with down to <10 nm spatial resolution, proving the square-root dependence also for this approach (Han *et al.* 2012; Rittweger *et al.* 2009b). Furthermore, optical nanoscopy of NVs was achieved by combining spin manipulation and optical read-out, allowing individual electronic spins to be detected, imaged and manipulated coherently with nanoscale resolution (Maurer *et al.* 2010).

3. The coordinate-stochastic approach

3.1 Basics: (F)PALM/STORM

The challenges posed by repeated cycling between molecular states for the coordinate-targeted STED/RESOLFT approaches are alleviated when transferring individual molecules between different states stochastically in space. For example, molecules that are initially OFF may be individually driven to their ON-state at unknown spatial coordinates. The molecules' coordinates can be determined with sub-diffraction precision from their images on a camera. While the image of a

single molecule is again blurred by diffraction, the molecular position can be determined by calculating the centroid of the blurred image spot (Bobroff, 1986; Heisenberg, 1930). Restrictions are: (1) only single isolated molecules further apart than the distance given by diffraction can be imaged at a time to avoid any bias in localization of molecular positions from overlapping (blurred) spots, and (2) molecules, once in their ON-state, have to emit a sufficient number of photons N, since the localization precision scales with the inverse square root of N (Thompson *et al.* 2002). It is however important to realize that localization *per se* cannot provide super-resolution, i.e. finding a position of an object with arbitrary precision is not the same as resolution. Resolution is about separating similar objects at small distances. This is why, although it had routinely been applied for decades, specifically for spatiotemporal tracking of single isolated particles or molecules, localization on its own did not provide nanoscale images. Resolution requires a criterion to discern neighboring molecules such as realized by driving molecular transitions between different states (Hell, 2009b; Hell & Kroug, 1995; Hell & Wichmann, 1994). Therefore, an approach first suggested as (F)PALM (Betzig *et al.* 2006; Hess *et al.* 2006) or STORM (Rust *et al.* 2006) assembles a super-resolved image by determining spatial positions molecule by molecule using molecular transitions: (1) only a few isolated molecules are stochastically transferred (or activated) into their ON-state at once; (2) these molecules are imaged onto a camera and their spatial coordinates are determined through localization and saved; (3) molecules are transferred into an OFF-state; (4) stochastic activation of another subset of isolated molecules allows the read-out of neighboring molecules; and (5) repetition of this cycle realizes the reconstruction of an image with sub-diffraction resolution from the spatial coordinates of all imaged molecules (Fig. 12*a*). Similar to upgrading conventional confocal scanning or SIM systems for RESOLFT-type nanoscopy, the setup for this stochastic-switching based nanoscopy concept is a simple expansion of a conventional camera-equipped wide-field or TIRF microscope, updated by a stronger excitation laser and/or a second laser for controlling the switching of molecules (Fig. 12*b*, where an implementation with two separate detection channels is shown).

3.2 Molecular transitions

Various ways of preparing molecular states with different fluorescence properties such as an ON- and an OFF-state have been suggested and implemented for this coordinate-stochastic nanoscopy. The strategy of combining stochastic molecular switching with localization was first used in methods called single-molecule high-resolution imaging with photobleaching (SHRImP) (Gordon *et al.* 2004) and nanometer-localized multiple single-molecule (NALMS) (Qu *et al.* 2004) imaging, in which the position of a small number of bright regular fluorophores was mapped by bleaching them (i.e. switching them off) consecutively, individually and stochastically. However, these methods start out from many bright molecules and hence from a bright total signal. They can therefore, in contrast to (F)PALM/STORM, accommodate only a small number of fluorophores. Similarly, the molecule-specific temporal characteristics of the blinking of nearby quantum-dots as recorded over consecutive camera frames were enough to separate two nearby emitters (Lidke *et al.* 2005), but it remains to be shown how many close-by emitters can be distinguished using the presented algorithms.

    The original (F)PALM experiments employed photoactivatable fluorescent proteins (Patterson & Lippincott-Schwartz, 2002), with the switch-on and -off accomplished using dedicated laser light and irreversible photobleaching, respectively (Fig. 12*c*) (Betzig *et al.* 2006; Hess *et al.* 2006). Similarly, photoactivatable organic dyes can be used (Fig. 12*e*) (Fölling *et al.* 2007, 2008a). This unfortunately comes at the expense of not being able to record a molecule several
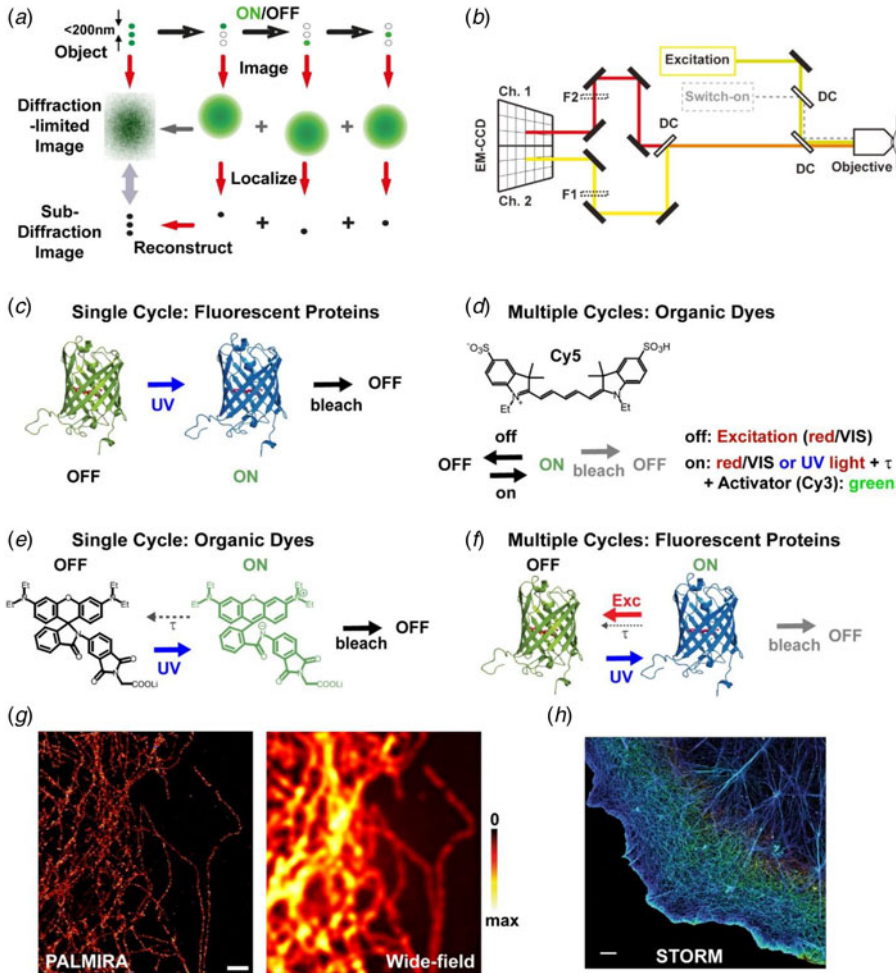
Fig. 12. Coordinate-stochastic (single-marker/single-molecule switching-based) nanoscopy ((F)PALM/ STORM). (*a*) Images with sub-diffraction spatial resolution are reconstructed from consecutive camera frames with simultaneous imaging and position-localization of single isolated (sparse) molecules only, which are switched on and off one after the other. (*b*) The setup is typically based on a conventional wide-field (TIRF) microscope with an excitation laser and, if required, an additional switching (or activation) laser, a microscope objective, dichroic mirrors (DC) for overlaying the lasers, de-coupling the fluorescence signal from the laser light and if required splitting up the fluorescence signal into two different wavelength ranges, fluorescence filters (here F1 and F2) for rejecting any residual laser scattering light and selecting the detected wavelength range, and a CCD camera detecting the fluorescence potentially in two channels (Ch. 1 and Ch. 2). (*c–f*) Various modes of (F)PALM/ STORM-based nanoscopy differing in the labels and molecular transitions: (*c*) the original (F)PALM approach using photoactivatable proteins that are initially dark or non-detectable, sparsely switched on by, for example, UV light and switched off by photobleaching. (*d*) The original STORM approach: Organic dyes such as Cy5 (or also fluorescent proteins) can be switched on and off by laser light of the same or different color or by spontaneous recovery (τ), with on- and off-switching potentially assisted by an additional activator dye such as Cy3 and by photobleaching, respectively. (*e*) Single-cycle switching using photoactivatable organic dyes that are initially dark or non-detectable, sparsely switched on by UV light and switched off by photobleaching or rarely by a spontaneous dark state return (τ). (*f*) Multiple-cycle switching using RSFPs that can be switched between a dark and bright isomer using the excitation and UV light (or spontaneous transitions (τ) and photobleaching). (*g*) Example PALM/ STORM image of a tubulin network in a fixed PtK2 cell stained with a photoactivatable rhodamine

times, i.e. to acquire structural changes in the specimen over time. The original STORM experiments applied reversible photoswitchable organic fluorophores such as cyanines (Fig. 12*d*) (Rust *et al.* 2006): under certain buffer conditions they can be transferred between a bright ON- and a dark OFF-state using red and green light, mediated by nearby activator fluorophores (Bates *et al.* 2005). Photoswitching in cyanines and other organic dyes may also be accomplished by other molecular transitions such as via the transient population of metastable dark states including the dyes' triplet states or redox states populated therefrom (Bock *et al.* 2007; Heilemann *et al.* 2008; Hu *et al.* 2008; Rust *et al.* 2006; Steinhauer *et al.* 2008; van de Linde *et al.* 2008). Similarly, RSFPs may be employed (Fig. 12*f*) (Dickson *et al.* 1997; Egner *et al.* 2007; Geisler *et al.* 2007). Harnessing reversible molecular transitions allows the recording of a molecule's position several times, i.e. to acquire a sequence of super-resolution images (Endesfelder *et al.* 2010; Jones *et al.* 2011; Shroff *et al.* 2008; Stiel *et al.* 2008). Beside fluorescent proteins and organic dyes, (F)PALM/STORM-like recordings were realized with other emitters such as luminescent single-walled carbon nanotubes (Cognet *et al.* 2008) or QDs (Hoyer *et al.* 2010; Lagerholm *et al.* 2006).

3.3 Continuous recording

The use of reversible molecular transitions led to the idea to continuously (and still stochastically) drive molecules between a bright and a dark state. Modalities termed 'PALM with independently running acquisition' (PALMIRA) (Egner *et al.* 2007; Geisler *et al.* 2007) and 'ground state depletion followed by individual molecule return' (GSDIM) (Fölling *et al.* 2008b) apply no activation or switch-on beam, and isolated fluorophores are allowed to blink stochastically and subsequently in time (not only in space) (Fig. 13*a*) (Fölling *et al.* 2008b; Hell, 2007). A single CW laser beam is used to generate the N photons and to switch the fluorophores off by transferring them into dark states. Dark state return is either promoted by switching cross-talk of the laser or by a spontaneous decay. The camera is run freely and the laser intensity and frame rate adjusted such that the average duration of the N-photon burst coincides with the duration of a camera frame. These purely stochastic concepts probably are the simplest far-field nanoscopy systems at present, because they require just uniform laser illumination, a freely running camera, and appropriate software. A straightforward advantage of such an acquisition mode is that it allows the use of conventional fluorophores such as many organic dyes or fluorescent proteins. Starting with STORM (Rust *et al.* 2006) and later GSDIM (Fölling *et al.* 2008b), experiments termed direct-STORM (dSTORM) (Heilemann *et al.* 2008; van de Linde *et al.* 2008) and Blinking Microscopy (Steinhauer *et al.* 2008), or single-molecule active control microscopy (SMACM) (Biteen *et al.* 2008, 2009; Sahl & Moerner, 2013; Sahl *et al.* 2012), spectral precision distance microscopy/spectral position determination microscopy with physically modifiable fluorochromes (SPDM/SPDM$_{Phymod}$) (Lemmer *et al.* 2008, 2009), or reversible photobleaching microscopy (RPM) (Baddeley *et al.* 2009) adapt buffer conditions and laser intensities to tune transitions to metastable dark states such as radical states of standard labels, producing super-resolution images of conventionally labelled samples (Fig. 13*b, c*) or even of autofluorescent cellular structures (Bierwagen *et al.* 2010). The return from long-lived metastable states can often be accelerated with additional UV or IR laser light, adding another parameter to optimize the acquisition of

---

(sub-diffraction (left) and diffraction-limited (right) counterparts, scale bar: 2 μm, adapted from (Fölling *et al.* 2007)). (*b*) Example STORM image of Alexa647-immunolabeled actin in a fixed COS-7 cell (scale bar: 2 μm, adapted from (Xu *et al.* 2012)).
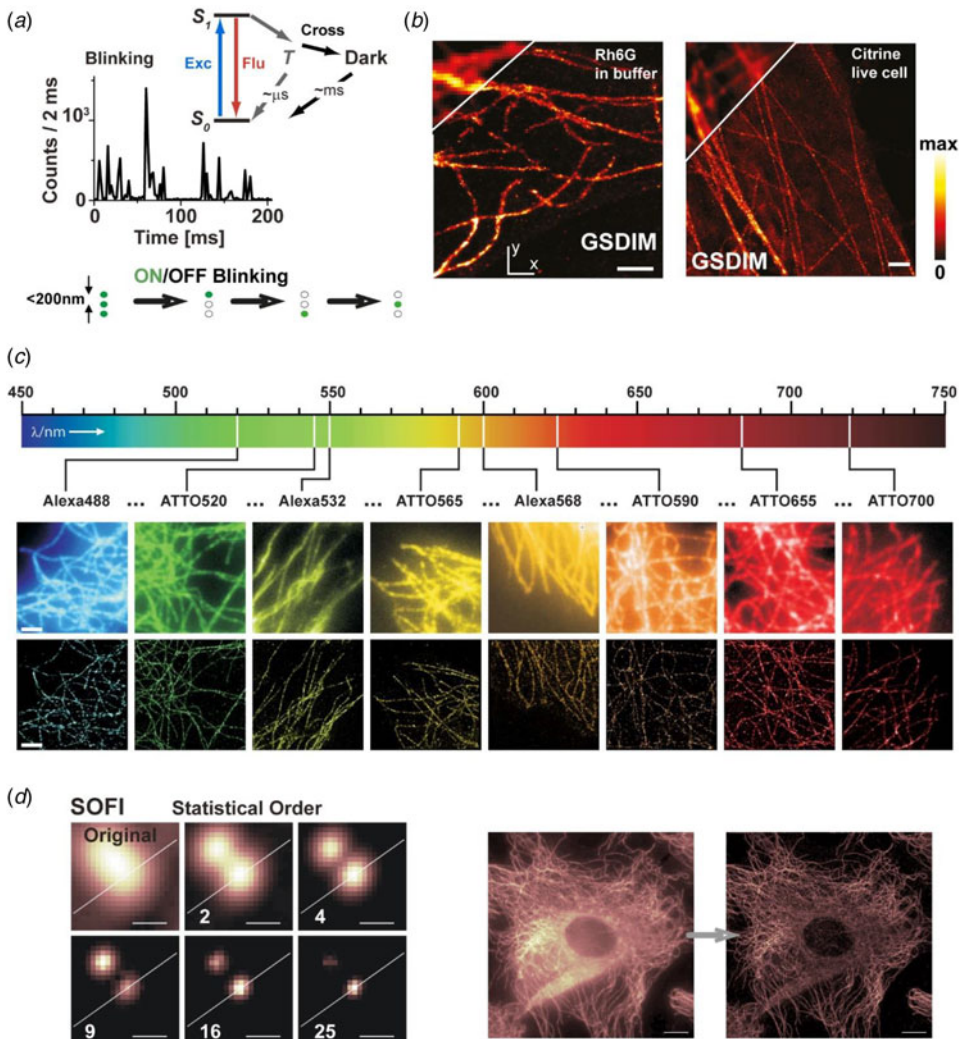
Fig. 13. Coordinate-stochastic single-marker/single-molecule switching: stochasticity in space and time (GSDIM, (d)STORM, . . .) and SOFI. (*a*) A fluorophore can continuously be cycled between its bright singlet (S_0 and S_1, emitting fluorescence (Flu)) and dark state (triplet T and other long-lived (µs-ms) dark states) system with a single excitation (Exc) laser, eliciting on-off blinking of fluorescence in time (as highlighted by a fluorescence time trace of a single Atto532 fluorophore in PVA, adapted from (Fölling *et al.* 2008b)) and space (as sketched in the lower panel for three different single molecules). (*b*) GSDIM/(d)STORM/. . . images of Rh6G-immunostained microtubules in PtK2 cells in aqueous buffer (left) and of the microtubule cytoskeleton of living PtK2 cells labeled with the fluorescent protein Citrine-Map2 (right). Upper left corner: Diffraction-limited wide-field recordings. Scale bars: 1 µm. Adapted from (Fölling *et al.* 2008b). (*c*) GSDIM/(d)STORM/. . . allows the use of a whole gamut of conventional organic dyes with different emission spectra as highlighted by super-resolution (lower panels) and corresponding diffraction-limited wide-field (upper panels) images of the cytoskeletal network of mammalian cells immunolabeled with eight different Alexa Fluor and Atto dyes spanning the visible wavelength range (emission maxima in upper color bar) according to the dSTORM principle (scale bar: 1 µm, adapted from (Heilemann *et al.* 2009b)). (*d*) Principle of SOFI imaging. SOFI is based on higher-order statistical analysis of temporal fluctuations recorded in a sequence of images. The spatial resolution increases with the order as exemplified by SOFI images of different order (as indicated) of two blinking quantum dots deposited on a cover slip (left, scale bars: 250 nm, adapted from (Dertinger *et al.* 2009)). (Right) Diffraction-limited wide-field (left) and SOFI (right) images of quantum-dot immunolabeled tubulin network of a 3T3 fibroblast (scale bar: 10 µm, adapted from (Dertinger *et al.* 2010)).

the single-molecule data (e.g. Fölling *et al.* 2008b). Transient stochastic on-switching may also be effected by molecular collisions or chemical reactions, where a fluorophore is only activated once interacting with other specific molecules such as single-walled carbon nanotubes (Cognet *et al.* 2008) or chemical reaction centres as in trajectory time distribution optical microscopy (TTDOM) (Mei & Hochstrasser, 2006), points accumulation for imaging in nanoscale topography (PAINT) (Sharonov & Hochstrasser, 2006), universal PAINT (uPAINT) (Giannone *et al.* 2010), NASCA (nanometer accuracy by stochastic chemical reactions) (Roeffaers *et al.* 2009), or CHemically Improved Resolution for Optical Nanoscopy (CHIRON) (Schwering *et al.* 2011). We have to note that albeit a whole gamut of different notations have been introduced ((F)PALM, STORM, PALMIRA, dSTORM, GSDIM, Blinking Microscopy, SMACM, SPDM, SPDM$_{Phymod}$, RPM, TTDOM, PAINT, uPAINT, NASCA, CHIRON or photoactuated unimolecular logical switching attained reconstruction (PULSAR) microscopy (Hu *et al.* 2008), they are all based on the same principle, namely, modulating the fluorescence emission of single molecules using molecular transitions. Differences appear only in details of the experimental design, i.e. switching mechanism, how many lasers used, camera running mode, choice of label, buffer conditions, etc.

3.4 SOFI

Molecule-specific ON–OFF blinking (Lidke *et al.* 2005) is the basis of a recent stochastic nanoscopy approach termed super-resolution optical fluctuation imaging (SOFI) (Fig. 13d) (Dertinger *et al.* 2009). Higher-order statistical analysis of the temporal fluctuations (recorded in a sequence of images) allows the identification of molecular positions with sub-diffraction spatial resolution. An example of such higher-order statistical analysis is the calculation of higher-order cumulants or autocorrelation functions (Dertinger *et al.* 2009, 2010; Geissbuehler *et al.* 2011, 2012). Similarly to FCS-based analysis of diffusing molecules, SOFI does not require temporal fluctuations recorded for single isolated molecules, but can be applied to up to ten-fold larger molecular densities than conventional (F)PALM/STORM. Furthermore, autocorrelations may be used to acquire, along with the spatial coordinates, temporal molecular parameters such as dark state kinetics, which might be, for example, a read-out for local oxygen concentrations (Geissbuehler *et al.* 2012). The spatial resolution increases with the order number, and images reconstructed from up to the 4th order cumulants have been demonstrated so far (Fig. 13d) (Dedecker *et al.* 2012; Dertinger *et al.* 2009, 2010; Geissbuehler *et al.* 2011, 2012). A face-to-face comparison to (F)PALM/STORM nanoscopy revealed 'that localization-based super-resolution can deliver higher resolution enhancements but imposes significant constraints on the blinking behavior of the probes, which limits its applicability for live-cell imaging. SOFI, on the other hand, works more consistently over different photo-switching kinetics and also delivers information about the specific blinking statistics. Its suitability for low SNR acquisition reveals SOFI's potential as a high-speed super-resolution imaging technique' (Geissbuehler *et al.* 2011).

3.5 General aspects

It becomes obvious that in the coordinate-stochastic approaches there is a tradeoff between spatial resolution, image acquisition speed and error rates: the spatial resolution of the final image may be increased by selecting only single-molecule emission events with high photon count numbers, and the acquisition time may be reduced by activating more molecules per imaging cycle, however introducing errors due to the neglect of some molecular positions (and thus lower sampling of
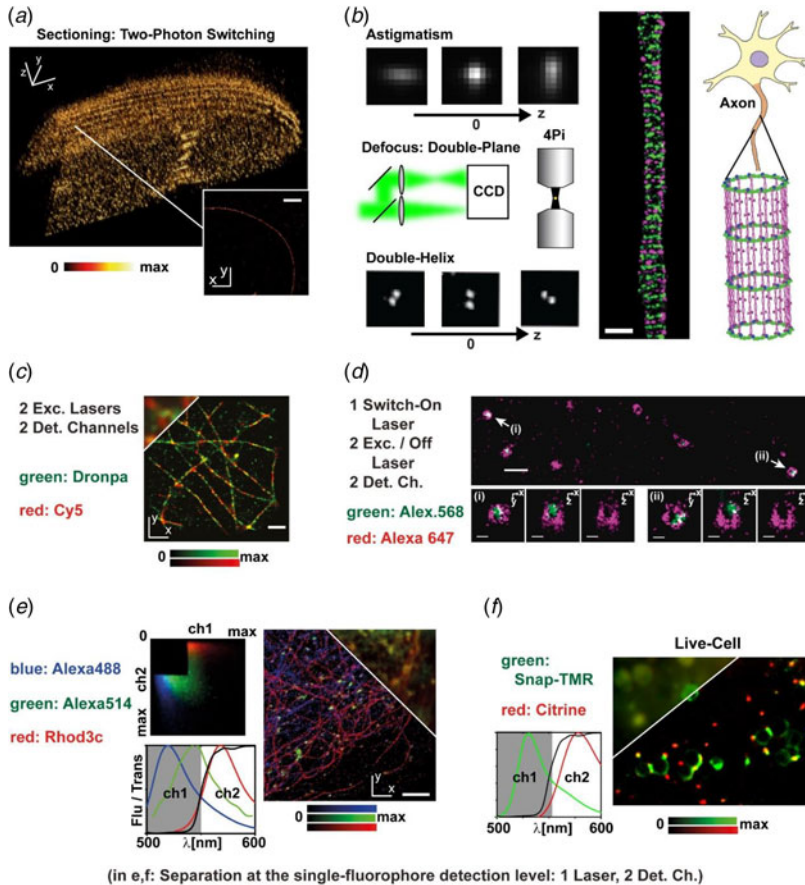
Fig. 14. 3D and multi-color imaging with coordinate-stochastic single-marker/single-molecule switching-based nanoscopy. (*a*) Optical sectioning and out-of-plane signal rejection achieved by two-photon on-switching or activation: Super-resolution images of lamin of a U373MG cell stained with a photoactivatable rhodamine (inset: equatorial slice as marked by the line, scale bar: 2 μm, adapted from (Fölling *et al.* 2007)). (*b*) (Left) Different approaches of 3D (F)PALM/STORM-based imaging: astigmatism using a cylindrical lens results in an elliptical distortion of the images of out-of-plane (axial z-direction) molecules, double plane imaging comparing focused and defocused camera images, 4Pi using two opposing objectives, and double-helix detection employing a 'doubled' detection of each single molecule where the orientation of the two lobes of intensity changes with the z-position of the molecule. (Right) Two-color STORM image of immunolabeled bII-spectrin (green) and adducin (magenta) in fixed axons reveals that actin, spectrin and adducin form a coordinated, quasi-1D lattice structure in axons (scale bar: 500 nm, adapted from (Xu *et al.* 2013), where 3D astigmatic imaging was also performed). (*c*) Two-color image of the microtubular network in a PtK2 cell stained with the reversibly photoswitchable protein rsFastLime (green) and the organic dye Cy5 (red) generated by subsequent recordings using two excitation lasers and two detection channels (upper left corner: diffraction-limited wide-field recording, scale bar: 1 μm, adapted from (Bock *et al.* 2007)). (*d*) Fast two-color 3D-STORM images of live BSC-1 cells using one activation and two excitation lasers inducing fluorescence blinking over time: Alexa 568-labeled transferrin (green) and clathrin-coated pits labeled with Alexa647 via a SNAP tag (magenta), x/y-projection of the recordings of multiple sections along z (upper panel), and different cross-sections through two objects (i, ii) indicated in the upper panel (x/y near the plasma membrane (left), x/z cutting through the middle of the invaginating pits (middle) and corresponding x/z cross-section of the clathrin channel only (right)). Scale bars: 500 nm (upper panel) and 100 nm (lower panels), adapted from (Jones *et al.* 2011). (*e, f*) Multi-color imaging via single-molecule signatures using one continuously running laser and two detection channels. Color separation is realized by applying fluorescence labels with slightly

the structure) and the risks of producing overlapping images of single molecules which hide information on molecular positions (e.g. Nieuwenhuizen *et al.* 2013; Shroff *et al.* 2008; Small, 2009). Therefore, quite a number of improvements in determining molecular positions from the isolated blurred spots of the camera frames have been promoted for (F)PALM/STORM-based nanoscopy, especially aiming at image reconstructions for more densely labeled samples, at low SNR, with improved localization precision, with increased acquisition and analysis speeds, and for different blinking/photoswitching statistics (e.g. Cox *et al.* 2012; Cronin *et al.* 2009; Endesfelder *et al.* 2010; Hedde *et al.* 2009; Henriques *et al.* 2010; Holden *et al.* 2011; Huang *et al.* 2011; Jones *et al.* 2011; Larson, 2010; Laurence & Chromy, 2010; Mortensen *et al.* 2010; Nieuwenhuizen *et al.* 2013; Pertsinidis *et al.* 2010; Smith *et al.* 2010; Wolter *et al.* 2010). In addition, one should bear in mind that rather immobile molecular orientations and out-of-focus sites may potentially result in significantly biased determinations of molecular positions (e.g. Enderlein *et al.* 2006; Engelhardt *et al.* 2011). Strategies to diagnose, mitigate and even fully correct molecular dipole orientation-related position artifacts have recently been emerging (Backer *et al.* 2014; Backlund *et al.* 2012, 2014; Lew *et al.* 2013; Lew & Moerner, 2014; Backer *et al.* 2013).

3.6 3D imaging

Sectioning or 3D imaging has been implemented for coordinate-stochastic switching-based nanoscopy. Sectioning along the axial direction is provided when activating molecules via two- or multi-photon processes (Fig. 14*a*) (Fölling *et al.* 2007, 2008a; York *et al.* 2011). On the other hand, most (F)PALM/STORM-based experiments have applied a TIRF illumination scheme from the very start, i.e. only planes of the sample that are within <100 nm near the microscope cover glass are selected and out-of-plane background rejected. Several different approaches have been proposed and demonstrated to supply real 3D resolution (Fig. 14*b*) (whether in wide-field or TIRF illumination mode), such as the introduction of astigmatism by the use of cylindrical lenses (Huang *et al.* 2008; Mlodzianoski *et al.* 2009; York *et al.* 2011) or adaptive optics (Izeddin *et al.* 2012), double-plane detection using two camera channels (Juette *et al.* 2008; Mlodzianoski *et al.* 2009), two opposing objectives in a 4Pi illumination and detection mode (Aquino *et al.* 2011; Shtengel *et al.* 2009), a double-helix modification to the emission path of the microscope (Lee *et al.* 2012, 2014; Pavani *et al.* 2009; Sahl & Moerner, 2013), bisected pupil 3D imaging (Backer *et al.* 2014), an Airy-beam point spread function (Jia *et al.* 2014), other novel information-optimal point spread function designs (Shechtman *et al.* 2014) or a combination of two opposing objectives and astigmatism (Xu *et al.* 2012). A nice example of 3D STORM nanoscopy recently presented novel details of the spatial organization of actin and other cytoskeletal filaments in mammalian cells (Fig. 12*b*) (Xu *et al.* 2012) and axons (Fig. 14*b*) (Xu *et al.* 2013). Observing single-molecule fluorescence from deep inside samples such as tissue may prove itself

---

shifted emission spectra, which emit differently into the two detection channels (lower panels: fluorescence emission spectra of the given fluorophores and (black) transmission spectrum of the applied dichroic mirror for splitting up the signal onto the two detection channels ch1 and ch2), and can be distinguished by a different ratio of photons detected in the two detection channels (upper left: two-dimensional histogram of photon pairs simultaneously registered in the two detection channels ch1 and ch2, allowing an accurate distinction of the three different fluorophores (color coded)). Super-resolution images and diffraction-limited counterparts (upper corners) of (*e*) Alexa488-labeled vimentin (blue), Alexa514-labeled clathrin (green), and Rhodamine 3c-labeled tubulin (red) in fixed PtK2 cells, and (*f*) Caveolin 1 (red) and Caveolin 2 (green) in live PtK2 cells labeled with TMR via SNAP tag and the fluorescent protein Citrine, respectively (scale bars: 2 μm, adapted from (Testa *et al.* 2010)).

difficult due to enhanced background signal stemming from scattered light or out-of-focus fluorescence. A remedy of this limitation may be the combination of the (F)PALM/STORM-based readout with selective-plane-illumination microscopy (SPIM) (Zanacchi *et al.* 2011) and/or the use of adaptive optics to correct for aberrations (Izeddin *et al.* 2012).

3.7 Dynamics

A limitation of stochastic single-molecule switching is the rather large total image acquisition time, since a sufficiently large number of single-molecule positions and thus camera frames (usually >10 000–100 000) have to be gathered for the reconstruction of an accurate and representative super-resolved image of a reasonably complex structure (Betzig *et al.* 2006). Furthermore, the initial use of photoactivatable, i.e. only one-cycle, photoswitchable fluorophores originally impeded the recording of multiple consecutive super-resolved images. However, the advent of reversibly photoswitchable labels (Fig. 12*d, f*) and the aforementioned sophisticated image reconstruction algorithms have since then enabled time-lapse studies of live-cell dynamics with (F)PALM/STORM-based techniques (e.g. Dedecker *et al.* 2012; Endesfelder *et al.* 2010; Flors *et al.* 2009; Hess *et al.* 2007; Jones *et al.* 2011; Shroff *et al.* 2008; Stiel *et al.* 2008; Testa *et al.* 2010; Wilmes *et al.* 2012; Wombacher *et al.* 2010). Longer observation times can thereby be achieved by using, for example, transiently binding fluorescent markers (Lukinavicius & Johnsson, 2011), such as a peptide that is designed to bind reversibly to the F-actin cytoskeleton (Izeddin *et al* 2011). With further optimization of the label brightness, labeling protocol, camera technology and image acquisition and reconstruction, time resolutions of down to <1 s have been anticipated for stochastic single-molecule switching-based nanoscopy techniques (Dempsey *et al.* 2011; Huang *et al.* 2013; Jones *et al.* 2011; Ondrus *et al.* 2012). Importantly, as well, photoswitching and continuous determination of molecular positions may be combined to perform single-molecule tracking at higher concentration of the labeled molecules (Eggeling *et al.* 2007; Hess *et al.* 2007; Manley *et al.* 2008).

3.8 Multi-colour recordings

Multi-color imaging is straightforward for the single-molecule-based nanoscopy techniques. The most obvious approach generates separate detection and localization of different labels by subsequently or simultaneously switching them on and off and detecting their emission at different colors using several dedicated laser lines and appropriate filtering (Fig. 14*c, d*) (e.g. Bates *et al.* 2007; Bock *et al.* 2007; Klein *et al.* 2011; Shroff *et al.* 2007; van de Linde *et al.* 2009; Wilmes *et al.* 2012). Discrimination of up to six different colors was introduced for the original STORM approach by applying different labels at different wavelengths for activation and emission (Bates *et al.* 2011). The simplest approach is to use single-molecule signatures not only for determining positions but also for identifying different species (Schoenle & Hell, 2007): a single continuously running excitation laser elicits fluorescence emission of various labels with slightly differing emission spectra (e.g. with their maxima 20–40 nm apart), two camera channels (preferably on the same chip) detect the fluorescence signal in nearby wavelength ranges, and single molecules are assigned through the ratios of photons detected in each channel (Bossi *et al.* 2008). Using this approach, up to four different colors have been separated with nanoscale resolution in fixed as well as living cells (Fig. 14*e, f*) (Gunewardene *et al.* 2011; Testa *et al.* 2010). Similarly, other spectroscopic parameters such as fluorescence anisotropy or lifetime may be used to distinguish between molecules of different rotational mobility (e.g. immobilized and freely diffusing

molecules) or lifetime but same emission color (Schoenle & Hell, 2007; Testa *et al.* 2008), or to simply image molecular positions and mobilities (Gould *et al.* 2008).

(F)PALM/STORM or GSDIM/(d)STORM-based nanoscopes have nowadays been commercialized and found their ways into a lot of laboratories all over the world, adding to the toolset for solving long-standing biological problems.

4. Conclusions: coordinate-targeted *versus* -stochastic

Both branches of nanoscopy (super-resolution optical microscopy) – coordinate-targeted STED/RESOLFT and coordinate-stochastic (F)PALM/STORM – are ultimately based on the same basic principle: transferring fluorescent labels between states of different emission characteristics (such as a bright ON- and a dark OFF-state) to allow the discerning of nearby objects (e.g. Hell, 2009b) (Fig. 15). Both branches are complementary and have their own advantages and disadvantages. The advantage of stochastically switching molecules is obvious: Whereas in the coordinate-targeted STED/RESOLFT read-out mode a molecule has to undergo many ON–OFF cycles, in the stochastic switching mode, a single OFF–ON–OFF cycle per molecule is in principle enough to produce an image, thus avoiding switching fatigue. However, in contrast to STED/RESOLFT nanoscopy, which usually creates a direct image of molecular distributions, computational algorithms are generally applied for (F)PALM/STORM to reconstruct the final image, a potential source of bias. For example, some molecules may be localized more precisely than others, because the number of photon emissions N follows a statistical distribution. Therefore, to ensure a certain resolution, the stochastic read-out mode usually defines a brightness threshold (e.g. $N > 50$) and molecules emitting less than this threshold in a bunch are discarded without contributing to the image. In a sense, this rejection of molecular events is to the stochastic read-out what switching fatigue (or photobleaching) is to its coordinate-targeted counterpart; the higher the required resolution, the more molecular events are discarded. Often, (F)PALM/STORM-based experiments have achieved focal plane resolution of <20 nm at the expense of discarding molecules (see e.g. Shroff *et al.* 2008; Small, 2009). In addition, some molecules may not be activated at all or counted several times, i.e. the molecular numbers assigned to the final image may be biased. While this imperfect assignment may not corrupt images of filament-like structures such as of microtubules, actin, mitochondrial or ER membrane renditions, it may compromise the accurate characterization of protein clusters (e.g. Annibale *et al.* 2011). In general, coming along with the increased sensitivity of the nanoscopy approach, greater care has to be taken when labelling cellular samples, especially with respect to unspecific background staining (Wurm *et al.* 2010). Artifacts due to, for example, improper fixation in immunolabeling or unspecific binding may not be observed in confocal but may be visible in nanoscopy images, due to the improved spatial resolution in the latter (Opazo *et al.* 2012; Tanaka *et al.* 2010). Also, due to the increased spatial resolution, the term "co-localization" may become invalid, since two objects (especially when labelled via a primary and secondary antibody as in most immunolabeling approaches) cannot occupy the same spot.

It is worth noting that the enhanced sensitivity of all nanoscopy concepts to artifacts calls for elaborate control measurements. For example, the results of previous protein cluster analyses using STED nanoscopy were ascertained using different labels as well as different STED set-ups, potentially introducing different switching fatigues (Sieber *et al.* 2007). At the same time, the multitude of different nanoscopy methods allows new ways of validating results. For example, both nanoscopy branches, the coordinate-targeted and the coordinate-stochastic, may
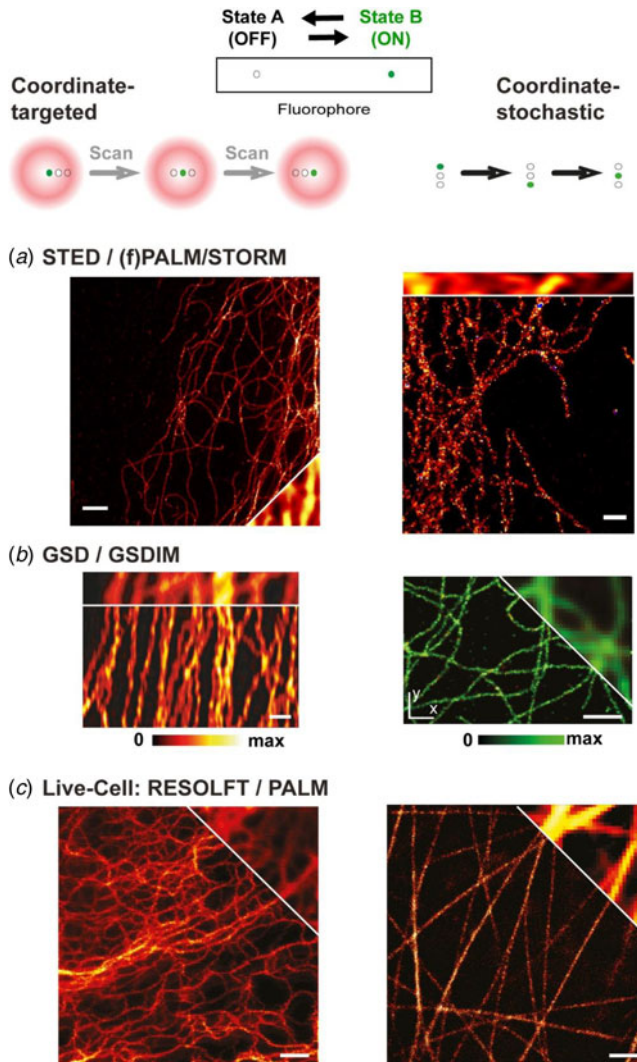
Fig. 15. Coordinate-targeted *versus* coordinate-stochastic nanoscopy. Both families of methods are based on transitions between molecular states of different fluorescence characteristics (such as a bright ON- and a dark OFF-state) realizing the separation of different molecules within a diffraction-limited area by subsequently confining emission either to sub-diffraction sized spots defined in space (coordinate-targeted (deterministic), left) or stochastically in space on single isolated molecules (coordinate-stochastic, right). Sub-diffraction coordinate-targeted and -stochastic imaging can be realized using the same fluorescence labels and switching mechanisms. (*a*) Coordinate-targeted STED (left) *versus* coordinate-stochastic (F)PALM/STORM images (right) of organic-dye-labeled microtubules in fixed PtK2 cells. (*b*) Coordinate-targeted GSD (left, scale bar 500 nm) *versus* coordinate-stochastic GSDIM images (right) of Atto532-labeled microtubules in fixed PtK2 cells. (*c*) Coordinate-targeted RESOLFT (left) *versus* coordinate-stochastic (F)PALM/STORM images (right) of the RSFP Dreiklang expressed in live PtK2 cells at Keratin19 (left) and Map2-micotubules (right). Adapted from (Brakemann *et al.* 2011). Diffraction-limited counterparts in upper parts. All other scale bars: 1 μm.

exploit the same molecular transitions and may thus be applicable to the same samples. Figure 15 depicts examples of STED *versus* (F)PALM/STORM (Fölling *et al.* 2007), GSD *versus* GSDIM (Bretschneider *et al.* 2007; Fölling *et al.* 2008b), and RESOLFT *versus* PALM (Brakemann *et al.* 2011) nanoscopy experiments, where the same or similar labels have been used for nanoscale cellular imaging. Consequently, both techniques could be applied for the validation of a specific result. Of course, while complementary, one approach may be more suitable for a concrete measurement than the other, and this argues for research environments having access to several of the above methodologies. For example, STED/RESOLFT has proven to be able to record fast live-cell dynamics, even deep inside tissue and *in vivo* (at times through the combination with single-molecule spectroscopic tools such as FCS), yet, to maintain reasonable signal-to-noise or -background levels, brightly labeled samples are often favored. On the other hand, (F)PALM/STORM-based experiments have shown remarkable results when imaging faintly labeled structures such as actin, but due to their acquisition mode have proven to be less versatile for dynamic live-cell and deep-tissue imaging, even if recent developments may improve their applicability in this regard. Quite generally, one should keep in mind and expect that new research will address such limitations where they are not of a fundamental nature. Still one should not expect one microscope to be optimized in all aspects of microscopy: high spatial and temporal resolution, low phototoxicity (and thus large live-cell compatibility), and high image contrast. For example, while (F)PALM/STORM- and STED-based nanoscopy approaches may suffer from still too low temporal resolution and potentially too high phototoxicity, respectively, recent ultrafast, low-phototoxic light-sheet based optical microscopes (Wu *et al.* 2013; Chen *et al.* 2014) so far do not give sub-diffraction spatial resolution.

It is becoming obvious that lens-based far-field fluorescence nanoscopy opens up unprecedented possibilities for biophysical and medical research. Wide-spread availability of instrumentation and expertise and the targeted application to important problems will enable the full impact of far-field nanoscopy to be realized, with many answers to long-standing scientific quests.

5. Acknowledgements

6. References

ABBE, E. (1873). Beiträge zur Theorie des Mikroskops und der mikroskopischen Wahrnehmung. *Archiv für Mikroskopische Anatomie* **9**, 413–468.

ALBERTS, B., JOHNSON, A., LEWIS, J., RAFF, M., ROBERTS, K. & WALTER, P. (2002). *Molecular Biology of the Cell*, 4 edn. New York: Garland Science.

ANBAR, M. & HART, E. J. (1964). Reactivity of aromatic compounds toward hydrated electrons. *Journal of the American Chemical Society* **86**(24), 5633–5637.

ANDO, R., MIZUNO, H. & MIYAWAKI, A. (2004). Regulated fast nucleocytoplasmic shuttling observed by reversible protein highlighting. *Science* **306**(5700), 1370–1373.

ANDRESEN, M., STIEL, A. C., TROWITZSCH, S., WEBER, G., EGGELING, C., WAHL, M. C., HELL, S. W. & JAKOBS, S. (2007). Structural basis for reversible photoswitching in Dronpa. *Proceedings of the National Academy of Sciences of the United States of America* **104**, 13005–13009.

ANDRESEN, M., WAHL, M. C., STIEL, A. C., GRATER, F., SCHAFER, L. V., TROWITZSCH, S., WEBER, G., EGGELING, C., GRUBMULLER, H., HELL, S. W. & JAKOBS, S. (2005). Structure and mechanism of the reversible photoswitch of a fluorescent protein. *Proceedings of the National Academy of Sciences of the United States of America* **102**(37), 13070–13074.

ANDREW, T. L., TSAI, H. Y. & MENON, R. (2009). Confining light to deep subwavelength dimensions to enable optical nanopatterning. *Science* **324**(5929), 917–921.

ANNIBALE, P., VANNI, S., SCARSELLI, M., ROTHLISBERGER, U. & RADENOVIC, A. (2011). Identification of clustering artifacts in photoactivated localization microscopy. *Nature Method* **8**, 527–528. doi: 10.1038/nmeth.1627.

AQUINO, D., SCHÖNLE, A., GEISLER, C., MIDDENDORFF, C. V., WURM, C. A., OKAMURA, Y., LANG, T., HELL, S. W. & EGNER, A. (2011). Two-color nanoscopy of three-dimensional volumes by 4Pi detection of stochastically switched fluorophores. *Nature Method* **8**(4), 353–359.

ASH, E. A. & NICHOLLS, G. (1972). Super-resolution aperture scanning microscope. *Nature* **237**, 510–512.

AUKSORIUS, E., BORUAH, B. R., DUNSBY, C., LANIGAN, P. M. P., KENNEDY, G., NEIL, M. A. A. & FRENCH, P. M. W. (2008). Stimulated emission depletion microscopy with a supercontinuum source and fluorescence lifetime imaging. *Optics Letters* **33** (2), 113–115.

AXELROD, D. (1981). Cell-substrate contacts illuminated by total internal reflection fluorescence. *Journal of Cell Biology* **89**, 141–145.

BACKER, A. S., BACKLUND, M. P., LEW, M. D. & MOERNER, W. E. (2013). Single-molecule orientation measurements with a quadrated pupil. *Optics Letters* **38** (9), 1521–1523.

BACKER, A. S., BACKLUND, M. P., VON DIEZMANN, A. R., SAHL, S. J. & MOERNER, W. E. (2014). A bisected pupil for studying single-molecule orientational dynamics and its application to three-dimensional super-resolution microscopy. *Applied Physics Letters* **104**(19), 193701.

BACKLUND, M. P., LEW, M. D., BACKER, A. S., SAHL, S. J., GROVER, G., AGRAWAL, A., PIESTUN, R. & MOERNER, W. E. (2012). Simultaneous, accurate measurement of the 3D position and orientation of single molecules. *Proceedings of the National Academy of Sciences* **109**(47), 19087–19092.

BACKLUND, M. P., LEW, M. D., BACKER, A. S., SAHL, S. J. & MOERNER, W. E. (2014). The role of molecular dipole orientation in single-molecule fluorescence microscopy and implications for super-resolution imaging. *ChemPhysChem* **15**(4), 587–599.

BADDELEY, D., JAYASINGHE, I. D., CREMER, C., CANNELL, M. B. & SOELLER, C. (2009). Light-induced dark states of organic fluochromes enable 30 nm resolution imaging in standard media. *Biophysical Journal* **96**(2), L22–L24.

BAILEY, B., FARKAS, D. L., TAYLOR, D. L. & LANNI, F. (1993). Enhancement of axial resolution in fluorescence microscopy by standing-wave excitation. *Nature* **366**, 44–48.

BALASUBRAMANIAN, G., CHAN, I. Y., KOLESOV, R., AL-HMOUD, M., TISLER, J., SHIN, C., KIM, C., WOJCIK, A., HEMMER, P. R., KRUEGER, A., HANKE, T., LEITENSTORFER, A., BRATSCHITSCH, R., JELEZKO, F. & WRACHTRUP, J. (2008). Nanoscale imaging magnetometry with diamond spins under ambient conditions. *Nature* **455**, 648–651.

BATES, M., BLOSSER, T. R. & ZHUANG, X. W. (2005). Short-range spectroscopic ruler based on a single-molecule optical switch. *Physical Review Letters* **94**, 108101.

BATES, M., DEMPSEY, G. T., CHEN, K. H. & ZHUANG, X. (2011). Multicolor super-resolution fluorescence imaging via multi-parameter fluorophore detection. *ChemPhysChem* **13**(1), 99–107.

BATES, M., HUANG, B., DEMPSEY, G. T. & ZHUANG, X. W. (2007). Multicolor super-resolution imaging with photo-switchable fluorescent probes. *Science* **317**, 1749–1753.

BATES, M., HUANG, B. & ZHUANG, X. W. (2008). Super-resolution microscopy by nanoscale localization of photo-switchable fluorescent probes. *Current Opinion in Chemical Biology* **12**(5), 505–514.

BERGERMANN, F., ALBER, L., SAHL, S. J., ENGELHARDT, J. & HELL, S. W. (2015). 2000-fold parallelized dual-color STED fluorescence nanoscopy *Optics Express* **23**(1), 211–223.

BERNING, S., WILLIG, K. I., STEFFENS, H., DIBAJ, P. & HELL, S. W. (2012). Nanoscopy in a living mouse brain. *Science* **335**, 551.

BERTERO, M. & BOCCACCI, P. (1998). *Introduction to Inverse Problems in Imaging*. Institute of Physics Publishing, Bristol, UK.

BERTERO, M., BOCCACCI, P., BRAKENHOFF, G. J., MALFANTI, F. & VAN DER VOORT, H. T. M. (1990). Three-dimensional image restoration and super-resolution in fluorescence confocal microscopy. *Journal of Microscopy* **157**, 3–20.

BETHGE, P., CHEREAU, R., AVIGNONE, E., MARSICANO, G. & NÄGERL, U. V. (2013). Two-photon excitation STED microscopy in two colors in acute brain slices. *Biophysical Journal* **104**, 778–785.

BETZIG, E., CHICHESTER, R. J., LANNI, F. & TAYLOR, D. L. (1993). Near-field fluorescence imaging of cytoskeletal actin. *Bioimaging* **1**, 129–136.

BETZIG, E., PATTERSON, G. H., SOUGRAT, R., LINDWASSER, O. W., OLENYCH, S., BONIFACINO, J. S., DAVIDSON, M. W., LIPPINCOTT-SCHWARTZ, J. & HESS, H. F. (2006). Imaging intracellular fluorescent proteins at nanometer resolution. *Science* **313**(5793), 1642–1645.

BEWERSDORF, J., BENNETT, B. T. & KNIGHT, K. L. (2006). H2AX chromatin structures and their response to DNA damage revealed by 4Pi microscopy. *Proceedings of the National Academy of Sciences of the United States of America* **103**, 18137–18142.

BIANCHINI, P. & DIASPRO, A. (2012). Fast scanning STED and two-photon fluorescence excitation microscopy with continuous wave beam. *Journal of Microscopy* **245**(3), 225–228.

BIERWAGEN, J., TESTA, I., FÖLLING, J., WENZEL, D., JAKOBS, S., EGGELING, C. & HELL, S. W. (2010). Far-field autofluorescence nanoscopy. *Nano Letters* **2010**(10), 4249–4252.

BINGEN, P., REUSS, M., ENGELHARDT, J. & HELL, S. W. (2011). Parrallelized STED fluorescence nanoscopy. *Optics Express* **19**(24), 23716–23726.

BITEEN, J. S., THOMPSON, M. A., TSELENTIS, N. K., BOWMAN, G. R., SHAPIRO, L. & MOERNER, W. E. (2008). Super-resolution imaging in live caulobacter crescentus cells using photoswitchable EYFP. *Nature Methods* **5**, 947–949.

BITEEN, J. S., THOMPSON, M. A., TSELENTIS, N. K., SHAPIRO, L. & MOERNER, W. E. (2009). Superresolution imaging in live Caulobacter crescentus cells using photoswitchable enhanced yellow fluorescent protein. *Proceedings SPIE* **7185**, 71850I.

BLOEMBERGEN, N. (1965). *Nonlinear Optics*. New York: Benjamin.

BLOM, H., KASTRUP, L. & EGGELING, C. (2006). Fluorescence fluctuation spectroscopy in reduced detection volumes. *Current Pharmaceutical Biotechnology* **7**(1), 51–66.

BLOM, H., RÖNNLUND, D., SCOTT, L., SPICAROVA, Z., RANTANEN, V., WIDENGREN, J., APERIA, A. & BRISMAR, H. (2012). Nearest neighbor analysis of dopamine D1 receptors and Na1-K1-ATPases in dendritic spines dissected by STED microscopy. *Microscopy Research and Technique* **75**, 220–228.

BLOM, H., RÖNNLUND, D., SCOTT, L., SPICAROVA, Z., WIDENGREN, J., BONDAR, A., APERIA, A. & BRISMAR, H. (2011). Spatial distribution of Na+-K+-ATPase in dendritic spines dissected by nanoscale superresolution STED microscopy. *BMC Neuroscience* **12**, 16.

BOBROFF, N. (1986). Position measurement with a resolution and noise-limited instrument. *Review of Scientific Instruments* **57**(6), 1152–1157.

BOCK, H. (2008). *High-Resolution Fluorescence Microscopy with Photoswitchable Fluorescent Proteins*. Germany: University Goettingen.

BOCK, H., GEISLER, C., WURM, C. A., VON MIDDENDORFF, C., JAKOBS, S., SCHÖNLE, A., EGNER, A., HELL, S. W. & EGGELING, C. (2007). Two-color far-field fluorescence nanoscopy based on photoswitchable emitters. *Applied Physics B: Lasers and Optics* **88**(8), 161–165.

BORLINGHAUS, R. T. (2006). Mrt letter: high speed scanning has the potential to increase fluorescence yield and to reduce photobleaching. *Microscopy Research and Technique* **69**, 689–692.

BORN, M. & WOLF, E. (2002). *Principles of Optics*, 7th edn. Cambridge, New York, Melbourne, Madrid, Cape Town: Cambridge University Press.

BOSSI, M., FOELLING, J., BELOV, V. N., BOYARSKIY, V. P., MEDDA, R., EGNER, A., EGGELING, C., SCHOENLE, A. & HELL, S. W. (2008). Multi-color far-field fluorescence nanoscopy through isolated detection of distinct molecular species. *Nano Letters* **8**(8), 2463–2468.

BOSSI, M., FOELLING, J., DYBA, M., WESTPHAL, V. & HELL, S. W. (2006). Breaking the diffraction resolution barrier in far-field microscopy by molecular optical bistability. *New Journal of Physics* **8**, 275.

BOYARSKIY, V. P., BELOV, V. N., MEDDA, R., HEIN, B., BOSSI, M. & HELL, S. W. (2008). Photostable, amino reactive and water-soluble fluorescent labels based on sulfonated rhodamine with a rigidized xanthene fragment. *Chemistry: A European Journal* **14**, 1784–1792.

BRAKEMANN, T., STIEL, A. C., WEBER, G., ANDRESEN, M., TESTA, I., GROTJOHANN, T., LEUTENEGGER, M., PLESSMANN, U., URLAUB, H., EGGELING, C., WAHL, M., HELL, S. W. & JAKOBS, S. (2011). A reversibly photoswitchable GFP-like protein with fluorescence excitation decoupled from switching. *Nature Biotechnology* **29**, 942–947.

BRETSCHNEIDER, S., EGGELING, C. & HELL, S. W. (2007). Breaking the diffraction barrier in fluorescence microscopy by optical shelving. *Physical Review Letters* **98**(21), 218103.

BROWN, D. A. & LONDON, E. (2000). Structure and function of sphingolipid- and cholesterol-rich membrane rafts. *Journal of Biological Chemistry* **275**(23), 17221–17224.

BÜCKERS, J., WILDANGER, D., VICIDOMINI, G., KASTRUP, L. & HELL, S. W. (2011). Simultaneous multi-lifetime multi-

color STED imaging for colocalization analyses. *Optics Express* **19**(4), 3130–3143.

BURNS, D. H., CALLIS, J. B., CHRISTIAN, G. D. & DAVIDSON, E. R. (1985). Strategies for attaining superresolution using spectroscopic data as constraints. *Applied Optics* **24**(2), 154–161.

CHEN, Y., MULLER, J. D., SO, P. T. C. & GRATTON, E. (1999). The photon counting histogram in fluorescence fluctuation spectroscopy. *Biophysical Journal* **77**, 553–567.

CHEN, B.-C., LEGANT, W.R., WANG, K., SHAO, L., MILKIE, D. E., DAVIDSON, M.W., JANETOPOULOS, C., WU, X.S., HAMMER III, J.A., LIU, Z., ENGLISH, B.P., MIMORI-KIYOSUE, Y., ROMERO, D.P., RITTER, A.T., LIPPINCOTT-SCHWARTZ, J., FRITZ-LAYLIN, L., MULLINS, R.D., MITCHELL, D.M., BEMBENEK, J.N., REYMANN, A.-C., BÖHME, R., GRILL, S.W., WANG, J.T., SEYDOUX, G., TULU, U.S., KIEHART, D.P., BETZIG, E. (2014). Lattice light-sheet microscopy: Imaging molecules to embryos at high spatiotemporal resolution. *Science* **346**, 1257998.

CHI, K. R. (2009). Super-resolution microscopy: breaking the limits. *Nature Methods* **6**(1), 15–18.

CHMYROV, A., ARDEN-JACOB, J., ZILLES, A., DREXHAGE, K. H. & WIDENGREN, J. (2008). Characterization of new fluorescent labels for ultra-high resolution microscopy. *Photochemical and Photobiological Sciences* **7**, 1378–1385.

CHMYROV, A., KELLER, J., GROTJOHANN, T., RATZ, M., D'ESTE, E., JAKOBS, S., EGGELING, C. & HELL, S. W. (2013). Nanoscopy with more than 100,000 'doughnuts'. *Nature Methods* **10**, 737–740.

CLAUSEN, M. & LAGERHOLM, B. C. (2011). The probe rules in single particle tracking. *Current Protein and Peptide Science* **12**, 699–713.

CLAUSEN, M. P., GALIANI, S., BERNARDINO DE LA SERNA, J., FRITZSCHE, M., CHOJNACKI, J., GEHMLICH, K., LAGERHOLM, B. C. & EGGELING, C. (2013). Pathways to optical STED microscopy. *NanoBioImaging* **1**(1), 1–12.

COGNET, L., TSYBOULSKI, D. A. & WEISMAN, R. B. (2008). Subdiffraction far-field imaging of luminescent single-walled carbon nanotubes. *Nano Letters* **8**(2), 749–753.

CONCHELLO, J.-A. & LICHTMAN, J. W. (2005). Optical sectioning microscopy. *Nature Methods* **2**(12), 920–931.

CONCHELLO, J. A. & MCNALLY, J. G. (1996). Fast regularization technique for expectation maximization alogorithm for optical sectioning microscopy. *Society of Photo-Optical Instrumentation Engineers. Proceedings* **2655**, 199–208.

COX, S., ROSTEN, E., MONYPENNY, J., JOVANOVIC-TALISMAN, T., BURNETTE, D.T., LIPPINCOTT-SCHWARTZ, J., JONES, G. E. & HEINTZMANN, R. (2012). Bayesian localization microscopy reveals nanoscale podosome dynamics. *Nature Methods* **9**(2), 195–200.

CREMER, C. & CREMER, T. (1978). Considerations on a laser-scanning-microscope with high-resolution and depth of field. *Microscopica Acta* **81**(1), 31–44.

CRONIN, B., DE WET, B. & WALLACE, M. I. (2009). Lucky imaging: improved localization accuracy for single molecule imaging. *Biophysical Journal* **96**(7), 2912–2917.

DAVE, R., TERRY, D. S., MUNRO, J. B. & BLANCHARD, S. C. (2009). Mitigating unwanted photophysical processes for improved single-molecule fluorescence imaging. *Biophysical Journal* **96**, 2371–2381.

DEAN, C., LIU, H., STAUDT, T., STAHLBERG, M. A., VINGILL, S., BUCKERS, J., KAMIN, D., ENGELHARDT, J., JACKSON, M. B., HELL, S. W. & CHAPMAN, E. R. (2012). Distinct subsets of Syt-IV/BDNF vesicles are sorted to axons versus dendrites and recruited to synapses by activity. *Journal of Neuroscience* **32**(16), 5398–5413.

DE BAKKER, B. I., DE LANGE, F., CAMBI, A., KORTERIK, J. P., VAN DIJK, E. M. H. P., VAN HULST, N. F., FIGDOR, C. G. & GARCIA-PARAJO, M. F. (2007). Nanoscale organization of the pathogen receptor DC-SIGN mapped by single-molecule high-resolution fluorescence microscopy. *ChemPhysChem* **8**(10), 1473–1480.

DEDECKER, P., HOFKENS, J. & HOTTA, J. I. (2008). Diffraction-unlimited optical microscopy. *Materials Today* **11**, 12–21.

DEDECKER, P., HOTTA, J. I., FLORS, C., SLIWA, M., UJI-I, H., ROEFFAERS, M. B.J., ANDO, R., MIZUNO, H., MIYAWAKI, A. & HOFKENS, J. (2007). Subdiffraction imaging through the selective donut-mode depletion of thermally stable photoswitchable fluorophores: numerical analysis and application to the fluorescent protein Dronpa. *Journal of the American Chemical Society* **129**(51), 16132–16141.

DEDECKER, P., MOA, G. C. H., DERTINGER, T. & ZHANG, J. (2012). Widely accessible method for superresolution fluorescence imaging of living systems. *Proceedings of the National Academy of Sciences of the United States of America* **109**(27), 10909–10914.

DEMPSEY, G. T., VAUGHAN, J. C., CHEN, K. H., BATES, M. & ZHUANG, X. (2011). Evaluation of fluorophores for optimal performance in localization-based super-resolution imaging. *Nature Methods* **8**(12), 1027–1036.

DENK, W. (1996). Two-photon excitation in functional biological imaging. *Journal of Biomedical Optics* **1**, 296–304.

DENK, W., STRICKLER, J. H. & WEBB, W. W. (1990). 2-photon laser scanning fluorescence microscopy. *Science* **248**, 73–76.

DERTINGER, T., COLYER, R., IYER, G., WEISS, S. & ENDERLEIN, J. (2009). Fast, background-free, 3D super-resolution optical fluctuation imaging (SOFI). *Proceedings of the National Academy of Sciences of the United States of America* **106**(52), 22287–22292.

DERTINGER, T., COLYER, R., VOGEL, R., ENDERLEIN, J. & WEISS, S. (2010). Achieving increased resolution and more pixels with Superresolution Optical Fluctuation Imaging (SOFI). *Optics Express* **18**(18), 18875–18885.

DICKSON, R. M., CUBITT, A. B., TSIEN, R. Y. & MOERNER, W. E. (1997). On/off blinking and switching

behaviour of single molecules of green fluorescent protein. *Nature* **388**(6640), 355–358.

DIGMAN, M. A., DALAL, R., HORWITZ, A. F. & GRATTON, E. (2008). Mapping the number of molecules and brightness in the laser scanning microscope. *Biophysical Journal* **94**, 2320–2332.

DING, J. B., TAKASAKI, K. T. & SABATINI, B. L. (2009). Supraresolution imaging in brain slices using stimulated-emission depletion two-photon laser scanning microscopy. *Neuron* **63**, 429–437.

DITTRICH, P. S. & SCHWILLE, P. (2001). Photobleaching and stabilization of fluorophores used for single-molecule analysis with one- and two-photon excitation. *Applied Physics B: Lasers and Optics* **73**, 829–837.

DONNERT, G., EGGELING, C. & HELL, S. W. (2007a). Major signal increase in fluorescence microscopy through dark-state relaxation. *Nature Methods* **4**(1), 81–86.

DONNERT, G., EGGELING, C. & HELL, S. W. (2009). Triplet-relaxation microscopy with bunched pulsed excitation. *Photochemistry and Photobiology* **8**, 481–485.

DONNERT, G., KELLER, J., MEDDA, R., ANDREI, M. A., RIZZOLI, S. O., LURMANN, R., JAHN, R., EGGELING, C. & HELL, S. W. (2006). Macromolecular-scale resolution in biological fluorescence microscopy. *Proceedings of the National Academy of Sciences of the United States of America* **103**(31), 11440–11445.

DONNERT, G., KELLER, J., WURM, C. A., RIZZOLI, S. O., WESTPHAL, V., SCHOENLE, A., JAHN, R., JAKOBS, S., EGGELING, C. & HELL, S. W. (2007b). Two-color far-field fluorescence nanoscopy. *Biophysical Journal* **92**(8), L67–L69.

DYBA, M. & HELL, S. W. (2002). Focal spots of size lambda/23 open up far-field florescence microscopy at 33 nm axial resolution. *Physical Review Letters* **88**(16), 163901.

DYBA, M. & HELL, S. W. (2003). Photostability of a fluorescent marker under pulsed excited-state depletion through stimulated emission. *Applied Optics* **42**(25), 5123–5129.

DYBA, M., JAKOBS, S. & HELL, S. W. (2003). Immunofluorescence stimulated emission depletion microscopy. *Nature Biotechnology* **21**(11), 1303–1304.

EGGELING, C. (2012). STED-FCS nanoscopy of membrane dynamics. In *Fluorescent Methods to Study Biological Membranes*, **vol. 13** (eds. Y. MELY & G. DUPORTAIL), pp. 291–309. Berlin: Springer-Verlag.

EGGELING, C., BERGER, S., BRAND, L., FRIES, J. R., SCHAFFER, J., VOLKMER, A. & SEIDEL, C. A. M. (2001a). Data registration and selective single-molecule analysis using multi-parameter fluorescence detection. *Journal of Biotechnology* **86**, 163–180.

EGGELING, C., HILBERT, M., BOCK, H., RINGEMANN, C., HOFMANN, M., STIEL, A. C., ANDRESEN, M., JAKOBS, S., EGNER, A., SCHÖNLE, A. & HELL, S. W. (2007). Reversible photoswitching enables single-molecule fluorescence fluctuation spectroscopy at high molecular

concentration. *Microscopy Research and Technique* **70**(12), 1003–1009.

EGGELING, C., RINGEMANN, C., MEDDA, R., SCHWARZMANN, G., SANDHOFF, K., POLYAKOVA, S., BELOV, V. N., HEIN, B., VON MIDDENDORFF, C., SCHÖNLE, A. & HELL, S. W. (2009). Direct observation of the nanoscale dynamics of membrane lipids in a living cell. *Nature* **457**, 1159–U1121.

EGGELING, C., SCHAFFER, J., VOLKMER, A., SEIDEL, C. A. M., BRAND, L., JAEGER, S. & GALL, K. (2001b). Multi-parameter fluorescence detection at the single-molecule level: techniques and applications. In *Proceedings: 2. Biosensor Symposium*, Tuebingen, Germany.

EGGELING, C., VOLKMER, A. & SEIDEL, C. A. M. (2005). Molecular photobleaching kinetics of rhodamine 6 G by one- and two-photon induced confocal fluorescence microscopy. *ChemPhysChem* **6**, 791–804.

EGGELING, C., WIDENGREN, J., BRAND, L., SCHAFFER, J., FELEKYAN, S. & SEIDEL, C. A. M. (2006). Analysis of photobleaching in single-molecule multicolor excitation and forster resonance energy transfer measurement. *Journal of Physical Chemistry Part A: Molecules, Spectroscopy, Kinetics, Environment and General Theory* **110**(9), 2979–2995.

EGGELING, C., WIDENGREN, J., RIGLER, R. & SEIDEL, C. A. M. (1998). Photobleaching of fluorescent dyes under conditions used for single-molecule detection: evidence of two-step photolysis. *Analytical Chemistry* **70**, 2651–2659.

EGGELING, C., WIDENGREN, J., RIGLER, R. & SEIDEL, C. A. M. (1999). Photostabilities of fluorescent dyes for single-molecule spectroscopy: mechanisms and experimental methods for estimating photobleaching in aqueous solution. In *Applied Fluorescence in Chemistry, Biology and Medicine* (eds. W. RETTIG, B. STREHMEL, M. SCHRADER & H. SEIFERT), pp. 193–240. Berlin: Springer.

EGGELING, C., WILLIG, K. I. & BARRANTES, F. J. (2013). STED microscopy of living cells – New frontiers in membrane and neurobiology. *Journal of Neurochemistry* **126**(2), 203–212.

EGNER, A., GEISLER, C., VON MIDDENDORFF, C., BOCK, H., WENZEL, D., MEDDA, R., ANDRESEN, M., STIEL, A.-C., JAKOBS, S., EGGELING, C., SCHOENLE, A. & HELL, S. W. (2007). Fluorescence nanoscopy in whole cells by asynchronous localization of photoswitching emitters. *Biophysical Journal* **93**, 3285–3290.

EGNER, A. & HELL, S. W. (2005). Fluorescence microscopy with super-resolved optical sections. *Trends in Cell Biology* **15**(4), 207–215.

EGNER, A., JAKOBS, S. & HELL, S. W. (2002). Fast 100-nm resolution three-dimensional microscope reveals structural plasticity of mitochondria in live yeast. *Proceedings of the National Academy of Sciences of the United States of America* **99**, 3370–3375.

EGNER, A., VERRIER, S., GOROSHKOV, A., SOLING, H. D. & HELL, S. W. (2004). 4Pi-microscopy of the Golgi

apparatus in live mammalian cells. *Journal of Structural Biology* **147**(1), 70–76.

EHRENBERG, M. & RIGLER, R. (1974). Rotational brownian motion and fluorescence intensity fluctuations. *Chemical Physics* **4**(3), 390–401.

ENDERLEIN, J., TOPRAK, E. & SELVIN, P. R. (2006). Polarization effect on position accuracy of fluorophore localization. *Optics Express* **14**(18), 8111–8120.

ENDESFELDER, U., VAN DE LINDE, S., WOLTER, S., SAUER, M. & HEILEMANN, M. (2010). Subdiffraction-resolution fluorescence microscopy of myosin–actin motility. *ChemPhysChem* **11**(4), 836–840.

ENGELHARDT, J., KELLER, J., HOYER, P., REUSS, M., STAUDT, T. & HELL, S. W. (2011). Molecular orientation affects localization accuracy in superresolution far-field fluorescence microscopy. *Nano Letters* **11**(1), 209–213.

EVANKO, D. (2009). Primer: fluorescence imaging under the diffraction limit. *Nature Methods* **6**(1), 19–20.

FAHEY, P. F., KOPPEL, D. E., BARAK, L. S., WOLF, D. E., ELSON, E. L. & WEBB, W. W. (1977). Lateral diffusion in planar lipid bilayers. *Science* **195**(4275), 305–306.

FEDER, T. J., BRUST-MASCHER, I., SLATTERY, J. P., BAIRD, B. A. & WEBB, W. W. (1996). Constrained diffusion or immobile fraction on cell surfaces: a new interpretation. *Biophysical Journal* **70**, 2767–2773.

FERINGA, B. L., ed. (2001). *Molecular Switches*. Weinheim: Wiley-VCH.

FERNANDEZ-SUAREZ, M. & TING, A. Y. (2008). Fluorescent probes for super-resolution imaging in living cells. Nature Reviews. *Molecular Cell Biology* **9**, 929–943.

FIELDING, C. J., ed. (2006). *Lipid Rafts and Caveolae*. Weinheim: Wiley-VCH.

FIOLKA, R., BECK, M. & STEMMER, A. (2008). Structured illumination in total internal reflection fluorescence microscopy using a spatial light modulator. *Optics Letters* **33**(14), 1629–1631.

FISCHER, J., FREYMANN, G. & WEGENER, M. (2010). The materials challenge in diffraction-unlimited direct-laser-writing optical lithography. *Advanced Materials* **22**(32), 3578–3582.

FITZPATRICK, J. A., YAN, Q., SIEBER, J. J., DYBA, M., SCHWARZ, U., SZENT-GYORGYI, C., WOOLFORD, C. A., BERGET, P. B., WAGGONER, A. S. & BRUCHEZ, M. P. (2009). STED nanoscopy in living cells using fluorogen activating proteins. *Bioconjugate Chemistry* **20**(10), 1843–1847.

FLORS, C., RAVARANI, N. J. & DRYDEN, D. T. F. (2009). Super-resolution imaging of DNA labelled with intercalating dyes. *ChemPhysChem* **10**, 2201–2204.

FÖLLING, J., BELOV, V., KUNETSKY, R., MEDDA, R., SCHÖNLE, A., EGNER, A., EGGELING, C., BOSSI, M. & HELL, S. W. (2007). Photochromic rhodamines provide nanoscopy with optical sectioning. *Angewandte Chemie (international Edition)* **46**, 6266–6270.

FÖLLING, J., BELOV, V., RIEDEL, D., SCHÖNLE, A., EGNER, A., EGGELING, C., BOSSI, M. & HELL, S. W.

(2008a). Fluorescence nanoscopy with optical sectioning by two-photon induced molecular switching using continuous-wave lasers. *ChemPhysChem* **9**, 321–326.

FÖLLING, J., BOSSI, M., BOCK, H., MEDDA, R., WURM, C. A., HEIN, B., JAKOBS, S., EGGELING, C. & HELL, S. W. (2008b). Fluorescence nanoscopy by ground-state depletion and single-molecule return. *Nature Methods* **5**, 943–945.

FRIEDEMANN, K., TURSHATOV, A., LANDFESTER, K. & CRESPY, D. (2011). Characterization via two-color STED microscopy of nanostructured materials synthesized by colloid electrospinning. *Langmuir* **27**(11), 7132–7139.

FRIEDRICH, M., GAN, Q., ERMOLAYEV, V. & HARMS, G. S. (2011). STED-SPIM: stimulated emission depletion improves sheet illumination microscopy resolution. *Biophysical Journal* **100**, L43–L45.

FROHN, J. T., KNAPP, H. F. & STEMMER, A. (2000). True optical resolution beyond the Rayleigh limit achieved by standing wave illumination. *Proceedings of the National Academy of Sciences of the United States of America* **97**, 7232–7236.

FU, C. C., LEE, H. Y., CHEN, K., LIM, T. S., WU, H. Y., LIN, P. K., WEI, P. K., TSAO, P. H., CHANG, H. C. & FANN, W. (2007). Characterization and application of single fluorescent nanodiamonds as cellular biomarkers. *Proceedings of the National Academy of Sciences of the United States of America* **104**(3), 727–732.

GEERTS, H., DEBRABANDER, M., NUYDENS, R., GEUENS, S., MOEREMANS, M., DEMEY, J. & HOLLENBECK, P. (1987). Nanovid Tracking – a New Automatic Method for the study of mobility in living cells based on colloidal gold and video microscopy. *Biophysical Journal* **52**, 775–782.

GEISLER, C., SCHOENLE, A., VON MIDDENDORFF, C., BOCK, H., EGGELING, C., EGNER, A. & HELL, S. W. (2007). Resolution of l/10 in fluorescence microscopy using fast single molecule photo-switching. *Applied Physics A: Materials Science and Processing* **88**(2), 223–226.

GEISSBUEHLER, S., BOCCHIO, N. L., DELLAGIACOMA, C., BERCLAZ, C., LEUTENEGGER, M. & LASSER, T. (2012). Mapping molecular statistics with balanced super-resolution optical fluctuation imaging (bSOFI). *Optical Nanoscopy* **1**(4).

GEISSBUEHLER, S., DELLAGIACOMA, C. & LASSER, T. (2011). Comparison between SOFI and STORM. *Biomedical Optics Express* **2**(3), 408–420.

GIANNONE, G., HOSY, E., LEVET, F., CONSTALS, A., SCHULZE, K., SOBOLEVSKY, A. I., ROSCONI, M. P., GOUAUX, E., TAMPE, R., CHOQUET, D. & COGNET, L. (2010). Dynamic superresolution imaging of endogenous proteins on living cells at ultra-high density. *Biophysical Journal* **2010**, 1303–1310.

GISKE, A. (2007). CryoSTED microscopy – a new spectroscopic approach for improving the resolution of STED

microscopy using low temperature. University of Heidelberg.

GORDON, M. P., HA, T. & SELVIN, P. R. (2004). Single-molecule high-resolution imaging with photo-bleaching. *Proceedings of the National Academy of Sciences of the United States of America* **101**, 6462–6465.

GÖTTFERT, F., WURM, C. A., MUELLER, V., BERNING, S., CORDES, V. C., HONIGMANN, A. & HELL, S. W. (2013). Coaligned dual-channel STED nanoscopy and molecular diffusion analysis at 20 nm resolution. *Biophysical Journal* **105**, L01–L03.

GOULD, T. J., BURKE, D., BEWERSDORF, J. & BOOTH, M. J. (2012). Adaptive optics enables 3D STED microscopy in aberrating specimens. *Optics Express* **20**(19), 20998.

GOULD, T. J., GUNEWARDENE, M. S., GUDHETI, M. V., VERKHUSHA, V. V., YIN, S. R., GOSSE, J. A. & HESS, S. T. (2008). Nanoscale imaging of molecular positions and anisotropies. *Nature Methods* **5**(12), 1027–1030.

GOULD, T. J., KROMANN, E. B., BURKE, D., BOOTH, M. J. & BEWERSDORF, J. (2013). Auto-aligning stimulated emission depletion microscope using adaptive optics. *Optics Letters* **38**(11), 1860–1862.

GOULD, T. J., MYERS, J. R. & BEWERSDORF, J. (2011). Total internal reflection STED microscopy. *Optics Express* **19**(14), 13351–13357.

GROTJOHANN, T., TESTA, I., LEUTENEGGER, M., BOCK, H., URBAN, N. T., LAVOIE-CARDINAL, F., WILLIG, K. I., EGGELING, C., JAKOBS, S. & HELL, S. W. (2011). Diffraction-unlimited all-optical imaging and writing with a photochromic GFP. *Nature*, **478**, 204–208.

GROTJOHANN, T., TESTA, I., REUSS, M., BRAKEMANN, T., EGGELING, C., HELL, S. W. & JAKOBS, S. (2012). rsEGFP2 enables fast RESOLFT nanoscopy of living cells. **eLIFE 1**, e00248.

GUGEL, H., BEWERSDORF, J., JAKOBS, S., ENGELHARDT, J., STORZ, R. & HELL, S. W. (2004). Cooperative 4pi excitation and detection yields sevenfold sharper optical sections in live-cell microscopy. *Biophysical Journal* **87**, 4146–4152.

GUNEWARDENE, M. S., SUBACH, F. V., GOULD, T. J., PENONCELLO, G. P., GUDHETI, M. V., VERKHUSHA, V. V. & HESS, S. T. (2011). superresolution imaging of multiple fluorescent proteins with highly overlapping emission spectra in living cells. *Biophysical Journal* **101**, 1522–1528.

GUSTAFSSON, M. G., AGARD, D. A. & SEDAT, J. W. (1996). 3D widefield microscopy with two objective lenses: experimental verification of improved axial resolution. In *Three-Dimensional Microscopy: Image Acquisition and Processing III*, vol. **2655** (ed. C. COGSWELL, G. S. KINO & T. WILSON), San Jose, CA, USA, pp. 62–66. Proc. SPIE.

GUSTAFSSON, M. G. L. (2000). Surpassing the lateral resolution limit by a factor of two using structured illumination microscopy. *Journal of Microscopy* **198**(2), 82–87.

GUSTAFSSON, M. G. L. (2005). Nonlinear structured-illumination microscopy: wide-field fluorescence imaging with theoretically unlimited resolution. *Proceedings of the National Academy of Sciences of the United States of America* **102**(37), 13081–13086.

GUSTAFSSON, M. G. L., AGARD, D. A. & SEDAT, J. W. (1995). Sevenfold improvement of axial resolution in 3D widefield microscopy using two objective lenses. *SPIE – the International Society for Optical Engineering. Proceedings* **2412**, 147–156.

GUSTAFSSON, M. G. L., AGARD, D. A. & SEDAT, J. W. (1999). (im)-m-5: 3d widefield light microscopy with better than 100 nm axial resolution. *Journal of Microscopy* **195**, 10–16.

GUSTAFSSON, M. G. L., SHAO, L., CARLTON, P. M., WANG, C. J. R., GOLUBOVSKAYA, I. N., CANDE, W. Z., AGARD, D. A. & SEDAT, J. W. (2008). Three-dimensional resolution doubling in wide-field fluorescence microscopy by structured illumination. *Biophysical Journal* **94**(12), 4957–4970.

HABUCHI, S., DEDECKER, P., HOTTA, J. I., FLORS, C., ANDO, R., MIZUNO, H., MIYAWAKI, A. & HOFKENS, J. (2006). Photo-induced protonation/deprotonation in the GFP-like fluorescent protein Dronpa: mechanism responsible for the reversible photoswitching. *Photochemistry and Photobiology* **5**, 567–576.

HAN, K. Y., KIM, S. K., EGGELING, C. & HELL, S. (2010). Metastable dark states enable ground state depletion microscopy of nitrogen vacancy centers in diamond with diffraction-unlimited resolution. *Nano Letters* **10**(8), 3199–3203.

HAN, K. Y., WILDANGER, D., RITTWEGER, E., MEIJER, J., PEZZAGNA, S., HELL, S. W. & EGGELING, C. (2012). Dark state photophysics of nitrogen–vacancy centres in diamond. *New Journal of Physics* **14**, 123002.

HAN, K. Y., WILLIG, K. I., RITTWEGER, E., JELEZKO, F., EGGELING, C. & HELL, S. W. (2009). Three-dimensional stimulated emission depletion microscopy of nitrogen-vacancy centers in diamond using continuous-wave light. *Nano Letters* **9**(9), 3323–3329.

HANCOCK, J. F. (2006). Lipid rafts: contentious only from simplistic standpoints. *Nature Reviews. Molecular Cell Biology* **7**, 457–462.

HANZAL-BAYER, M. F. & HANCOCK, J. F. (2007). Lipid rafts and membrane traffic. *F E B S Letters* **581**, 2098–2104.

HARKE, B. (2008). *3D STED Microscopy with Pulsed and Continuous Wave Lasers*. PhD thesis, Georg-August-University Goettingen.

HARKE, B., BIANCHINI, P., BRANDI, F. & DIASPRO, A. (2012). Photopolymerization inhibition dynamics for sub-diffraction direct laser writing lithography. *ChemPhysChem* **13**(6), 1429–1434.

HARKE, B., KELLER, J., ULLAL, C. K., WESTPHAL, V., SCHOENLE, A. & HELL, S. W. (2008a). Resolution scaling in STED microscopy. *Optics Express* **16**(6), 4154–4162.

HARKE, B., ULLAL, C. K., KELLER, J. & HELL, S. W. (2008b). Three-dimensional nanoscopy of colloidal crystals. *Nano Letters* **8**(5), 1309–1313.

HAUSTEIN, E. & SCHWILLE, P. (2003). Ultrasensitive investigations of biological systems by fluorescence correlation spectroscopy. *Methods* **29**(2), 153–166.

HE, H. T. & MARGUET, D. (2011). Detecting nanodomains in living cell membrane by fluorescence correlation spectroscopy. *Annual Review of Physical Chemistry* **62**, 417–436.

HEDDE, P. N., FUCHS, J., OSWALD, F., WIEDENMANN, J. & NIENHAUS, G. U. (2009). Online image analysis software for photoactivation localization microscopy. *Nature Methods* **6**(10), 689–690.

HEILEMANN, M., DEDECKER, P., HOFKENS, J. & SAUER, M. (2009a). Photoswitches: key molecules for subdiffraction-resolution fluorescence imaging and molecular quantification. *Laser and Photonics Reviews* **3**(1–2), 180–202.

HEILEMANN, M., VAN DE LINDE, S., MUKHERJEE, A. & SAUER, M. (2009b). Super-resolution imaging with small organic fluorophores. *Angewandte Chemie (international Edition)* **48**(37), 6903–6908.

HEILEMANN, M., VAN DE LINDE, S., SCHUTTPELZ, M., KASPER, R., SEEFELDT, B., MUKHERJEE, A., TINNEFELD, P. & SAUER, M. (2008). Subdiffraction-resolution fluorescence imaging with conventional fluorescent probes. *Angewandte Chemie (international Edition)* **47**, 6172–6176.

HEIN, B., WILLIG, K. I. & HELL, S. W. (2008). Stimulated emission depletion (sted) nanoscopy of a fluorescent protein-labeled organelle inside a living cell. *Proceedings of the National Academy of Sciences of the United States of America* **105**(38), 14271–14276.

HEIN, B., WILLIG, K. I., WURM, C. A., WESTPHAL, V., JAKOBS, S. & HELL, S. W. (2010). Stimulated emission depletion nanoscopy of living cells using SNAP-Tag fusion proteins. *Biophysical Journal* **98**, 158–163.

HEINTZMANN, R. & FICZ, G. (2007). Breaking the resolution limit in light microscopy. *Methods in Cell Biology* **81**, 561–580.

HEINTZMANN, R. & GUSTAFSSON, M. G. L. (2009). Subdiffraction resolution in continuous samples. *Nature Photonics* **3**(7), 362–364.

HEINTZMANN, R., JOVIN, T. M. & CREMER, C. (2002). Saturated patterned excitation microscopy – a concept for optical resolution improvement. *Optical Society of America. Journal A: Optics, Image Science, and Vision* **19**(8), 1599–1609.

HEISENBERG, W. (1930). *The Physical Principles of the Quantum Theory.* Chicago: Chicago University Press.

HELL, S. (2009a). Far-field optical nanoscopy. In *Single Molecule Spectroscopy in Chemistry* (eds. A. GRÄSLUND, R. RIGLER & J. WIDENGREN), pp. 365–398. Berlin: Springer.

HELL, S. W. (2007). Verfahren und Fluoreszenzlichtmikroskop zum raeumlich hochaufloesenden Abbilden einer Struktur einer Probe German Patent, vol. DE 10 2006 021 317.

HELL, S. W. (1992). Double-scanning confocal microscope. European Patent 0491289, vol. 0491289.

HELL, S. W. (1994). Improvement of lateral resolution in far-field light microscopy using two-photon excitation with offset beams. *Optics Communications* **106**, 19–24.

HELL, S. W. (2003). Toward fluorescence nanoscopy. *Nature Biotechnology* **21**(11), 1347–1355.

HELL, S. W. (2004). Strategy for far-field optical imaging and writing without diffraction limit. *Physics Letters. Section A: General, Atomic and Solid State Physics* **326**(1–2), 140–145.

HELL, S. W. (2007). Far-field optical nanoscopy. *Science* **316**(5828), 1153–1158.

HELL, S. W. (2009b). Microscopy and its focal switch. *Nature Methods* **6**(1), 24–32.

HELL, S. W., DYBA, M. & JAKOBS, S. (2004). Concepts for nanoscale resolution in fluorescence microscopy. *Current Opinion in Neurobiology* **14**(5), 599–609.

HELL, S. W., JAKOBS, S. & KASTRUP, L. (2003). Imaging and writing at the nanoscale with focused visible light through saturable optical transitions. *Applied Physics A: Materials Science and Processing* **77**, 859–860.

HELL, S. W. & KROUG, M. (1995). Ground-state depletion fluorescence microscopy, a concept for breaking the diffraction resolution limit. *Applied Physics B: Lasers and Optics* **60**, 495–497.

HELL, S. W., LINDEK, S., CREMER, C. & STELZER, E. H. K. (1994). Measurement of the 4Pi-confocal point spread function proves 75 nm resolution. *Applied Physics Letters* **64**(11), 1335–1338.

HELL, S. W., SCHMIDT, R. & EGNER, A. (2009). Diffraction-3unlimited three-dimensional optical nanoscopy with opposing lenses. *Nature Photonics* **3**, 381–387.

HELL, S. W. & STELZER, E. H. K. (1992). Properties of a 4pi confocal fluorescence microscope. *Optical Society of America. Journal A: Optics, Image Science, and Vision* **9**, 2159–2166.

HELL, S. W. & WICHMANN, J. (1994). Breaking the diffraction resolution limit by stimulated-emission – stimulated-emission-depletion fluorescence microscopy. *Optics Letters* **19**(11), 780–782.

HENRIQUES, R., LELEK, M., FORNASIERO, E. F., VALTORTA, F., ZIMMER, C. & MHLANGA, M. M. (2010). QuickPALM: 3D real-time photoactivation nanoscopy image processing in ImageJ. *Nature Methods* **7**(5), 339–340.

HERNANDEZ, I. C., D'AMORA, M., DIASPRO, A. & VICIDOMINI, G. (2014a). Influence of laser intensity noise on gated CW-STED microscopy Laser *Physics Letters* **11**(9), 095603.

HERNANDEZ, I. C., PERES, C., ZANACCHI, F. C., D'AMORA, M., CHRISTODOULOU, S., BIANCHINI, P., DIASPRO, A. & VICIDOMINI, G. (2014b). A new filtering technique for removing anti-Stokes emission background in gated CW-STED microscopy. *J. Biophotonics* **7**, 376–380.

HESS, S. T., GIRIRAJAN, T. P. K. & MASON, M. D. (2006). Ultra-high resolution imaging by fluorescence photoactivation localization microscopy. *Biophysical Journal* **91**(11), 4258–4272.

HESS, S. T., GOULD, T. J., GUDHETI, M. V., MAAS, S. A., MILLS, K. D. & ZIMMERBERG, J. (2007). Dynamic clustered distribution of hemagglutinin resolved at 40 nm in living cell membranes discriminates between raft theories. *Proceedings of the National Academy of Sciences of the United States of America* **104**(44), 17370–17375.

HOEBE, R. A., VAN OVEN, C. H., GADELLA, T. W. J., DHONUKSHE, P. B., VAN NOORDEN, C. J. F. & MANDERS, E. M. M. (2007). Controlled light-exposure microscopy reduces photobleaching and phototoxicity in fluorescence live-cell imaging. *Nat Biotech* **25**(2), 249–253.

HOFMANN, M. (2007). *RESOLFT-Mikroskopie mit photo-schaltbaren Proteinen*. Germany: University of Heidelberg.

HOFMANN, M., EGGELING, C., JAKOBS, S. & HELL, S. W. (2005). Breaking the diffraction barrier in fluorescence microscopy at low light intensities by using reversibly photoswitchable proteins. *Proceedings of the National Academy of Sciences of the United States of America* **102**(49), 17565–17569.

HOLDEN, S. J., UPHOFF, S. & KAPANIDIS, A. N. (2011). DAOSTORM: an algorithm for highdensity super-resolution microscopy. *Nature Methods* **8**(4), 279–280.

HONIGMANN, A., EGGELING, C., SCHULZE, M. & LEPERT, A. (2012). Super-resolution STED microscopy advances with yellow CW OPSL. *Laser Focus World* **48**(1), 75–79.

HONIGMANN, A., MUELLER, V., FERNANDO, U. P., EGGELING, C. & SPERLING, J. (2013a). Simplifying STED microscopy of photostable red-emitting labels. *Laser + Potonik* **5**, 40–42.

HONIGMANN, A., MUELLER, V., HELL, S. W. & EGGELING, C. (2013b). STED microscopy detects and quantifies liquid phase separation in lipid membranes using a new far-red emitting fluorescent phosphoglycerolipid analogue. *Faraday Discussion* **161**, 77–89.

HONIGMANN, A., MUELLER, V., TA, H., SCHOENLE, A., SEZGIN, E., HELL, S.W. & EGGELING, C. (2014). Scanning STED-FCS reveals spatiotemporal heterogeneity of lipid interaction in the plasma membrane of living cells. *Nature Communications* **5**:5412 doi: 10.1038/ncomms6412.

HOTTA, J., FRON, E., DEDECKER, P., JANSSEN, K. P. F., LI, C., MUELLEN, K., HARKE, B., BÜCKERS, J., HELL, S. W. & HOFKENS, J. (2010). Spectroscopic rationale for efficient stimulated-emission depletion microscopy fluorophores. *Journal of the American Chemical Society* **132**(14), 5021–5023.

HOYER, P., STAUDT, T., ENGELHARDT, J. & HELL, S. W. (2010). Quantum dot blueing and blinking enables fluorescence nanoscopy. *Nano Letters* **11**(1), 245–250.

HU, D. H., TIAN, Z. Y., WU, W. W., WAN, W. & LI, A. D. Q. (2008). Photoswitchable nanoparticles enable high-resolution cell imaging: PULSAR microscopy. *Journal of the American Chemical Society* **130**(46), 15279–15281.

HUANG, B. (2010). Super-resolution optical microscopy: multiple choices. *Current Opinion in Chemical Biology* **14**, 10–14.

HUANG, B., BABCOCK, H. & ZHUANG, X. (2010). Breaking the diffraction barrier: super-resolution imaging of cells. *Cell*, **143**, 1047–1058.

HUANG, B., BATES, M. & ZHUANG, X. (2009). Super-resolution fluorescence microscopy. *Annual Reviews of Biochemistry* **78**, 993–1016.

HUANG, B., WANG, W. Q., BATES, M. & ZHUANG, X. W. (2008). Three-dimensional super-resolution imaging by stochastic optical reconstruction microscopy. *Science* **319**, 810–813.

HUANG, F., HARTWICH, T. M. P., RIVERA-MOLINA, F. E., LIN, Y., DUIM, W. C., LONG, J. J., UCHIL, P. D., MYERS, J. R., BAIRD, M. A., MOTHES, W., DAVIDSON, M. W., TOOMRE, D. & BEWERSDORF, J. (2013). Video-rate nanoscopy using sCMOSCMOSCMOSCMOS camera–specific single-molecule localization algorithms. *Nature Methods* **10**(7), 653–658.

HUANG, F., SCHWARTZ, S. L., BYARS, J. M. & LIDKE, K. A. (2011). Simultaneous multiple-emitter fitting for single molecule super-resolution imaging. *Biomedical Optics Express* **2**(5), 1377–1393.

IRIE, M., FUKAMINATO, T., SASAKI, T., TAMAI, N. & KAWAI, T. (2002). A digital fluorescent molecular photo-switch. *Nature* **420**(6917), 759–760.

IRVINE, S. E., STAUDT, T., RITTWEGER, E., ENGELHARDT, J. & HELL, S. W. (2008). Direct light-driven modulation of luminescence from Mn-doped ZnSe quantum dots. *Angewandte Chemie (international Edition)* **47**(14), 2685–2688.

IZEDDIN, I., EL BEHEIRY, M., ANDILLA, J., CIEPIELEWSKI, D., DARZACQ, X. & DAHAN, M. (2012). PSF shaping using adaptive optics for threedimensional single-molecule super-resolution imaging and tracking. *Optics Express* **20**(5), 4957–4967.

IZEDDIN, I., SPECHT, C. G., LELEK, M., DARZACQ, X., TRILLER, A., ZIMMER, C. & DAHAN, M. (2011). Super-resolution dynamic imaging of dendritic spines using a low-affinity photoconvertible actin probe. *PloS ONE* **6**, e15611.

JACOBSON, K., MOURITSEN, O. G. & ANDERSON, G. W. (2007). Lipid rafts: at a crossroad between cell biology and physics. *Nature Cell Biology* **9**(1), 7–14.

JELEZKO, F. & WRACHTRUP, J. (2006). Single defect centres in diamond: a review. *Physica Status Solidi. A: Applications and Materials Science (Print)* **203**, 3207–3225.

JIA, S., VAUGHAN, J. C. & ZHUANG, X. (2014). Isotropic three-dimensional super-resolution imaging with a self-bending point spread function. *Nat Photon* **8**(4), 302–306.

JOLY, E. (2004). Hypothesis: could the signalling function of membrane microdomains involve a localized transition of lipids from liquid to solid state? *BMC Cell Biology* **5**(5), 3.

JONES, S. A., SHIM, S.-H., HE, J. & ZHUANG, X. (2011). Fast, three-dimensional super-resolution imaging of live cells. *Nature Methods* **8**(6), 499–505.

JUETTE, M. F., GOULD, T. J., LESSARD, M. D., MLODZIANOSKI, M. J., NAGPURE, B. S., BENNETT, B. T., HESS, S. T. & BEWERSDORF, J. (2008). Three-dimensional sub-100 nm resolution fluorescence microscopy of thick samples. *Nature Methods* **5**(6), 527–529.

KASHA, M. (1950). Characterization of electronic transitions in complex molecules. *Faraday Discussions* **9**, 14–19.

KASK, P., PALO, K., ULLMANN, D. & GALL, K. (1999). Fluorescence-intensity distribution analysis and its application in biomolecular detection technology. *Proceedings of the National Academy of Sciences of the United States of America* **96**, 13756–13761.

KASPER, R., HARKE, B., FORTHMANN, C., TINNEFELD, P., HELL, S. W. & SAUER, M. (2010). Single-molecule STED microscopy with photostable organic fluorophores. *Small* **6**(13), 1379–1384.

KASTRUP, L., BLOM, H., EGGELING, C. & HELL, S. W. (2005). Fluorescence fluctuation spectroscopy in sub-diffraction focal volumes. *Physical Review Letters* **94**, 178104.

KASTRUP, L., WILDANGER, D., RANKIN, B. & HELL, S. W. (2010). STED microscopy with compact light sources. In *Nanoscopy and Multidimensional Optical Fluorescence Microscopy* (ed. A. DIASPRO), pp. 1–13. Boca Raton: Chapman & Hall/CRC.

KELLER, J. (2006). *Optimal de-excitation patterns for RESOLFT-Microscopy*. PhD thesis, University of Heidelberg, Germany.

KELLNER, R., BAIER, J., WILLIG, K. I., HELL, S. W. & BARRANTES, F. J. (2007). Nanoscale organization of nicotinic acetylcholine receptors revealed by STED microscopy. *Neuroscience* **144**(1), 135–143.

KIRSCH, A., MEYER, C. & JOVIN, T. M. (1996). Integrating of optical techniques in scanning probe microscopes; the scanning near-field optical microscope (SNOM). In *Analytical Use of Fluorescenct Probes in Oncology* (eds. E. Kohen & J. G. Hirschberg), pp. 317–323. New York: Plenum Press.

KITTEL, R. J., WICHMANN, C., RASSE, T. M., FOUQUET, W., SCHMIDT, M., SCHMID, A., WAGH, D. A., PAWLU, C., KELLNER, R. R., WILLIG, K. I., HELL, S. W., BUCHNER, E., HECKMANN, M. & SIGRIST, S. J. (2006). Bruchpilot promotes active zone assembly, ca2+ channel clustering, and vesicle release. *Science* **312**, 1051–1054.

KLAR, T. A. & HELL, S. W. (1999). Subdiffraction resolution in far-field fluorescence microscopy. *Optics Letters* **24**(14), 954–956.

KLAR, T. A., JAKOBS, S., DYBA, M., EGNER, A. & HELL, S. W. (2000). Fluorescence microscopy with diffraction resolution barrier broken by stimulated emission. *Proceedings of the National Academy of Sciences of the United States of America* **97**, 8206–8210.

KLEIN, T., LOESCHBERGER, A., PROPPERT, S., WOLTER, S., VAN DE LINDE, S. & SAUER, M. (2011). Live-cell dSTORM with SNAP-tag fusion proteins. *Nature Methods* **8**(1), 7–9.

KOLMAKOV, K., BELOV, V. N., BIERWAGEN, J., RINGEMANN, C., MUELLER, V., EGGELING, C. & HELL, S. W. (2010a). Red-emitting rhodamine dyes for fluorescence microscopy and nanoscopy. *Chemistry – A European Journal* **16**(1), 158–166.

KOLMAKOV, K., BELOV, V. N., WURM, C. A., HARKE, B., LEUTENEGGER, M., EGGELING, C. & HELL, S. W. (2010b). A versatile route to red-emitting carbo-pyronine dyes for optical microscopy and nanoscopy. *European Journal of Organic Chemistry* **2010**(19), 3593–3610.

KOLMAKOV, K., WURM, C. A., HENNIG, R., RAPP, E., JAKOBS, S., BELOV, V. N. & HELL, S. W. (2012). Red-emitting rhodamines with hydroxylated, sulfonated, and phosphorylated dye residues and their use in fluorescence nanoscopy. *Chemistry – A European Journal* **18** (41), 12986–12998.

KOOPMAN, M., CAMBI, A., DE BAKKER, B. I., JOSTEN, B., FIGDOR, C. G., VAN HULST, N. F. & GARCIA-PARAJO, M. F. (2004). Near-field scanning optical microscopy in liquid for high resolution single molecule detection on dendritic cells. *FEBS Letters* **573**, 6–10.

KRUEGER, A. (2008). New carbon materials: biological applications of functionalized nanodiamond materials. *Chemistry – A European Journal* **14**, 1382–1390.

KUSUMI, A., NAKADA, C., RITCHIE, K., MURASE, K., SUZUKI, K., MURAKOSHI, H., KASAI, R. S., KONDO, J. & FUJIWARA, T. (2005). Paradigm shift of the plasmamembrane concept from the two-dimensional continuum fluid to the partitioned fluid: high-speed single-molecule tracking of membrane molecules. *Annual Review of Biophysics and Bioengineering* **34**, 351–378.

LAGERHOLM, B. C., AVERETT, L., WEINREB, G. E., JACOBSON, K. & THOMPSON, N. L. (2006). Analysis method for measuring submicroscopic distances with blinking quantum dots. *Biophysical Journal* **91**, 3050–3060.

LARSON, D. R. (2010). The economy of photons. *Nature Methods* **7**(5), 357–359.

LAU, L., LEE, Y. L., SAHL, S. J., STEARNS, T. & MOERNER, W. E. (2012). STED microscopy with optimized labeling density reveals 9-fold arrangement of a centriole protein. *Biophysical Journal* **102**, 2926–2935.

LAURENCE, T. A. & CHROMY, B. A. (2010). Efficient maximum likelihood estimator fitting of histograms. *Nature Methods* **5**(7), 338–339.

LAUTERBACH, M. A., KELLER, J., SCHÖNLE, A., KAMIN, D., WESTPHAL, V., RIZZOLI, S. O. & HELL, S. W. (2010a). Comparing video-rate STED nanoscopy and confocal microscopy of living neurons. *Journal of Biophotonics* **3** (7), 417–424.

LAUTERBACH, M. A., ULLAL, C. K., WESTPHAL, V. & HELL, S. (2010b). Dynamic imaging of colloidal-crystal

nanostructures at 200 frames per second. *Langmuir* **26** (18), 14400–14404.

LEE, H.-L. D., SAHL, S. J., LEW, M. D. & MOERNER, W. E. (2012). The double-helix microscope super-resolves extended biological structures by localizing single blinking molecules in three dimensions with nanoscale precision. *Applied Physics Letters* **100**(15), 153701.

LEE, M. K., RAI, P., WILLIAMS, J., TWIEG, R. J. & MOERNER, W. E. (2014). Small-molecule labeling of live cell surfaces for three-dimensional super-resolution microscopy. *Journal of the American Chemical Society* **136** (40), 14003–14006.

LEMMER, P., GUNKEL, M., BADDELEY, D., KAUFMANN, R., URICH, A., WEILAND, Y., REYMANN, J., MULLER, P., HAUSMANN, M. & CREMER, C. (2008). Spdm: light microscopy with single-molecule resolution at the nanoscale. *Applied Physics B: Lasers and Optics* **93**, 1–12.

LEMMER, P., GUNKEL, M., WEILAND, Y., MUELLER, P., BADDELEY, D., KAUFMANN, R., URICH, A., EIPEL, H., AMBERGER, R., HAUSMANN, M. & CREMER, C. (2009). Using conventional fluorescent markers for far-field fluorescence localization nanoscopy allows resolution in the 10-nm range. *Journal of Microscopy* **235**(2), 163–171.

LEUTENEGGER, M., EGGELING, C. & HELL, S. W. (2010). Analytical description of STED microscopy performance. *Optics Express* **18**(25), 26417.

LEUTENEGGER, M., GOESCH, M., PERENTES, A., HOFFMANN, P., MARTIN, O. J. F. & LASSER, T. (2006). Confining the sampling volume for Fluorescence Correlation Spectroscopy using a sub-wavelength sized aperture. *Optics Express* **14**(2), 956–969.

LEUTENEGGER, M., RINGEMANN, C., LASSER, T., HELL, S. W. & EGGELING, C. (2012). Fluorescence correlation spectroscopy with a total internal reflection fluorescence STED microscope (TIRF-STED-FCS). *Optics Express* **20**(5), 5243–5263.

LEVENE, M. J., KORLACH, J., TURNER, S. W., FOQUET, M., CRAIGHEAD, H. G. & WEBB, W. W. (2003). Zero-mode waveguides for single-molecule analysis at high concentrations. *Science* **299**, 682–686.

LEW, M. D., BACKLUND, M. P. & MOERNER, W. E. (2013). Rotational mobility of single molecules affects localization accuracy in super-resolution fluorescence microscopy. *Nano Letters* **13**(9), 3967–3972.

LEW, M. D. & MOERNER, W. E. (2014). Azimuthal polarization filtering for accurate, precise, and robust single-molecule localization microscopy. *Nano Letters* **14**(11), 6407–6413.

LEWIS, A., ISAACSON, M., HAROOTUNIAN, A. & MURRAY, A. (1984). Development of a 500 a resolution light microscope. *Ultramicroscopy* **13**, 227–231.

LI, L., GATTASS, R. R., GERSHGOREN, E., HWANG, H. & FOURKAS, J. T. (2009a). Achieving l/20 resolution by one-color initiation and deactivation of polymerization. *Science* **324**(5929), 910–913.

LI, Q., WU, S. S. H. & CHOU, K. C. (2009b). Subdiffraction-limit two-photon fluorescence microscopy for GFP-Tagged cell imaging. *Biophysical Journal* **97**(12), 3224–3228.

LIDKE, K. A., RIEGER, B., JOVIN, T. M. & HEINTZMANN, R. (2005). Superresolution by localization of quantum dots using blinking statistics. *Optics Express* **13**(18), 7052–7062.

LIETO, A. M., CUSH, R. C. & THOMPSON, N. L. (2003). Ligand-receptor kinetics measured by total internal reflection with fluorescence correlation spectroscopy. *Biophysical Journal* **85**, 3294–3302.

LINGWOOD, D. & SIMONS, K. (2010). Lipid rafts as a membrane-organizing principle. *Science* **327**, 46–50.

LIPPINCOTT-SCHWARTZ, J. & MANLEY, S. (2009). Putting super-resolution fluorescence microscopy to work. *Nature Methods* **6**(1), 21–23.

LIU, Z. W., LEE, H., XIONG, Y., SUN, C. & ZHANG, X. (2007). Far-field optical hyperlens magnifying sub-diffraction-limited objects. *Science* **315**(5819), 1686–1686.

LOMMERSE, P. H. M., SPAINK, H. P. & SCHMIDT, T. (2004). *In vivo* plasma membrane organization: results of biophysical approaches. *Biochimica et Biophysica Acta* **1664**, 119–131.

LORD, S. J., LEE, H.-L. D. & MOERNER, W. E. (2010). Single-molecule spectroscopy and imaging of biomolecules in living cells. *Analytical Chemistry* **82**(6), 2192–2203.

LUKINAVICIUS, G. & JOHNSSON, K. (2011). Switchable fluorophores for protein labeling in living cells. *Current Opinion in Chemical Biology* **15**(6), 768–774.

LUKINAVICIUS, G., UMEZAWA, K., OLIVIER, N., HONIGMANN, A., YANG, G., PLASS, T., MUELLER, V., REYMOND, L., CORREA, I. R., LUO, Z.-G., SCHULTZ, C., LEMKE, E. A., HEPPENSTALL, P., EGGELING, C. & JOHNSSON, K. (2013). A near-infrared fluorophore for live-cell superresolution microscopy of cellular proteins. *Nature Chemistry* **5**, 132–139.

LUKINAVICIUS, G., REYMOND, L., D'ESTE, E., MASHARINA, A., GÖTTFERT, F., TA, H., GÜTHER, A., FOURNIER, M., RIZZO, S., WALDMANN, H., BLAUKOPF, C., SOMMER, C., GERLICH, D. W., ARNDT, H., HELL, S. W. & JOHNSSON, K. (2014). Fluorogenic probes for live-cell imaging of the cytoskeleton *Nature Methods* **11**(7), 731–733.

LUKOSZ, W. (1966). Optical systems with resolving powers exceeding the classical limit. *Journal of the Optical Society of America* **56**, 1463–1471.

LUKYANOV, K. A., FRADKOV, A. F., GURSKAYA, N. G., MATZ, M. V., LABAS, Y. A., SAVITSKY, A. P., MARKELOV, M. L., ZARAISKY, A. G., ZHAO, X. N., FANG, Y., TAN, W. Y. & LUKYANOV, S. A. (2000). Natural animal coloration can be determined by a nonfluorescent green fluorescent protein homolog. *Journal of Biological Chemistry* **275**(34), 25879–25882.

MAGDE, D., WEBB, W. W. & ELSON, E. (1972). Thermodynamic fluctuations in a reacting system – measurement by fluorescence correlation spectroscopy. *Physical Review Letters* **29**(11), 705–708.

MANLEY, S., GILLETTE, J. M., PATTERSON, G. H., SHROFF, H., HESS, H. F., BETZIG, E. & LIPPINCOTT-SCHWARTZ, J. (2008). High-density mapping of single-molecule trajectories with photoactivated localization microscopy. *Nature Methods* **5**(2), 155–157.

MANZO, C., VAN ZANTEN, T. S. & GARCIA-PARAJO, M. F. (2011). Nanoscale fluorescence correlation spectroscopy on intact living cell membranes with NSOM probes. *Biophysical Journal* **100**, L08–L10.

MAURER, P. C., MAZE, J., STANWIX, P. L., JIANG, L., GORSHKOV, A. V., ZIBROV, A. A., HARKE, B., HODGES, J. S., ZIBROV, A. S., YACOBY, A., TWITCHEN, D., HELL, S. W., WALSWORTH, R. L. & LUKIN, M. D. (2010). Far-field optical imaging and manipulation of individual spins with nanoscale resolution. *Nature Physics* **6**, 912–918.

MAZE, J. R., STANWIX, P. L., HODGES, J. S., HONG, S., TAYLOR, J. M., CAPPELLARO, P., JIANG, L., DUTT, M. V. G., TOGAN, E., ZIBROV, A. S., YACOBY, A., WALSWORTH, R. L. & LUKIN, M. D. (2008). Nanoscale magnetic sensing with an individual electronic spin in diamond. *Nature* **455**, 644–647.

MCCABE, E. M., FEWER, D. T., OTTEWILL, A. C., HEWLETT, S. J. & HEGARTY, J. (1996). Direct-view microscopy: optical sectioning strength for finite-sized, multiple-pinhole arrays. *Journal of Microscopy* **184**(2), 95–105.

MEI, E. & HOCHSTRASSER, R. M. (2006). High-resolution optical imaging from trajectory time distributions. *Journal of Physical Chemistry B* **110**, 25101–25107.

MEYER, L., WILDANGER, D., MEDDA, R., PUNGE, A., RIZZOLI, S. O., DONNERT, G. & HELL, S. W. (2008). Dual-color sted microscopy at 30-nm focal-plane resolution. *Small* **4**(8), 1095–1100.

MINSKY, M. (1961). Microscopy apparatus US Patent.

MITRONOVA, G. Y., BELOV, V. N., BOSSI, M. L., WURM, C. A., MEYER, L., MEDDA, R., MONERON, G., BRETSCHNEIDER, S., EGGELING, C., JAKOBS, S. & HELL, S. W. (2010). New fluorinated rhodamines for optical microscopy and nanoscopy. *Chemistry A European Journal* **16**(15), 4477–4488.

MLODZIANOSKI, M. J., JUETTE, M. F., BEANE, G. L. & BEWERSDORF, J. (2009). Experimental characterization of 3D localization techniques for particle-tracking and super-resolution microscopy. *Optics Express* **17**(10), 8264–8277.

MOERNER, W. E. (2006). Single-molecule mountains yield nanoscale cell images. *Nature Methods* **3**(10), 781–782.

MOERNER, W. E. (2007). New directions in single-molecule imaging and analysis. *Proceedings of the National Academy of Sciences of the United States of America* **104**(31), 12596–12602.

MOERNER, W. E. & KADOR, L. (1989). Optical-detection and spectroscopy of single molecules in a solid. *Physical Review Letters* **62**(21), 2535–2538.

MOERTELMAIER, M., BRAMESHUBER, M., LINIMEIER, M., SCHUTZ, G. J. & STOCKINGER, H. (2005). Thinning out clusters while conserving stoichiometry of labeling. *Applied Physics Letters* **87**, 263903.

MOFFITT, J. R., OSSEFORTH, C. & MICHAELIS, J. (2011). Time-gating improves the spatial resolution of STED microscopy. *Optics Express* **19**(5), 4242–4254.

MONERON, G. & HELL, S. (2009). Two-photon excitation STED microscopy. *Optics Express* **17**(17), 14567–14573.

MONERON, G., MEDDA, R., HEIN, B., GISKE, A., WESTPHAL, V. & HELL, S. W. (2010). Fast STED microscopy with continuous wave fiber lasers. *Optics Express* **18**(2), 1302–1309.

MOROZOVA, K. S., PIATKEVICH, K. D., GOULD, T. J., ZHANG, J., BEWERSDORF, J. & VERKHUSHA, V. V. (2010). Far-red fluorescent protein excitable with red lasers for flow cytometry and superresolution STED nanoscopy. *Biophysical Journal* **99**, L13–L15.

MORTENSEN, K. I., CHURCHMAN, S. L., SPUDICH, J. A. & FLYVBJERG, H. (2010). Optimized localization analysis for single-molecule tracking and super-resolution microscopy. *Nature Methods* **7**(5), 377–381.

MUELLER, V. (2012). Nanoscale studies of membrane dynamics via STED – Fluorescence Correlation Spectroscopy, University Heidelberg.

MUELLER, V., EGGELING, C., KARLSSON, H. & VON GEGERFELT, D. (2012). CW DPSS lasers make STED microscopy more practical. *Biophotonics* **19**(5), 30–32.

MUELLER, V., HONIGMANN, A., RINGEMANN, C., MEDDA, R., SCHWARZMANN, G. & EGGELING, C. (2013). FCS in STED microscopy: studying the nanoscale of lipid membrane dynamics. In *Methods in Enzymology*, **vol. 591** (ed. S. Y. Tetin), pp. 1–38. Burlington: Academic Press: Elsevier.

MUELLER, V., RINGEMANN, C., HONIGMANN, A., SCHWARZMANN, G., MEDDA, R., LEUTENEGGER, M., POLYAKOVA, S., BELOV, V. N., HELL, S. W. & EGGELING, C. (2011). STED nanoscopy reveals molecular details of cholesterol- and cytoskeleton-modulated lipid interactions in living cells. *Biophysical Journal* **101**, 1651–1660.

MULLER, C. B. & ENDERLEIN, J. (2010). Image scanning microscopy. *Physical Review Letters* **104**(19), 198101.

MULLER, T., SCHUMANN, C. & KRAEGELOH, A. (2012). STED microscopy and its applications: new insights into cellular processes on the nanoscale. *ChemPhysChem* **13**(8), 1986–2000.

MUNRO, S. (2003). Lipid rafts: elusive or illusive? *Cell* **115**, 377–388.

NÄGERL, U. V., WILLIG, K. I., HEIN, B., HELL, S. W. & BONHOEFFER, T. (2008). Live-cell imaging of dendritic spines by STED microscopy. *Proceedings of the National Academy of Sciences of the United States of America* **105**, 18982–18987.

NEUMANN, D., BÜCKERS, J., KASTRUP, L., HELL, S. & JAKOBS, S. (2010). Two-color STED microscopy reveals different degrees of colocalization between hexokinase-I and the three human VDAC isoforms. *PMC Biophysics* **5** (3), 1–4.

NIEUWENHUIZEN, R. P. J., LIDKE, K. A., BATES, M., LEYTON PUIG, D., GRÜNWALD, D., STALLINGA, S. & RIEGER, B. (2013). Measuring image resolution in optical nanoscopy. *Nature Methods* **10**, 557–562.

NOVOTNY, L. & HECHT, B. (2006). *Principles of Nano-optics.* Cambridge: Cambridge University Press.

ONDRUS, A. E., LEE, H.-LU D., IWANAGA, S., PARSONS, W. H., ANDRESEN, B. M., MOERNER, W. E. & DU BOIS, J. (2012). Fluorescent saxitoxins for live cell imaging of single voltage-gated sodium ion channels beyond the optical diffraction limit. *Chemistry and Biology* **19** (7), 902–912.

OPAZO, F., LEVY, M., BYROM, M., SCHAEFER, C., GEISLER, C., GROEMER, T. W., ELLINGTON, A. D. & RIZZOLI, S. O. (2012). Aptamers as potential tools for super-resolution microscopy. *Nature Methods* **9**, 938–939.

OPAZO, F., PUNGE, A., BÜCKERS, J., HOOPMANN, P., KASTRUP, L., HELL, S. W. & RIZZOLI, S. O. (2010). Limited intermixing of synaptic vesicle components upon vesicle recycling. *Traffic: the International Journal of Intracellular Transport* **11**(6), 800–812.

ORRIT, M. & BERNARD, J. (1990). Single pentacene molecules detected by fluorescence excitation in a p-terphenyl crystal. *Physical Review Letters* **65**, 2716–2719.

OSSEFORTH, C., MOFFITT, J. R., SCHERMELLEH, L. & MICHAELIS, J. (2013). Simultaneous dual-color 3D STED microscopy. *Optics Express* **22**(6), 7028–7039.

PATTERSON, G., DAVIDSON, M., MANLEY, S. & LIPPINCOTT-SCHWARTZ, J. (2010). Superresolution imaging using single-molecule localization. *Annual Review of Physical Chemistry* **61**, 345–367.

PATTERSON, G. H. & LIPPINCOTT-SCHWARTZ, J. (2002). A photoactivatable GFP for selective photolabeling of proteins and cells. *Science* **297**(5588), 1873–1877.

PAVANI, S. R. P., THOMPSON, M. A., BITEEN, J. S., LORD, S. J., LIU, N., TWIEG, R. J., PIESTUN, R. & MOERNER, W. E. (2009). Three-dimensional, single-molecule fluorescence imaging beyond the diffraction limit by using a double-helix point spread function. *Proceedings of the National Academy of Sciences of the United States of America* **106**(9), 2995–2999.

PAWLEY, J. B. (2006). *Handbook of Biological Confocal Microscopy,* 2nd edn. New York: Springer.

PELLETT, P. A., SUN, X., GOULD, T. J., ROTHMAN, J. E., XU, M.-Q., CORREA, J. R., I. R. & BEWERSDORF, J. (2011). Two-color STED microscopy in living cells. *Biomedical Optics Express* **2**(8), 2364–2371.

PENDRY, J. B. (2000). Negative refraction makes a perfect lens. *Physical Review Letters* **85**(18), 3966–3969.

PERSSON, F., BINGEN, P., STAUDT, T., ENGELHARDT, J., TEGENFELDT, J. O. & HELL, S. W. (2011). Fluorescence nanoscopy of single DNA molecules by using stimulated emission depletion (STED). *Angewandte Chemie International Edition* **50**(24), 5581–5583.

PERTSINIDIS, A., ZHANG, Y. & CHU, S. (2010). Subnanometre single-molecule localization, registration and distance measurements. *Nature* **466**(7306), 647–651.

PETERSEN, N. O., HODDELIUS, P. L., WISEMAN, P. W., SEGER, O. & MAGNUSSON, K.-E. (1986). Quantification of membrane receptor distributions by image correlation spectroscopy: concept and application. *Biophysical Journal* **65**, 1135–1146.

PIKE, L. J. (2006). Rafts defined: a report on the Keystone symposium on lipid rafts and cell function. *Journal of Lipid Research* **47**, 1597–1598.

PODOLSKIY, V. A. & NARIMANOV, E. E. (2005). Near-sighted superlens. *Optics Letters* **30**, 75–77.

POHL, D. W., DENK, W. & LANZ, M. (1984). Optical stethoscopy – image recording with resolution lambda/20. *Applied Physics Letters* **44**, 651–653.

QU, X. H., WU, D., METS, L. & SCHERER, N. F. (2004). Nanometer-localized multiple single-molecule fluorescence microscopy. *Proceedings of the National Academy of Sciences of the United States of America* **101**(31), 11298–11303.

RANKIN, B. R. & HELL, S. W. (2009). STED microscopy with a MHz pulsed stimulated-Raman-scattering source. *Optics Express* **17**(18), 15679–15684.

RANKIN, B. R., KELLNER, R. R. & HELL, S. W. (2008). Stimulated-emission-depletion microscopy with a multicolor stimulated-Raman-scattering light source. *Optics Letters* **33**(21), 2491–2493.

RANKIN, B. R., MONERON, G., WURM, C. A., NELSON, J. C., WALTER, A., SCHWARZER, D., SCHROEDER, J., COLON-RAMOS, D. A. & HELL, S. W. (2011). Nanoscopy in a living multicellular organism expressing GFP. *Biophysical Journal* **100**, L63–L65.

RASNIK, I., MCKINNEY, S. A. & HA, T. (2006). Nonblinking and longlasting single-molecule fluorescence imaging. *Nature Methods* **3**(11), 891–893.

REGO, E. H., SHAO, L., MACKLIN, J. J., WINOTO, L., JOHANSSON, G. A., KAMPS-HUGHES, N., DAVIDSON, M. W. & GUSTAFSSON, M. G. L. (2012). Nonlinear structured-illumination microscopy with a photoswitchable protein reveals cellular structures at 50-nm resolution. *Proceedings of the National Academy of Sciences of the United States of America* **109**(3), E135–E143.

REISINGER, E., BRESEE, C., NEEF, J., NAIR, R., REUTER, K., BULANKINA, A., NOUVIAN, R., KOCH, M., BÜCKERS, J., KASTRUP, L., ROUX, I., PETIT, C., HELL, S. W., BROSE, N., RHEE, J., KÜGLER, S., BRIGANDE, J. V. & MOSER, T. (2011). Probing the functional equivalence of otoferlin and synaptotagmin 1 in exocytosis. *Journal of Neuroscience* **31**(13), 4886–4895.

REUSS, M., ENGELHARDT, J. & HELL, S. (2010). Birefringent device converts a standard scanning microscope into a STED microscope that also maps molecular orientation. *Optics Express* **18**(2), 1049–1058.

REUTHER, A., LAUBEREAU, A. & NIKOGOSYAN, D. N. (1996). Primary photochemical processes in water. *Journal of Physical Chemistry* **100**, 16794–16800.

RICE, J. H. (2007). Beyond the diffraction limit: far-field fluorescence imaging with ultrahigh resolution. *Molecular BioSystems* **3**(11), 781–793.

RINGEMANN, C., HARKE, B., MIDDENDORFF, C. V., MEDDA, R., HONIGMANN, A., WAGNER, R., LEUTENEGGER, M., SCHOENLE, A., HELL, S. & EGGELING, C. (2009). Exploring single-molecule dynamics with fluorescence nanoscopy. *New Journal of Physics* **11**, 103054.

RINGEMANN, C., SCHÖNLE, A., GISKE, A., VON MIDDENDORFF, C., HELL, S. W. & EGGELING, C. (2008). Enhancing fluorescence brightness: effect of reverse intersystem crossing studied by fluorescence fluctuation spectroscopy. *ChemPhysChem* **9**(9), 612–624.

RITTWEGER, E., HAN, K. Y., IRVINE, S. E., EGGELING, C. & HELL, S. W. (2009a). Sted microscopy reveals crystal colour centres with nanometric resolution. *Nature Photonics* **3**, 144–147.

RITTWEGER, E., WILDANGER, D. & HELL, S. W. (2009b). Far-field fluorescence nanoscopy of diamond color centers by ground state depletion. *Europhysics Letters* **86** (14001), 14001.

ROEFFAERS, M. B. J., DE CREMER, G., LIBEERT, J., AMELOOT, R., DEDECKER, P., BONS, A.-J., BUCKINS, M., MARTENS, J. A., SELS, B. F., DE VOS, D. E. & HOFKENS, J. (2009). *Super-Resolution Reactivity Mapping of Nanostructured Catalyst Particles* **48**, 9285–9289.

RUPRECHT, V., WIESER, S., MARGUET, D. & SCHUETZ, G. J. (2011). Spot variation fluorescence correlation spectroscopy allows for superresolution chronoscopy of confinement times in membranes. *Biophysics Journal* **100**, 2839–2845.

RUST, M. J., BATES, M. & ZHUANG, X. W. (2006). Sub-diffraction-limit imaging by stochastic optical reconstruction microscopy (STORM). *Nature Methods* **3**, 793–795.

SAHL, S. J., LEUTENEGGER, M., HELL, S. W. & EGGELING, C. (2014). High-resolution tracking of single-molecule diffusion in membranes by confocalized and spatially differentiated fluorescence photon stream recording. *ChemPhysChem* **15**(4), 771–783.

SAHL, S. J., LEUTENEGGER, M., HILBERT, M., HELL, S. W. & EGGELING, C. (2010). Fast molecular tracking maps nanoscale dynamics of plasma membrane lipids. *Proceedings of the National Academy of Sciences of the United States of America* **107**(15), 6829–6834.

SAHL, S. J. & MOERNER, W. E. (2013). Super-resolution fluorescence imaging with single molecules. *Current Opinion in Structural Biology* **23**(5), 778–787.

SAHL, S. J., WEISS, L. E., DUIM, W. C., FRYDMAN, J. & MOERNER, W. E. (2012). Cellular inclusion bodies of mutant huntingtin exon 1 obscure small fibrillar aggregate species. *Scientific Reports* **2**, 895.

SAKATA, T., YAN, Y. & MARRIOT, G. (2005). Family of site-selective molecular optical switches. *Journal of Organic Chemistry* **70**, 2009–2013.

SCHERMELLEH, L., CARLTON, P. M., HAASE, S., SHAO, L., WINOTO, L., KNER, P., BURKE, B., CARDOSO, M. C., AGARD, D. A., GUSTAFSSON, M. G. L., LEONHARDT, H. & SEDAT, J. W. (2008). Subdiffraction multicolor imaging of the nuclear periphery with 3D structured illumination microscopy. *Science* **320**(5881), 1332–1336.

SCHMIDT, R., WURM, C. A., JAKOBS, S., ENGELHARDT, J., EGNER, A. & HELL, S. W. (2008). Spherical nanosized focal spot unravels the interior of cells. *Nature Methods* **5**(6), 539–544.

SCHMIDT, R., WURM, C. A., PUNGE, A., EGNER, A., JAKOBS, S. & HELL, S. W. (2009). Mitochondrial cristae revealed with focused light. *Nano Letters* **9**(6), 2508–2510.

SCHOENLE, A. & HELL, S. W. (2007). Fluorescence nanoscopy goes multicolor. *Nature Biotechnology* **25**(11), 1234–1235.

SCHÖNLE, A., HANNINEN, P. E. & HELL, S. W. (1999). Nonlinear fluorescence through intermolecular energy transfer and resolution increase in fluorescence microscopy. *Annalen der Physik* **8**(2), 115–133.

SCHRADER, M., MEINECKE, F., BAHLMANN, K., KROUG, M., CREMER, C., SOINI, E. & HELL, S. W. (1995). Monitoring the excited state of a dye in a microscope by stimulated emission. *Bioimaging* **3**, 147–153.

SCHRÖDER, J., BENINK, H., DYBA, M. & LOS, G. V. (2008). *In vivo* labeling method using a genetic construct for nanoscale resolution microscopy. *Biophysical Journal* **96**(1), L1–L3.

SCHROF, S., STAUDT, T., RITTWEGER, E., WITTENMAYER, N., DRESBACH, T., ENGELHARDT, J. & HELL, S. W. (2011). STED nanoscopy with mass-produced laser diodes. *Optics Express* **19**(9), 8066–8072.

SCHUTZ, G. J., SCHINDLER, H. & SCHMIDT, T. (1997). Single-molecule microscopy on model membranes reveals anomalous diffusion. *Biophysical Journal* **73**, 1073–1080.

SCHWENTKER, M. A. (2007). *Parallelized Ground State Depletion*. Germany: University of Heidelberg.

SCHWENTKER, M. A., BOCK, H., HOFMANN, M., JAKOBS, S., BEWERSDORF, J., EGGELING, C. & HELL, S. W. (2007). Wide-field subdiffraction RESOLFT microscopy using fluorescent protein photoswitching. *Microscopy Research and Technique* **70**(3), 269–280.

SCHWERING, M., KIEL, A., KURZ, A., LYMPEROPOULOS, K., SPRODEFELD, A., KRAMER, R. H. & HERTEN, D. P. (2011). Far-field nanoscopy with reversible chemical reactions. *Angewandte Chemie (international Edition)* **50**, 2940–2945.

SCHWILLE, P., KORLACH, J. & WEBB, W. W. (1999). Fluorescence correlation spectroscopy with single-molecule sensitivity on cell and model membranes. *Cytometry* **36**, 176–182.

SCOTT, T. F., KOWALSKI, B. A., SULLIVAN, A. C., BOWMAN, C. N. & MCLEOD, R. R. (2009). Two-color single-photon photoinitiation and photoinhibition for sub-diffraction photolithography. *Science* **324**(5929), 913–917.

SERGEEV, M., COSTANTINO, S. & WISEMAN, P. W. (2006). Measurement of monomer-oligomer distributions via fluorescence moment image analysis. *Biophysical Journal* **91**, 3884–3896.

SEZGIN, E., LEVENTAL, I., GRZYBEK, M., SCHWARZMANN, G., MUELLER, V., HONIGMANN, A., BELOV, V. N., EGGELING, C., COSKUN, Ü., SIMONS, K. & SCHWILLE, P. (2012). Partitioning, diffusion, and ligand binding of raft lipid analogs in model and cellular plasma membranes. *Biochimica et Biophysica Acta (BBA) – Biomembranes* **1818**, 1777–1784.

SHARONOV, A. & HOCHSTRASSER, R. M. (2006). Wide-field subdiffraction imaging by accumulated binding of diffusing probes. *Proceedings of the National Academy of Sciences of the United States of America* **103**(50), 18911–18916.

SHAW, A. S. (2006). Lipid rafts: now you see them, now you don't. *Nature Immunology* **7**(11), 1139–1142.

SHECHTMAN, Y., SAHL, S. J., BACKER, A. S. & MOERNER, W. E. (2014). Optimal point spread function design for 3D imaging. *Physical Review Letters* **113**(13), 133902.

SHEETZ, M. P., TURNEY, S., QIAN, H. & ELSON, E. L. (1989). Nanometer-level analysis demonstrates that lipid flow does not drive membrane glycoprotein movements. *Nature* **340**, 284–288.

SHEPPARD, C. J. R. & KOMPFNER, R. (1978). Resonant scanning optical microscope. *Applied Optics* **17**, 2879–2882.

SHERA, E. B., SEITZINGER, N. K., DAVIS, L. M., KELLER, R. A. & SOPER, S. A. (1990). Detection of single fluorescent molecules. *Chemical Physics Letters* **174**(6), 553–557.

SHROFF, H., GALBRAITH, C. G., GALBRAITH, J. A. & BETZIG, E. (2008). Live-cell photoactivated localization microscopy of nanoscale adhesion dynamics. *Nature Methods* **5**(5), 417–423.

SHROFF, H., GALBRAITH, C. G., GALBRAITH, J. A., WHITE, H., GILLETTE, J., OLENYCH, S., DAVIDSON, M. W. & BETZIG, E. (2007). Dual-color superresolution imaging of genetically expressed probes within individual adhesion complexes. *Proceedings of the National Academy of Sciences of the United States of America* **104**(51), 20308–20313.

SHTENGEL, G., GALBRAITH, J. A., GALBRAITH, C. G., LIPPINCOTT-SCHWARTZ, J., GILLETTE, J. M., MANLEY, S., SOUGRAT, R., WATERMAN, C. M., KANCHANAWONG, P., DAVIDSON, M. W., FETTER, R. D. & HESS, H. F. (2009). Interferometric fluorescent super-resolution microscopy resolves 3D cellular ultrastructure. *Proceedings of the National Academy of Sciences of the United States of America* **106**(9), 3125–3130.

SIEBER, J. J., WILLIG, K. I., HEINTZMANN, R., HELL, S. W. & LANG, T. (2006). The snare motif is essential for the formation of syntaxin clusters in the plasma membrane. *Biophysical Journal* **90**, 2843–2851.

SIEBER, J. J., WILLIG, K. I., KUTZNER, C., GERDING-REIMERS, C., HARKE, B., DONNERT, G., RAMMNER, B., EGGELING, C., HELL, S. W., GRUBMULLER, H. & LANG, T. (2007). Anatomy and dynamics of a supramolecular membrane protein cluster. *Science* **317**, 1072–1076.

SIMONS, K. & IKONEN, E. (1997). Functional rafts in cell membranes. *Nature* **387**, 569–572.

SMALL, A. R. (2009). Theoretical limits on errors and acquisition rates in localizing switchable fluorophores. *Biophysical Journal* **96**(2), L16–L18.

SMITH, B. R., INGLIS, D. W., SANDNES, B., RABEAU, J. R., ZVYAGIN, A. V., GRUBER, D., NOBLE, C. J., VOGEL, R., OSAWA, E. & PLAKHOTNIK, T. (2009). Five-nanometer diamond with luminescent nitrogen-vacancy defect centers. *Small* **5**(14), 1649–1653.

SMITH, C. S., JOSEPH, N., RIEGER, B. & LIDKE, K. A. (2010). Fast, single-molecule localization that achieves theoretically minimum uncertainty. *Nature Methods* **7**(5), 373–375.

SMOLYANINOV, II, HUNG, Y. J. & DAVIS, C. C. (2007). Magnifying superlens in the visible frequency range. *Science* **315**(5819), 1699–1701.

STAUDT, T., ENGLER, A., RITTWEGER, E., HARKE, B., ENGELHARDT, J. & HELL, S. W. (2011). Far-field optical nanoscopy with reduced number of state transition cycles. *Optics Express* **19**(6), 5644–5657.

STEINHAUER, C., FORTHMANN, C., VOGELSANG, J. & TINNEFELD, P. (2008). Superresolution microscopy on the basis of engineered dark states. *Journal of the American Chemical Society* **130**, 16840–16841.

STIEL, A. C., ANDRESEN, M., BOCK, H., HILBERT, M., SCHILDE, J., SCHÖNLE, A., EGGELING, C., EGNER, A., HELL, S. W. & JAKOBS, S. (2008). Generation of monomeric reversibly switchable red fluorescent proteins for far-field fluorescence nanoscopy. *Biophysical Journal* **95**, 2989–2997.

STIEL, A. C., TROWITZSCH, S., WEBER, G., ANDRESEN, M., EGGELING, C., HELL, S. W., JAKOBS, S. & WAHL, M. C. (2007). 1·8 angstrom bright-state structure of the reversibly switchable fluorescent protein dronpa guides the generation of fast switching variants. *Biochemical Journal* **402**(1), 35–42.

SYNGE, E. H. (1928). A suggested method for extending microscopic resolution into the ultra-microscopic region. *Philosophical Magazine* **6**, 356–362.

TAKASAKI, K. T., DING, J. B. & SABATINI, B. L. (2013). Live-cell superresolution imaging by pulsed STED two-photon excitation microscopy. *Biophysical Journal* **104**, 770–777.

TANAKA, K. A. K., SUZUKI, K. G. N., SHIRAI, Y. M., SHIBUTANI, S. T., MIYAHARA, M. S. H., TSUBOI, H., YAHARA, M., YOSHIMURA, A., MAYOR, S., FUJIWARA, T. K., KUSUMI, A. (2010). Membrane molecules mobile

even after chemical fixation. *Nature Methods* **7**(11), 865–866.

TONNESEN, J., KATONA, G., ROZSA, B. & NÄGERL, U.V. (2014). Spine neck plasticity regulates compartmentalization of synapses *Nature Neuroscience* **17**(5):678–685.

TESTA, I., SCHÖNLE, A., MIDDENDORFF, C. V., GEISLER, C., MEDDA, R., WURM, C. A., STIEL, A. C., JAKOBS, S., BOSSI, M., EGGELING, C., HELL, S. W. & EGNER, A. (2008). Nanoscale separation of molecular species based on their rotational mobility. *Optics Express* **16** (25), 21093–21104.

TESTA, I., URBAN, N. T., JAKOBS, S., EGGELING, C., WILLIG, K. I. & HELL, S. W. (2012). Nanoscopy of living brain slices with low light levels. *Neuron* **75**, 992–1000.

TESTA, I., WURM, C. A., MEDDA, R., ROTHERMEL, E., V. MIDDENDORFF, C., FÖLLING, J., JAKOBS, S., HELL, S. W. & EGGELING, C. (2010). Multicolor fluorescence nanoscopy in fixed and living cells by exciting conventional fluorophores with a single wavelength. *Biophysical Journal* **99**(8), 2686–2694.

THOMPSON, R. E., LARSON, D. R. & WEBB, W. W. (2002). Precise nanometer localization analysis for individual fluorescent probes. *Biophysical Journal* **82**, 2775–2783.

TINNEFELD, P., EGGELING, C., HELL, S.W. (2015). (Eds.) Far-Field Optical Nanoscopy, *Springer Series on Fluorescence*, Vol. 14. Springer (Berlin & Heidelberg, Germany).

TONNESEN, J., NADRIGNY, F., WILLIG, K. I., WEDLICH-SOLDNER, R. & NÄGERL, U. V. (2011). Two-color STED microscopy of living synapses using a single laser-beam pair. *Biophysical Journal* **101**, 2545–2552.

TORALDO DI FRANCIA, G. (1952). Super-gain antennas and optical resolving power. *Il Nuovo Cimento* **9**, 426–435.

TSIEN, R. Y., ERNST, L. & WAGGONER, A. (2006). Fluorophores for confocal microscopy: photophysics and photochemistry. In *Handbook of Biological Confocal Microscopy* (ed. J. B. PAWLEY), pp. 338–352. New York: Springer.

TZENG, Y. K., FAKLARIS, O., CHANG, B. M., KUO, Y. M., HSU, J. H. & CHANG, H. C. (2011). Superresolution imaging of albumin-conjugated fluorescent nanodiamonds in cells by stimulated emission depletion. *Angewandte Chemie International Edition* **50**, 2262–2265.

ULLAL, C. K., PRIMPKE, S., SCHMIDT, R., BÖHM, U., EGNER, A., VANA, P. & HELL, S. W. (2011). Flexible microdomain specific staining of block copolymers for 3D optical nanoscopy. *Macromolecules* **44**(19), 7508–7510.

ULLAL, C. K., SCHMIDT, R., HELL, S. W. & EGNER, A. (2009). Block copolymer nanostructures mapped by far-field optics. *Nano Letters* **9**(6), 2497–2500.

URBAN, N. T., WILLIG, K. I., HELL, S. W. & NÄGERL, U. V. (2011). STED nanoscopy of actin dynamics in synapses deep inside living brain slices. *Biophysical Journal* **101**(5), 1277–1284.

VAN DE LINDE, S., ENDESFELDER, U., MUKHERJEE, A., SCHUTTPELZ, M., WIEBUSCH, G., WOLTER, S., HEILEMANN, M. & SAUER, M. (2009). Multicolor photoswitching microscopy for subdiffraction-resolution fluorescence imaging. *Photochemistry and Photobiology* **8**, 465–469.

VAN DE LINDE, S., KASPER, R., HEILEMANN, M. & SAUER, M. (2008). Photoswitching microscopy with standard fluorophores. *Applied Physics B: Lasers and Optics* **93**(4), 725–731.

VAN ZANTEN, T. S., GOMEZ, J., MANZO, C., CAMBI, A., BUCET, J., REIGAD, R. & GARCIA-PARAJO, M. F. (2010). Direct mapping of nanoscale compositional connectivity on intact cell membranes. *Proceedings of the National Academy of Sciences of the United States of America* **107**(35), 15437–15442.

VICIDOMINI, G., MONERON, G., EGGELING, C., RITTWEGER, E. & HELL, S. W. (2012). STED with wavelengths closer to the emission maximum. *Optics Express* **20**(5), 5225–5236.

VICIDOMINI, G., MONERON, G., HAN, K. Y., WESTPHAL, V., TA, H., REUSS, M., ENGELHARDT, H., EGGELING, C. & HELL, S. W. (2011). Sharper low-power STED nanoscopy by time gating. *Nature Methods* **8**(7), 571–573.

VICIDOMINI, G., SCHOENLE, A., TA, H., HAN, K. Y., MONERON, G., EGGELING, C. & HELL, S. W. (2013). STED nanoscopy with time-gated detection: theoretical and experimental aspects. *PloS ONE* **8**(1), e54421.

VOGELSANG, J., KASPER, R., STEINHAUER, C., PERSON, B., HEILEMANN, M., SAUER, M. & TINNEFELD, P. (2008). A reducing and oxidizing system minimizes photobleaching and blinking of fluorescent dyes. *Angewandte Chemie (international Edition)* **47**(29), 5465–5469.

VUKOJEVIC, V., HEIDKAMP, M., MINGA, Y., JOHANSSON, B., TERENIUSA, L. & RIGLER, R. (2008). Quantitative single-molecule imaging by confocal laser scanning microscopy. *Proceedings of the National Academy of Sciences of the United States of America* **105**(47), 18176–18181.

WAGNER, E., LAUTERBACH, M., KOHL, T., WESTPHAL, V., WILLIAMS, G. S. B., STEINBRECHER, J. H., STREICH, J. H., KORFF, B., TUAN, H.-T. M., HAGEN, B., LUTHER, S., HASENFUSS, G., PARLITZ, U., JAFRI, M. S., HELL, S. W., LEDERER, W. J. & LEHNART, S. E. (2012). STED live cell super-resolution imaging shows proliferative remodeling of T-tubule membrane structures after myocardial infarction. *Circulation Research* **111**, 402–414.

WAWREZINIECK, L., RIGNEAULT, H., MARGUET, D. & LENNE, P. F. (2005). Fluorescence correlation spectroscopy diffusion laws to probe the submicron cell membrane organization. *Biophysical Journal* **89**, 4029–4042.

WEBB, W. W., WELLS, K. S., SANDISON, D. R. & STRICKLER, J. (1990). Criteria for quantitative dynamical confocal fluorescence imaging. In *Optical Microscopy for Biology* (eds. B. Herman & K. Jacobson), pp. 73–108. New York: Wiley.

WEIL, T., PARTON, R., HERPERS, B., SOETAERT, J., XANTHAKIS, D., DOBBIE, I., HALSTEAD, J., HAYASHI, R., RABOUILLE, C. & DAVIS, I. (2012). Drosophila

patterning is established by differential association of mRNAs with P bodies. *Nature Cell Biology* **14**, 1305–1313.

WEISS, S. (1999). Fluorescence spectroscopy of single biomolecules. *Science* **283**, 1676–1683.

WEISS, S. (2000). Shattering the diffraction limit of light: a revolution in fluorescence microscopy? *Proceedings of the National Academy of Sciences of the United States of America* **97**(16), 8747–8749.

WENGER, J., CONCHONAUD, F., DINTINGER, J., WAWREZINIECK, L., EBBESEN, T. W., RIGNEAULT, H., MARGUET, D. & LENNE, P. F. (2007). Diffusion analysis within single nanometric apertures reveals the ultrafine cell membrane organization. *Biophysical Journal* **92**(3), 913–919.

WESTPHAL, V., BLANCA, C. M., DYBA, M., KASTRUP, L. & HELL, S. W. (2003). Laser-diode-stimulated emission depletion microscopy. *Applied Physics Letters* **82**(18), 3125–3127.

WESTPHAL, V. & HELL, S. W. (2005). Nanoscale resolution in the focal plane of an optical microscope. *Physical Review Letters* **94**, 143903.

WESTPHAL, V., LAUTERBACH, M. A., DI NICOLA, A. & HELL, S. W. (2007). Dynamic far-field fluorescence nanoscopy. *New Journal of Physics* **9**, 435.

WESTPHAL, V., RIZZOLI, S. O., LAUTERBACH, M. A., KAMIN, D., JAHN, R. & HELL, S. W. (2008). Video-rate far-field optical nanoscopy dissects synaptic vesicle movement. *Science* **320**(5873), 246–249.

WIDENGREN, J., CHMYROV, A., EGGELING, C., LOFDAHL, P. A. & SEIDEL, C. A. M. (2007). Strategies to improve photostabilities in ultrasensitive fluorescence spectroscopy. *Journal of Physical Chemistry Part A: Molecules, Spectroscopy, Kinetics, Environment and General Theory* **111**, 429–440.

WIDENGREN, J. & RIGLER, R. (1996). Mechanisms of photobleaching investigated by fluorescence correlation spectroscopy. *Bioimaging* **4**(3), 149–156.

WIDENGREN, J. & SCHWILLE, P. (2000). Characterization of photoinduced isomerization and back-isomerization of the cyanine dye cy5 by fluorescence correlation spectroscopy. *Journal of Physical Chemistry Part A: Molecules, Spectroscopy, Kinetics, Environment and General Theory* **104**, 6416–6428.

WIESBAUER, M., WOLLHOFEN, R., VASIC, B., SCHILCHER, K., JACAK, J. & KLAR, T. A. (2013). Nano-anchors with single protein capacity produced with STED lithography. *Nano Letters* **13**(11), 5672–5678.

WILDANGER, D., BÜCKERS, J., WESTPHAL, V., HELL, S. W. & KASTRUP, L. (2009a). A STED microscope aligned by design. *Optics Express* **17**(18), 16100–16110.

WILDANGER, D., MAZE, J. & HELL, S. W. (2011). Diffraction unlimited all-optical recording of electron spin resonances. *Physical Review Letters* **107**, 017601.

WILDANGER, D., MEDDA, R., KASTRUP, L. & HELL, S. W. (2009b). A compact STED microscope providing 3D nanoscale resolution. *Journal of Microscopy* **236**, 35–43.

WILDANGER, D., PATTON, B.R., SCHILL, H., MARSEGLIA, L., HADDEN, J.P., KNAUER, S., SCHÖNLE, A., RARITY, J.G., O'BRIEN, J.L., HELL, S.W. & SMITH, J.M. (2012). Solid immersion facilitates fluorescence microscopy with nanometer resolution and sub-ångström emitter localization. *Advanced Optical Materials* **24**(44), 309–313.

WILDANGER, D., RITTWEGER, E., KASTRUP, L. & HELL, S. W. (2008). STED microscopy with a supercontinuum laser source. *Optics Express* **16**(13), 9614–9621.

WILLIG, K. I., HARKE, B., MEDDA, R. & HELL, S. W. (2007). STED microscopy with continuous wave beams. *Nature Methods* **4**(11), 915–918.

WILLIG, K. I., KELLER, J., BOSSI, M. & HELL, S. W. (2006a). STED microscopy resolves nanoparticle assemblies. *New Journal of Physics* **8**, 106.

WILLIG, K. I., KELLNER, R. R., MEDDA, R., HEIN, B., JAKOBS, S. & HELL, S. W. (2006b). Nanoscale resolution in GFP-based microscopy. *Nature Methods* **3**(9), 721–723.

WILLIG, K. I., RIZZOLI, S. O., WESTPHAL, V., JAHN, R. & HELL, S. W. (2006c). STED microscopy reveals that synaptotagmin remains clustered after synaptic vesicle exocytosis. *Nature* **440**(7086), 935–939.

WILLIG, K. I., STIEL, A. C., BRAKEMANN, T., JAKOBS, S. & HELL, S. W. (2011). Dual-label STED nanoscopy of living cells using photochromism. *Nano Letters* **11**(9), 3970–3973.

WILMANN, P. G., PETERSEN, J., DEVENISH, R. J., PRESCOTT, M. & ROSSJOHN, J. (2005). Variations on the GFP chromophore. *Journal of Biological Chemistry* **280**(4), 2401–2404.

WILMES, S., STAUFENBIEL, M., LIßE, D., RICHTER, C. P., BEUTEL, O., BUSCH, K., HESS, S. T. & PIEHLER, J. (2012). Triple-color super-resolution imaging of live cells: resolving submicroscopic receptor organization in the plasma membrane. *Angewandte Chemie (international Edition)* **51**(20), 4868–4871.

WILSON, T. & SHEPPARD, C. J. R. (1984). *Theory and Practice of Scanning Optical Microscopy*. New York: Academic Press.

WOLLHOFEN, R., KATZMANN, J., HRELESCU, C., JACAK, J. & KLAR, T. A. (2013). 120 nm resolution and 55 nm structure size in STED-lithography. *Optics Express* **21**(9), 10831–10840.

WOLTER, S., SCHUTTPELZ, M., TSCHEREPANOW, M., VAN DE LINDE, S., HEILEMANN, M. & SAUER, M. (2010). Real-time computation of subdiffraction-resolution fluorescence images. *Journal of Microscopy* **237**(1), 12–22.

WOMBACHER, R., HEIDBREDER, M., VAN DE LINDE, S., SHEETZ, M. P., HEILEMANN, M., CORNISH, V. W. & SAUER, M. (2010). Live-cell super-resolution imaging with trimethoprim conjugates. *Nature Methods* **7**, 717–719. doi: 10.1038/nmeth.1489.

WU, Y., WAWRZUSIN, P., SENSENEY, J., FISCHER, R.S., CHRISTENSEN, R., SANTELLA, A., YORK, A.G.,

WINTER, P. W., WATERMAN, C. M., BAO, Z., COLÓN-RAMOS, D. A., MCAULIFFE, M. & SHROFF, H. (2013). Spatially isotropic four-dimensional imaging with dual-view plane illumination microscopy *Nature Biotechnology*, **31**(11), 1032–1038.

WURM, C. A., NEUMANN, D., SCHMIDT, R., EGNER, A., JAKOBS, S. (2010). Sample Preparation for STED Microscopy. In: PAPKOVSKY, D. B. (ed) *Live Cell Imaging, Methods in Molecular Biology*. Springer, Heidelberg, pp 185–199.

WURM, C. A., KOLMAKOV, K., GÖTTFERT, F., TA, H., BOSSI, M., SCHILL, H., BERNING, S., JAKOBS, S., DONNERT, G., BELOV, V. N. & HELL, S. W. (2012). Novel red fluorophores with superior performance in STED microscopy. *Optical Nanoscopy* **1**(7), 1–7.

XU, K., BABCOCK, H. P. & ZHUANG, X. (2012). Dual-objective STORM reveals three-dimensional filament organization in the actin cytoskeleton. *Nature Methods* **9**(2), 185–188.

XU, K., ZHONG, G. & ZHUANG, X. (2013). Actin, spectrin, and associated proteins form a periodic cytoskeletal structure in Axons. *Science* **339**, 452–456.

YANG, B., PRZYBILLA, F., MESTRE, M., TREBBIA, J.-B. & LOUNIS, B. (2014). Large parallelization of STED nanoscopy using optical lattices *Optics Express* **22**(5), 5581–5589.

YECHIEL, E. & EDIDIN, M. (1987). Micrometer-scale domains in fibroblast plasma-membranes. *Journal of Cell Biology* **105**(2), 755–760.

YILDIZ, A., FORKEY, J. N., MCKINNEY, S. A., HA, T., GOLDMAN, Y. E. & SELVIN, P. R. (2003). Myosin V walks hand-over-hand: single fluorophore imaging with 1·5-nm localization. *Science* **300**(5628), 2061–2065.

YORK, A. G., GHITANI, A., VAZIRI, A., DAVIDSON, M. W. & SHROFF, H. (2011). Confined activation and subdiffractive localization enables whole-cell PALM with genetically expressed probes. *Nature Methods* **8**, 327–333. doi: 10.1038/nmeth.1571.

YORK, A. G., PAREKH, S. H., NOGARE, D. D., FISCHER, R. S., TEMPRINE, K., MIONE, M., CHITNIS, A. B., COMBS, C. A. & SHROFF, H. (2012). Resolution doubling in live, multicellular organisms via multifocal structured illumination microscopy. *Nature Methods* **9**, 749–754. doi: 10.1038/nmeth.2025.

ZANACCHI, F. C., LAVAGNINO, Z., DONNORSO, M. P., DEL BUE, A., FURIA, L., FARETTA, M. & DIASPRO, A. (2011). Live-cell 3D super-resolution imaging in thick biological samples. *Nature Methods* **8**(12), 1047–1049.

ZANDER, C., ENDERLEIN, J. & KELLER, R. A. (2002). *Single-molecule Detection in Solution*, 1st edn. Berlin, Germany: Wiley-VCH.

ZONDERVAN, R., KULZER, F., ORLINSKII, S. B. & ORRIT, M. (2003). Photoblinking of rhodamine 6 G in poly(vinyl alcohol): radical dark state formed through the triplet. *Journal of Physical Chemistry Part A: Molecules, Spectroscopy, Kinetics, Environment and General Theory* **107**(35), 6770–6776.